Fano resonances in nanoscale structures

Andrey E. Miroshnichenko*

Nonlinear Physics Centre and Centre for Ultrahigh Bandwidth Devices for Optical Systems (CUDOS), Research School of Physics and Engineering, Australian National University, Canberra, Australian Capital Territory 0200, Australia

Sergej Flach

Max-Planck-Institut für Physik Komplexer Systeme, Nöthnitzer Strasse 38, D-01187 Dresden, Germany

Yuri S. Kivshar

Nonlinear Physics Centre and Centre for Ultrahigh Bandwidth Devices for Optical Systems (CUDOS), Research School of Physics and Engineering, Australian National University, Canberra, Australian Capital Territory 0200, Australia

(Published 11 August 2010)

Modern nanotechnology allows one to scale down various important devices (sensors, chips, fibers, etc.) and thus opens up new horizons for their applications. The efficiency of most of them is based on fundamental physical phenomena, such as transport of wave excitations and resonances. Short propagation distances make phase-coherent processes of waves important. Often the scattering of waves involves propagation along different paths and, as a consequence, results in interference phenomena, where constructive interference corresponds to resonant enhancement and destructive interference to resonant suppression of the transmission. Recently, a variety of experimental and theoretical work has revealed such patterns in different physical settings. The purpose of this review is to relate resonant scattering to Fano resonances, known from atomic physics. One of the main features of the Fano resonance is its asymmetric line profile. The asymmetry originates from a close coexistence of resonant transmission and resonant reflection and can be reduced to the interaction of a discrete (localized) state with a continuum of propagation modes. The basic concepts of Fano resonances are introduced, their geometrical and/or dynamical origin are explained, and theoretical and experimental studies of light propagation in photonic devices, charge transport through quantum dots, plasmon scattering in Josephson-junction networks, and matter-wave scattering in ultracold atom systems, among others are reviewed.

DOI: 10.1103/RevModPhys.82.2257 PACS number(s): 32.80.−t, 81.07.−b, 42.79.−e, 73.23.−b

CONTENTS

*aem124@physics.anu.edu.au

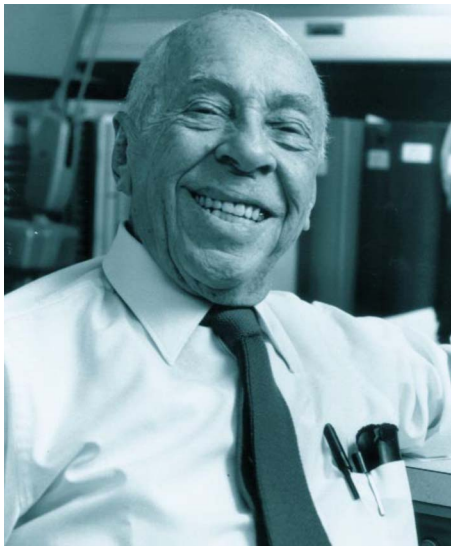

FIG. 1. (Color online) Ugo Fano (1912–2001). "Outstanding interpreter of how radiation interacts with atoms and cells" (Clark, 2001) and much more (this review).

I. HISTORICAL REMARKS

One of the important diagnostic tools in physics is scattering of radiation (waves) by matter. It allows us to investigate properties of matter and to control the radiation. For example, Rydberg spectral lines (1888) of the hydrogen atom allowed Niels Bohr to deduce his model of an atom (1913), which laid the basis of quantum mechanics. Later, Beutler (1935) observed that some of the Rydberg spectral atomic lines exhibit sharp asymmetric profiles in absorption. It was Ugo Fano (1935) (Fig. 1) who suggested the first theoretical explanation of this effect and suggested a formula (also known as the Beutler-Fano formula) that predicts the shape of spectral lines based on a superposition principle from quantum mechanics. The complexity of the physical phenomena was encapsulated in a few key parameters, which made this formula a workhorse in many fields of physics, including nuclear, atomic, molecular, and condensed-matter physics. According to Fano (1977): "the Beutler spectra showed unusual intensity profiles which struck me as reflecting interference between alternative mechanisms of excitation." The interpretation provided by Fano of these "strange-looking shapes" of spectral absorption lines is based on the interaction of a discrete excited state of an atom with a continuum sharing the same energy level, which results in interference phenomena. The first paper with a derivation of the line-shape formula (Fano, 1935) was published in 1935 when Fano was a young postdoctoral fellow in the group of Enrico Fermi. Fano has acknowledged the influence of his teacher on the derivation of this key result. The second, much more elaborated, paper (Fano, 1961) became one of the most important publications in the physics of the 20th century rated among the first three most relevant works published in *Physical Review* (Redner, 2004), with over 5700 citations by now (July 2010). "The paper appears to owe its success to accidental circumstances, such as the timing of its publication and some successful features of its formulation. The timing coincided with a rapid expansion of atomic and condensed matter spectroscopy, both optical and collisional. The formulation drew attention to the generality of the ingredients of the phenomena under consideration. In fact, however, the paper was a rehash of work done 25 years earlier" (Fano, 1977; Vittorini-Orgeas and Bianconi, 2009). In his pioneering papers, Fano introduced an important new ingredient of matter-radiation interaction in atomic physics, making him a key player in 20th-century physics. This was also acknowledged by the Fermi Award in 1995 for "his seemingly formal use of fundamental theory" leading to "the underpinning of a vast variety of practical results which developed naturally from this understanding."

Remarkably, the first observation of the asymmetric line shapes can be traced back to the discovery made by Wood in 1902, namely, the presence of unexpected narrow bright and dark bands in the spectrum of an optical reflection grating illuminated by a light source with slowly varying wavelength (Wood, 1902). Wood was astounded to see that under special illumination conditions the grating efficiency in a given order dropped from maximum to minimum illumination, within a wavelength range not greater than the distance between the sodium lines. These rapid variations in intensities of the various diffracted spectral orders in certain narrow frequency bands were termed *anomalies* since the effects could not be explained by the conventional grating theory (Wood, 1935). The first theoretical treatment of these anomalies is due to Lord Rayleigh (1907). His "dynamical theory of the grating" was based on an expansion of the scattered electromagnetic field in terms of outgoing waves only. This theory correctly predicted the wavelengths (Rayleigh wavelengths) at which anomalies occurred. However, one of the limitations of Rayleigh's approach is that it yields a singularity at the Rayleigh wavelength and, therefore, does not give the shape of the bands associated with the anomaly. Fano tried to overcome this difficulty in a series of papers (Fano, 1936, 1937, 1938, 1941) by assuming a grating consisting of lossy dielectric material and suggesting that anomalies could be associated with the excitation of a surface wave along the grating. The resonant excitation of leaky surface waves near the grating, which occurs when a suitable phase matching between the incident plane wave and the guided wave is satisfied, leads to a strong enhancement of the field near the grating surface (Hessel and Oliner, 1965; Sarrazin *et al.*, 2003; de Abajo, 2007). As pointed out by Sarrazin *et al.* (2003), the observed asymmetric profiles can be fitted by the Fano formula with good accuracy. Thus, the interaction of excited leaky modes with incoming radiation leads to similar interference phenomena as in absorption by Rydberg atoms, where a leaky mode can be associated with a discrete state and the incoming radiation with a continuum. These examples reveal the universality of Fano's approach in describing the origin of asymmetric line

shapes in terms of interference phenomena, regardless of the nature of the constituting waves, as well as in predicting both the position and the width of the resonance.

Similar asymmetric profiles were observed in various other systems and settings. But sometimes it is not obvious to determine the origin of the interference. In the present review, we provide a general explanation of the appearance of the Fano resonances in various physical systems based on a simple model, which sheds light on the origin of the interference phenomena, and is well along the lines of Steven Weinberg: "our job in physics is to see things simply, to understand many complicated phenomena in a unified way, in terms of a few simple principles" (1979 Nobel Prize lecture). The aim of this review is to demonstrate that the concept of the Fano resonance can be applied to control transport and scattering properties of waves in nanoscale devices.

II. THE FANO RESONANCE

We start from a description of systems where the Fano resonance is typically observed. It will allow us to demonstrate its basic properties and necessary conditions, which will be covered in more detail below.

A. Two oscillators with a driving force

Usually, a resonance is thought to be an enhancement of the response of a system to an external excitation at a particular frequency. It is referred to as the resonant frequency or natural frequency of the system. In many classical textbooks a resonance is introduced by the means of a harmonic oscillator with periodic forcing. When the frequency of the driving force is close to the eigenfrequency of the oscillator, the amplitude of the latter is growing toward its maximal value. Often many physical systems may also exhibit the opposite phenomenon when their response is suppressed if some resonance condition is met (which has, even lead to the term *antiresonance*). The simplest example can be illustrated using two weakly coupled harmonic oscillators, where one of them is driven by a periodic force [see Fig. 2(a)]. In such a system, in general, there are two resonances located close to the eigenfrequencies ω_1 and ω_2 of the oscillators (Joe *et al.*, 2006). One of the resonances of the forced oscillator demonstrates the standard enhancement of the amplitude near its eigenfrequency ω_-, while in correspondence with the resonance ω_+ we see an unusual sharp peak in the amplitude [see Figs. 2(b) and 2(c)]. The first resonance is characterized by a symmetric profile, described by a Lorentzian function and known as a Breit-Wigner resonance (Breit and Wigner, 1936). The second resonance is characterized by an asymmetric profile. It exhibits total suppression of the amplitude of the forced oscillator at the eigenfrequency of the second oscillator ω_2. The amplitude of the first oscillator becomes zero as a result of destructive interference of oscillations from the external force and the second oscillator. Indeed, it is known that the phase of the single

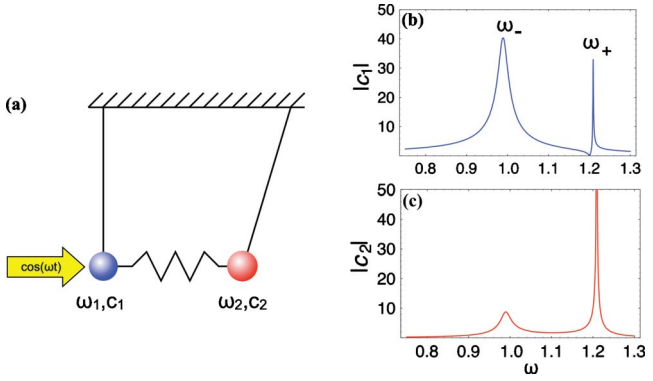

FIG. 2. (Color online) Resonances of parametrically driven coupled oscillators. (a) Schematic view of two coupled damped oscillators with a driving force applied to one of them; (b) the resonant dependence of the amplitude of the forced oscillator $|c_1|$, and (c) the coupled one $|c_2|$. There are two resonances in the system. The forced oscillator exhibits resonances with symmetric and asymmetric profiles near the eigenfrequencies $\omega_1 = 1$ and $\omega_2 = 1.2$ (b), respectively. The second coupled oscillator responds only with symmetric resonant profiles (c). Adapted from Joe *et al.*, 2006.

forced oscillator exhibits a π jump at the resonance, meaning that below the resonance the oscillator is in phase with the driving force, and it becomes out of phase above the resonance (Joe *et al.*, 2006). In the case of two coupled oscillators at the resonance of the second oscillator there are effectively two driving forces acting on the first oscillator, which are out of phase and cancel each other. This example demonstrates one of the basic properties of the Fano resonance, namely, resonant destructive interference, which makes it unique among other resonances.

B. Light and atoms

The resonances with asymmetric line shape were first described by Fano (1935, 1961) when he was attracted by unusual sharp peaks in the absorption spectra of noble gases observed by Beutler (1935). The nature of the asymmetry was established with the theory of configuration by Fano (1961). The photoionization of an atom can proceed in various ways (Fig. 3). The first, straightforward one, is the excitation of the inner-shell electron above the ionization threshold $A+\hbar\nu \rightarrow A^+ + e$. Another possibility is to excite the atom into some quasidiscrete level, which can spontaneously ionize by ejecting an electron into the continuum, $A+\hbar\nu \rightarrow A^* \rightarrow A^+ + e$. Such levels were said to be autoionizing, after Jevons and Shenstone (1938). In other words, the autoionized state is a bound state of an atom with energy above the first ionizing threshold. Autoionization is one of the most fundamental electron-electron correlation phenomena, and it is forbidden in the noninteracting-particle approximation (Connerade, 1998). One of the possible autoionized states follows from the excitation of two electrons by one photon when the excitation energies of each electron are of the same order of magnitude and

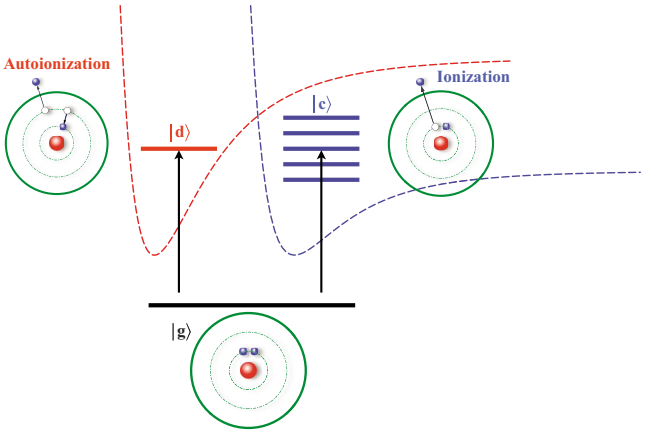

FIG. 3. (Color online) Fano resonance as a quantum interference of two processes: direct ionization of a deep inner-shell electron and autoionization of two excited electrons followed by the Auger effect. This process can be represented as a transition from the ground state of an atom $|g\rangle$ either to a discrete excited autoionizing state $|d\rangle$ or to a continuum $|c\rangle$. Dashed lines indicate double excitations and ionization potentials.

the total excitation energy exceeds the atom ionization threshold. The interaction between electrons leads to the decay of this state when one electron transfers into a lower state and the second electron is ejected into the continuum, using the energy of the relaxed electron. In spectroscopy, this process is known as the Auger effect (Auger, 1925a, 1925b, 1926). Different types of other autoionizing states are described by Smirnov (2003). In general, autoionization can be considered as a mechanism that couples bound states of one channel with continuum states of another. Because of the superposition principle of quantum mechanics, whenever two states are coupled by different paths, interference may occur.

Fano used a perturbation approach to explain the appearance of asymmetric resonances. He considered a so-called prediagonalized state by putting the coupling between discrete bound states, which is degenerate in energy with a continuum of states, to zero. Such a prediagonalized state may or may not have a clear physical analogy but serves in any case as a convenient mathematical construction, which allows us to solve the problem. As a result, Fano obtained the formula for the shape of the resonance profile (Fano, 1935, 1961) of a scattering cross section:

$$\sigma = \frac{(\epsilon + q)^2}{\epsilon^2 + 1}, \tag{1}$$

using a phenomenological shape parameter q and a reduced energy ϵ defined by $2(E-E_F)/\Gamma$. E_F is a resonant energy and Γ is the width of the autoionized state. Equation (1) suggests that there are exactly one maximum and one minimum in the Fano profile,

$$\sigma_{\min} = 0 \quad \text{at } \epsilon = -q, \tag{2}$$

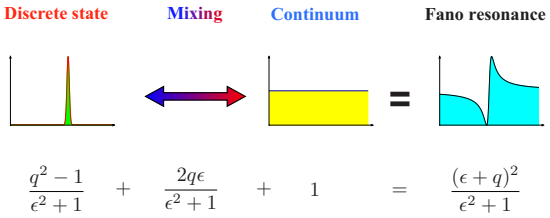

FIG. 4. (Color online) Illustration of the Fano formula (1) as a superposition of the Lorentzian line shape of the discrete level with a flat continuous background.

$$\sigma_{\max} = 1 + q^2 \quad \text{at } \epsilon = 1/q.$$

In his original paper, Fano (1961) introduced the asymmetry parameter q as a ratio of the transition probabilities to the mixed state and to the continuum (Fig. 4). In the limit $|q| \to \infty$, the transition to the continuum is very weak, and the line shape is entirely determined by the transition through the discrete state only with the standard Lorentzian profile of a Breit-Wigner resonance. When the asymmetry parameter q is of the order of unity, both the continuum and discrete transitions are of the same strength, resulting in the asymmetric profile [Eq. (1)], with the maximum value at $E_{\max} = E_F + \Gamma/(2q)$ and minimum at $E_{\min} = E_F - \Gamma q/2$. The case of zero asymmetry parameter $q=0$ is unique to the Fano resonance and describes a symmetrical dip, sometimes called an antiresonance (see Fig. 5). The main feature of the Fano resonance is the possibility of destructive interference, leading to asymmetric line shapes (Piao *et al.*, 1990; Nockel and Stone, 1994; Lee and Kim, 2000a; Bianconi, 2003; Bandopadhyay *et al.*, 2004; Rau, 2004). The actual resonant frequency of the discrete level E_F may lie somewhere between the maximum and the minimum of the asymmetric profile, and the parameter q defines the relative deviation. In the situation $|q| \to \infty$, the resonant frequency coincides with the maximum of the profile, while in the case $q=0$ the resonant frequency coincides with the minimum. For $q=1$ it is located exactly at half the distance between the minimum and maximum (see Fig. 5).

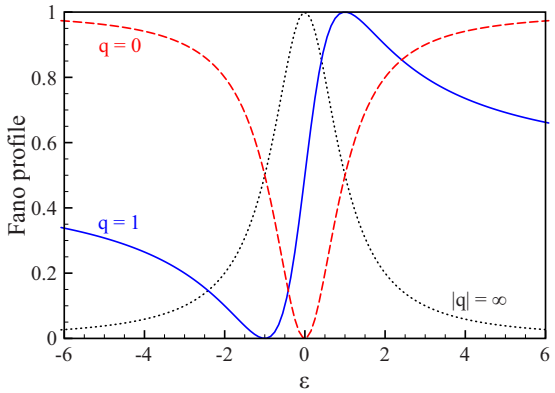

FIG. 5. (Color online) Normalized Fano profiles (1) with the prefactor $1/(1+q^2)$ (2) for various values of the asymmetry parameter q.

Because of recent advances in the generation of ultrashort attosecond pulses, Wickenhauser *et al.* (2005) theoretically investigated the possibility of observing the buildup of Fano resonances in time using attosecond streaking techniques. Excitation by an ultrashort pump pulse opens two interfering paths from the ground state to the continuum, which are then studied by a weak probe pulse. After the characteristic time of the autoionizing level, the transient coupling to the resonant state starts to "burn a hole" in the energy distribution of the initial Gaussian. This method may become useful in determining both coherent and incoherent pathways to ionization.

The Fano formula (1) was successfully used to fit and explain various experimental data (Simpson and Fano, 1963; Fano, 1964, 1965; Fano and Cooper, 1965, 1968; Heinzmann *et al.*, 1970; Kessler and Lorenz, 1970; Fano and Lee, 1973; Smith *et al.*, 1973; Ramaker and Schrader, 1974; Bandrauk and Laplante, 1976; Kleinpoppen and McDowell, 1976; Davis and Feldkamp, 1977; Druger, 1977; Armstrong *et al.*, 1978; Dixit and Lambropoulos, 1979; Feneuille *et al.*, 1979; Heller and Mukamel, 1979; Yafet, 1981; Ganz *et al.*, 1984; Ley *et al.*, 1984; Harmin, 1985; Janzen *et al.*, 1985; Oliveira and Wilkins, 1985; Becker *et al.*, 1986; Syage and Wessel, 1987; Ueda, 1987; Meijerink and Blasse, 1989; Nussenzweig *et al.*, 1990; Chergui *et al.*, 1991; Winstead and Langhoff, 1991; Maeda *et al.*, 1992; Sturm *et al.*, 1992; Taylor and Johnson, 1993; Nockel and Stone, 1994; Roney, 1994a, 1994b, 1995; Sanchez and Martin, 1994; dell'Orto *et al.*, 1995; Siegner *et al.*, 1995; Simonian *et al.*, 1995; Aoki *et al.*, 1996; Bar-Ad *et al.*, 1997; Waligorski *et al.*, 1997; Lee, 1998; Mehlhorn, 1998; Patthey *et al.*, 1999; Pichl *et al.*, 2000; Marinho *et al.*, 2001; Glutsch, 2002; Kokoouline *et al.*, 2002; Bortchagovsky and Fischer, 2003; Eichmann *et al.*, 2003; Bandopadhyay *et al.*, 2004; Margulis and Pyataev, 2004; Kolorenc *et al.*, 2005; Wickenhauser *et al.*, 2005; Hase *et al.*, 2006; Xu and Xiong, 2006; Fransson and Balatsky, 2007), thus revealing the underlying mechanism of the observed resonances in terms of quantum-mechanical interaction between discrete and continuous states. In nuclear and atomic physics, interferences often originate from the interaction of open (continuum) and closed (discrete-level) channels (Feshbach, 1958, 1962). Bhatia and Temkin (1984) unified the approaches of Fano and Feshbach with *ab initio* calculations and derived a rigorous expression for the asymmetry parameter q (Bhatia and Temkin, 1984).

There are certain limitations to the applicability of the Fano formula (1) (Connerade, 1998). First, it can be applied to describe only single isolated resonances. The appearance of more than two propagation paths will change the profiles. Second, the width of the discrete level should be narrow compared to other resonant structures in the scattering profile.

In general, the Coulomb interaction between an outgoing electron e^- and a charged ion core A^+ during autoionization leads to a renormalization of the energy levels of the many-electron system. Such a renormalization is known as the quantum defect of the Rydberg series. To precisely describe the positions and width of the resonances, a multichannel quantum-defect theory was developed by Seaton (1966) and Fano (1970), which provides a rigorous description of the process. It allows us to derive all asymptotic quantities such as phase shifts or amplitudes of the autoionized levels. Equation (1) was derived by Fano by neglecting effects due to long-range Coulomb interaction. Still, it provides a physical insight into the autoionization process in terms of quantum-mechanical interference of discrete and continuum states.

At the resonance the phase of the scattering wave changes sharply by π. Thus, the interaction of scattering waves will result in constructive and destructive interference phenomena located very close to each other, corresponding to a maximum $E_{\max}$ and a minimum $E_{\min}$ of the transmission and absorption, respectively. The width of the resonance is proportional to the distance between them, $\Gamma \sim |E_{\max} - E_{\min}|$. In principle, they may be located close to each other $E_{\max} \approx E_{\min}$, resulting in a very narrow resonance $\Gamma \approx 0$, corresponding to a long-lived quasibound state (Stillinger and Herrick, 1975). Using artificial one-dimensional potentials, one can even achieve $\Gamma = 0$ (von Neumann and Wigner, 1929), as a proof of concept. By applying Feshbach's theory of resonances to two overlapping Fano resonances, Friedrich and Wintgen (1985a, 1985b) demonstrated that the interference of several autoionization levels of a Rydberg atom may lead to the formation of bound states in the continuum with anomalously narrow resonances.

C. Light and structured matter

Experiments on the absorption cross section of a single quantum dot, which is often considered as an artificial atom, revealed that the asymmetry parameter q can be continuously tuned with the power of the laser (Kroner *et al.*, 2008). In this system, the transition rate to the discrete level saturates at high power, while with increasing laser power, the rate of the continuum transition does not (Zhang *et al.*, 2006). Eventually, the initially weak continuum transition rate will match the saturated transition rate to the discrete level. As a result, a symmetric Lorentzian profile at low power will transform to an asymmetric Fano profile at sufficiently large power (see Fig. 6).

While probing bound-state formation in quantum point contacts, the detector conductance exhibits a well-defined Fano resonance, whose asymmetry can be changed by contact separation (Yoon *et al.*, 2009). This effect became known as detector backaction in quantum-mechanical measurement, because there is wave-function overlap between the bound state and the detector. This interaction, however, can be controlled with the use of additional gates (Yoon *et al.*, 2009). This approach may become important in quantum computing during qubit manipulation processes (Mourokh *et al.*, 2005).

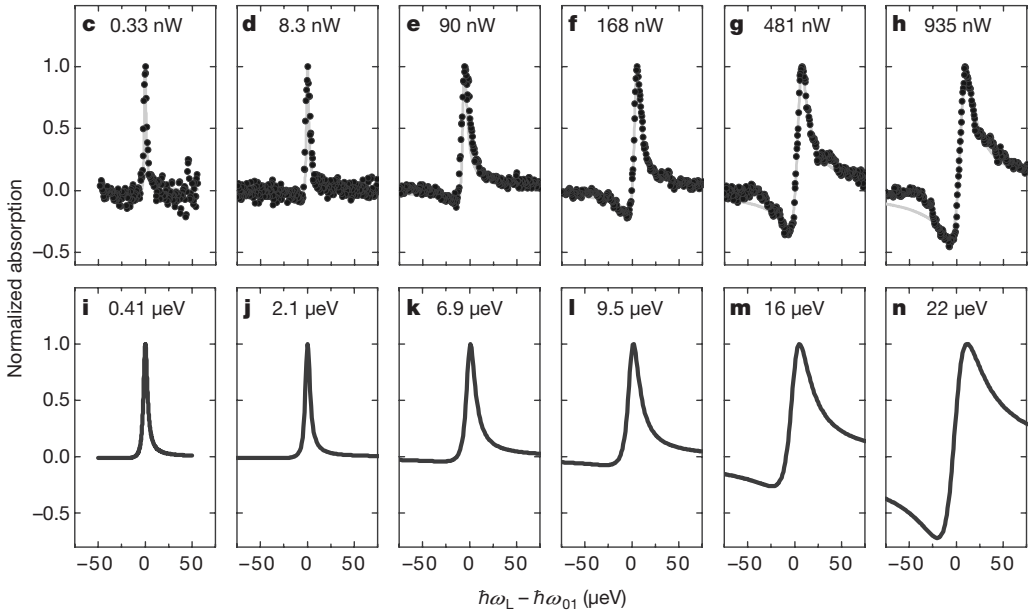

FIG. 6. Tuning of the asymmetry parameter of the Fano resonance. Measured (upper row) and calculated (bottom row) absorption spectra of a single quantum dot for various laser powers. The absorption profile varies from a symmetrical to an asymmetrical one with increase of the laser power, indicating the enhancement of the continuum transition. From Kroner *et al.*, 2008.

In biased semiconductor superlattices, the Fano coupling parameter Γ between the discrete state and the continuum can be continuously tuned by variation of the applied electric field (Holfeld *et al.*, 1998). The external bias gives rise to Wannier-Stark states, which interact with excitons and result in asymmetric absorption spectra of the Wannier-Stark transitions (Hino and Toshima, 2005; Xu and Xiong, 2006). The external bias determines the energy spacing of a Wannier-Stark subband and thus controls the effective coupling between the discrete states and the continua. It allows us to study the dephasing dynamics of the Fano resonance.

In general, the asymmetry parameter q is not restricted to be only real (Kobayashi *et al.*, 2003). In systems with broken time-reversal symmetry, transition amplitudes to the discrete level and to the continuum may become complex, as does the asymmetry parameter. The Fano resonance in such systems can be studied by analyzing the dynamical response. In particular, Misochko *et al.* (2005) found that the time-dependent reflection of light by a bismuth single crystal after excitation by an ultrashort laser pulse exhibits Fano asymmetric profiles in the Fourier transform of a time-periodic signal. They demonstrated that the asymmetric parameter varies periodically with the time delay between pump and probe pulses. The breaking of time-reversal symmetry is indicated by a change in the sign of the asymmetry parameter. Moreover, Bärnthaler *et al.* (2010) suggested using the complex q parameter as a probe of decoherence in wave transport either via dissipation or dephasing. The parameter variation of Fano resonances and the degree of decoherence was implemented in transport through microwave billiards (Rotter *et al.*, 2004).

Asymmetric line shapes were also observed in Raman spectra of heavily doped semiconductors (Hopfield *et al.*, 1967; Bell *et al.*, 1973; Cerdeira *et al.*, 1973a; Bechstedt and Peuker, 1975; Chandrasekhar *et al.*, 1978; Magidson and Beserman, 2002) and high-T_c superconductors (Friedl *et al.*, 1990; Limonov *et al.*, 1998, 2000; Misochko *et al.*, 2000). Although almost any asymmetric profile of these spectra can be fitted by the Fano formula (Cerdeira *et al.*, 1973b; Cardona *et al.*, 1974; Cardona, 1983; Menéndez and Cardona, 1985; Belitsky *et al.*, 1997; Jin *et al.*, 2001; Hase *et al.*, 2006; Lee *et al.*, 2006; Aleshkin *et al.*, 2007; Jin and Xu, 2007), a suitable theory for a quantitative description of these cases is still lacking. The general qualitative understanding is that the absorbed photon can initiate two kinds of processes. The first one is the interband or intraband electronic transition from the ground state to the continuum. The second process is the transition to an intermediate state followed by a one-phonon Raman emission and electron transition to either the initial ground state or the excited donor state. Thus, the interference of two processes may in principle result in Fano resonance.

D. Atoms and atoms

When two atoms collide with each other, a quasibound state can be formed, which is characterized by a complex energy $E=E_F+i\Gamma$. In scattering theory this quasibound state is called a resonance since it possesses a finite lifetime $\hbar/\Gamma$. The quasibound state is formed due to the excitation and sharing of electrons and can be interpreted as an interaction between discrete and continuous states (see Fig. 3). In a similar manner, the observed asymmetric resonances in predissociation (Bandrauk and Laplante, 1976; Cotting *et al.*, 1994; Lewis *et al.*, 2001; Lebech *et al.*, 2006; Palffy *et al.*, 2007) (or frag-

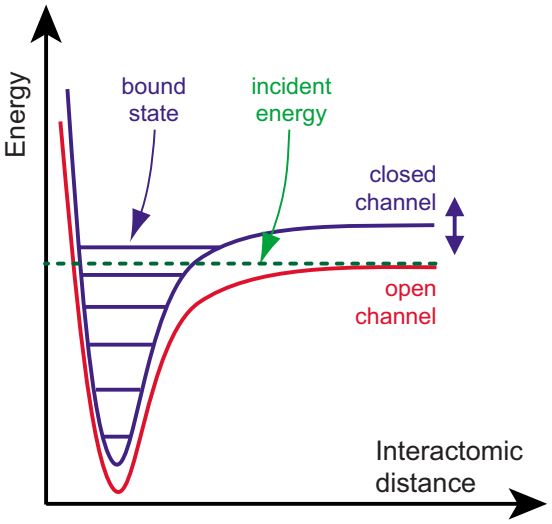

FIG. 7. (Color online) Two-channel model for a Feshbach resonance. Atoms that are prepared in the open channel undergo a collision at low incident energy. In the course of the collision, the open channel is coupled to the closed channel. When a bound state of the closed channel has energy close to zero, a scattering resonance occurs. From Bloch *et al.*, 2008.

mentation) of molecules were explained by Rice (1933) in terms of autoionization. The concept was introduced by Feshbach (1958) in the context of reactions forming a compound nucleus. A Feshbach resonance in a two-particle collision appears whenever a bound state in a closed channel is coupled resonantly with a scattering continuum of an open channel (Bloch *et al.*, 2008). The scattered particles are temporarily captured in the quasibound state, and the associated long time delay gives rise to a Breit-Wigner-type resonance in the scattering cross section (see Fig. 7).

A recent series of studies was devoted to the explicit calculation of scattering states for one-dimensional chains with two interacting bosons or fermions (Grupp *et al.*, 2007; Nygaard *et al.*, 2008a, 2008b; Valiente and Petrosyan, 2009). These systems allowed for two-particle continuum states but also for bound states of two particles. By tuning of the Bloch wave number, the bound state dissolves into the two-particle continuum. However, its trace inside the continuum remains, leading to a π phase shift of the scattering phase and to corresponding Fano or Feshbach resonances in the scattering length. Notably in these problems a clear notion of resonant transport is absent since there is no difference between a probe beam and a target owing to indistinguishability of the two particles.

Efimov predicted that a three-body quantum system can support weakly bound states (trimers) under conditions when none of the three constituent pairs are bound (Efimov, 1970, 1971). Efimov trimer states appear in the limit where the two-body interaction is too weak to support a two-body bound state (dimer). Such trimer states should exist regardless of the nature of the two-body interaction and thus are generic in few-body systems. Recently, the first experimental observation of Efimov states has been reported in ultracold cesium trimers (Kraemer *et al.*, 2006) by measurement of the three-body recombination process $Cs+Cs+Cs \rightarrow Cs_2+Cs$. The fingerprint of Efimov trimers in this system appears as a resonant enhancement and suppression of three-body collisions as a function of the two-atom interaction strength (Esry and Greene, 2006; Kraemer *et al.*, 2006) with typical asymmetric profiles. Mazumdar *et al.* (2006) explained this asymmetric response in terms of a Fano resonance, suggesting that the asymmetry can be used as a diagnostic tool for the Efimov effect.

Despite the complexity of the original system where the Fano resonance was first observed, the phenomenon turned out to be a universal phenomenon in wave propagation and interference, observed in various physical systems. It is for these reasons that the Fano resonance can be equally observed in the transport of waves described by classical or quantum-mechanical processes.

III. MODELING: COMPLEX GEOMETRIES

One possibility to model a Fano resonance is to choose the geometry of a given system in such a way that at least two scattering paths are available. In this section we consider the basic geometries that do the job and discuss several extensions.

A. Fano-Anderson model

One of the simplest models that describes the physics and the main features of the Fano resonance is the Fano-Anderson model (Mahan, 1993), which mimics the energy level structures (see Fig. 3) of the model proposed by Fano (1961). In a simplified version (Miroshnichenko, Mingaleev, *et al.*, 2005) it can be described by the following Hamiltonian, which can be treated in a classical way:

$$H = C\sum_n (\phi_n \phi_{n-1}^* + \text{c.c.}) + E_F|\psi|^2 + V_F(\psi^* \phi_0 + \text{c.c.}), \tag{3}$$

where the asterisk denotes complex conjugation. This model describes the interaction of two subsystems. One subsystem is a linear discrete chain with the complex field amplitude ϕ_n at site n and nearest-neighbor coupling with strength C. This system supports propagation of plane waves with dispersion $\omega_k = 2C \cos k$. The second subsystem consists of a single Fano state ψ with energy E_F. The interaction between these two subsystems is given by the coupling coefficient V_F between the state ψ and one site of the discrete chain ϕ_0. A propagating wave may directly pass through the chain or instead visit the Fano state, return back, and continue with propagation. These two paths are the ingredients of the Fano resonance.

The lattice Hamiltonian (3) generates the following differential equations:

$$i\dot{\phi}_n = C(\phi_{n-1} + \phi_{n+1}) + V_F\psi\delta_{n0},$$
$$i\dot{\psi} = E_F\psi + V_F\phi_0. \tag{4}$$

With the ansatz

$$\phi_n(\tau) = A_n e^{-i\omega\tau}, \quad \psi(\tau) = Be^{-i\omega\tau}, \tag{5}$$

we obtain a set of algebraic equations for the amplitudes:

$$\omega A_n = C(A_{n-1} + A_{n+1}) + V_F B\delta_{n0},$$
$$\omega B = E_F B + V_F A_0. \tag{6}$$

For a scattering problem, the system Eq. (6) should be solved for frequencies chosen from the propagation band $\omega=\omega_k$ with the following boundary conditions:

$$A_n = \begin{cases} Ie^{ikn} + \rho e^{-ikn}, & n<0, \\ \tau e^{ikn}, & n>0, \end{cases} \tag{7}$$

where I, r, and t represent the incoming, reflected, and transmitted wave amplitudes, respectively.

From Eq. (6) it follows that

$$B = \frac{V_F A_0}{\omega_k - E_F} \tag{8}$$

and finally

$$\omega_k A_n = C(A_{n-1} + A_{n+1}) + \frac{V_F^2}{\omega_k - E_F} A_0\delta_{n0}. \tag{9}$$

The main resulting action of the Fano state is that the strength of the effective scattering potential $V_F^2/(\omega_k - E_F)$ resonantly depends on the frequency of the incoming wave ω_k. If E_F lies inside the propagation band of the linear chain $|E_F|<2C$, the scattering potential will become infinitely large for $\omega_{k_F}=E_F$, completely blocking propagation. Therefore meeting the resonance condition leads to a resonant suppression of the transmission, which is the main feature of the Fano resonance.

The transmission coefficient $T=|\tau/I|^2$ can be computed using the transfer matrix approach (Tong *et al.*, 1999) and expressed in the following form (Miroshnichenko, Mingaleev, *et al.*, 2005):

$$T = \frac{\alpha_k^2}{\alpha_k^2 + 1}, \tag{10}$$

where

$$\alpha_k = c_k(E_F - \omega_k)/V_F^2, \quad c_k = 2C\sin k. \tag{11}$$

Transmission vanishes at $\omega_k=E_F$. The expression for the transmission coefficient [Eq. (10)] corresponds to the Fano formula (1) with $q=0$, where α_k corresponds to the dimensionless energy and E_F is the resonant frequency. The Fano state is an additional degree of freedom which allows waves propagating in the chain to interfere with those propagating through the discrete state.

The width of the resonance is defined as

$$\Gamma = \frac{V_F^2}{C\sin k_F}, \tag{12}$$

where k_F is the wave number at the resonance $E_F=\omega_{k_F}$. The width of the resonance is proportional to the square of the coupling strength V_F^2.

The Fano-Anderson model [Eq. (3)] is perhaps the simplest one-dimensional model that shows up with a Fano resonance. Since its asymmetry parameter $q=0$, the location of the maximum in the Fano profile is tuned to infinity. The essence of the Fano resonance (destructive interference) is therefore not encapsulated in an asymmetric scattering profile with both a maximum and a minimum. It is the minimum that is generated by interference along several propagation paths. Because of its analytical simplicity the model may serve as a guideline for the analysis of more complicated physical models. There are many variations of this model (Burioni *et al.*, 2005, 2006; Miroshnichenko and Kivshar, 2005a; Chakrabarti, 2006) studied recently.

B. Tuning the asymmetry parameter

The Fano-Anderson model [Eq. (3)] describes the resonant suppression of the transmission with a symmetric line shape ($q=0$), emphasizing the main property of the Fano resonance, which is destructive interference (resonant reflection). It can be easily extended in order to obtain a nonzero asymmetry parameter q with asymmetric line shapes, such that both resonant suppression and resonant enhancement of the transmission will be located close to each other. When a defect $E_L\phi_L\delta_{nL}$ is introduced in the main array [Eq. (4)] [see Fig. 8(a)], both paths for scattering waves will yield phase shifts. As a result, both constructive and destructive interference phenomena may coexist, generating asymmetric transmission profiles [see Fig. 8(b)]. As shown in Fig. 8(b), the sign of the asymmetry parameter q alternates with increasing distance between the side-coupled defect and the defect in the main array [which is known as q reversal (Kim and Yoshihara, 1993)];

$$\mathrm{sgn}(\omega_{T_{\max}} - \omega_{T_{\min}}) = (-1)^L. \tag{13}$$

Note that the maximum of the transmission does not need to reach the value $T=1$. This incomplete constructive interference is due to additional phase accumulation along the propagation distance between two defects. It does not affect the destructive interference, at which strictly $T=0$, confirming that $T=0$ is the only necessary and sufficient result of destructive interference and the Fano resonance.

C. Many resonances

Consider now a replacement of the Fano site in the Fano-Anderson model by a finite chainlet, consisting of N coupled sites (Burioni *et al.*, 2005; Miroshnichenko and Kivshar, 2005a); see Fig. 8(c). If the chainlet is decoupled from the linear discrete chain, the standing

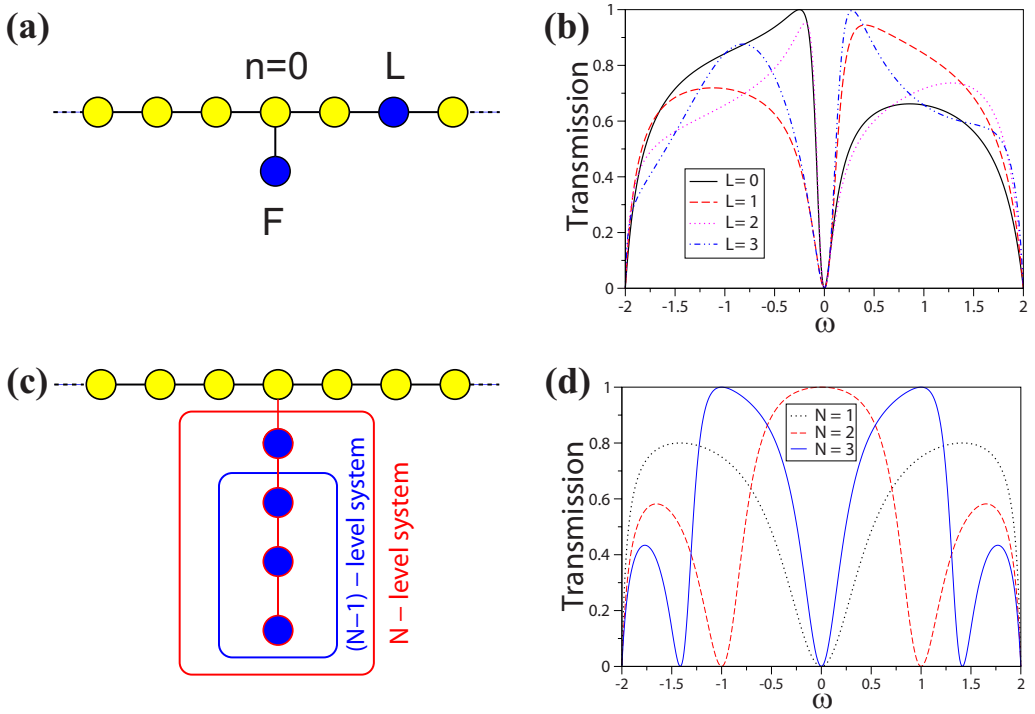

FIG. 8. (Color online) Variations in the Fano-Anderson model. (a) Schematic view of the Fano-Anderson model with an additional defect in the chain. (b) Transmission coefficient for different distances between the Fano site and the additional defect for parameters $C=1$, $V_F=0.5$, $E_F=0$, and $E_L=1$. (c) Schematic view of the Fano-Anderson model with a locally coupled N-defect chainlet. (d) Transmission coefficient of the N-site chainlet model. All sites in the chainlet are identical and with zero eigenfrequencies $E_m=0$, and the couplings are $C=V_m=1$. Adapted from Miroshnichenko and Kivshar, 2005a.

waves of the chainlet will give rise to N eigenfrequencies. Once the chainlet is coupled back to the linear discrete chain, each of the standing waves will provide an additional path for a propagating wave, leading to a variety of interference phenomena. The finite chainlet could be considered as an approximation of a complex N-level system, such as a quantum dot, for example. Miroshnichenko and Kivshar (2005a) showed that, in general, there are exactly N total reflection ($T=0$) and $N-1$ total transmission ($T=1$) resonances [see Fig. 8(d)]. Each frequency of the total reflection corresponds to an eigenfrequency of the chainlet standing wave, and each total transmission corresponds to an eigenfrequency of the chainlet with $N-1$ sites, shown in Fig. 8(c). At resonances, some particular eigenstates of the side-coupled chainlet are excited.

Many other inhomogeneous networks have been considered in design of various topological filters (Burioni *et al.*, 2005, 2006). One can even plant Cayley trees into a discrete array and gather well-pronounced Fano resonances [see Fig. 9(a)].

D. Nonlinear Fano resonance

The Fano state amplitude becomes largest

$$|B_{\max}|^2 = 4V_F^2|I|^2/\Gamma^2 \tag{14}$$

exactly at the resonant value of the wave number k_F, and it diverges (and is therefore much larger than the amplitudes in the chain, which are bounded by I) in the limit of small coupling strength V_F.

Whatever the physical origin of the waves whose scattering is studied, large amplitudes call for corrections—either many-body interactions in a quantum setting or nonlinear response corrections in a classical setting. Notably, these corrections apply in first order only for the Fano state. Taking the classical setting, nonlinear Fano resonances (Miroshnichenko, Mingaleev, *et al.*, 2005) were studied by introducing nonlinear corrections to the evolution equation for the Fano state only [Eq. (6)],

$$\omega B = E_F B + \lambda|B|^2 B + V_F A_0. \tag{15}$$

The nonlinear transmission coefficient can be expressed in the following form (Miroshnichenko, Mingaleev, *et al.*, 2005):

$$T = \frac{x^2}{x^2+1}, \tag{16}$$

where $x=-\cot\delta(k)$ is a function of the scattering phase $\delta(k)$ and satisfies the cubic equation

$$(x^2+1)(x-\alpha_k) - \gamma_k = 0 \tag{17}$$

with the parameter $\gamma_k=\lambda c_k^3|I|^2/V_F^4$. The nonlinear Fano resonance condition corresponds to $x=0$ in Eq. (17), which needs the condition $\gamma_k=-\alpha_k$ to be satisfied [see Fig. 10(c)]. The transmission coefficient depends not only on the frequency of the incoming wave ω_k but on its intensity $|I|^2$ as well. The presence of nonlinearity

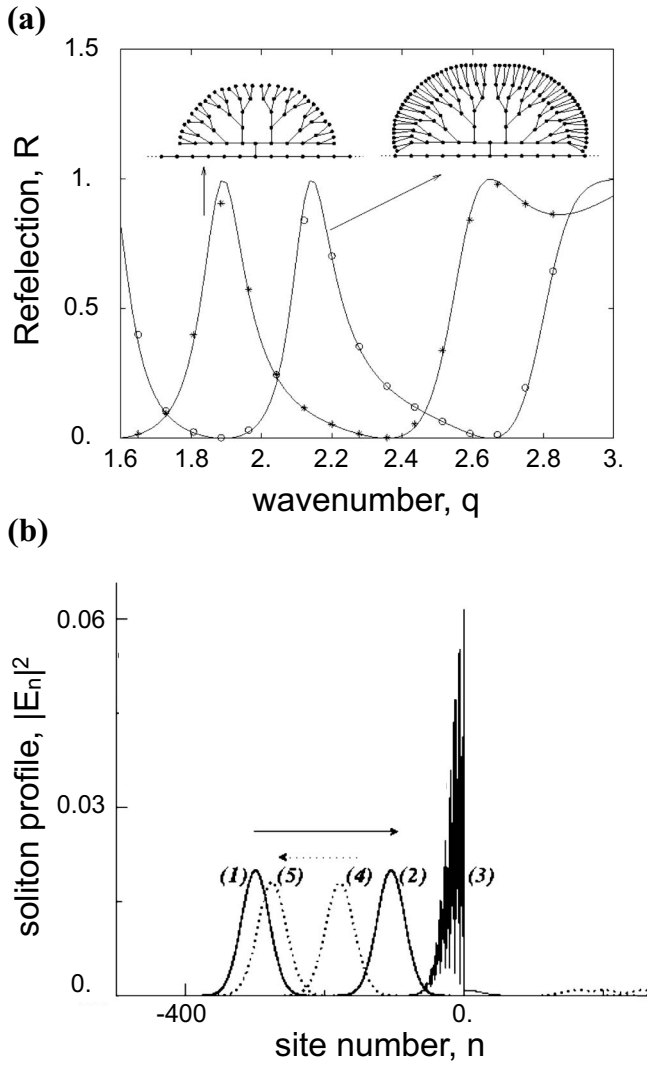

FIG. 9. Resonant reflection of a soliton in topological networks. (a) The reflection coefficient vs wave number k for two Cayley trees of length $M=5$ (line) and $M=6$ (line) attached to the discrete array. Empty circles and stars correspond to direct numerical simulations of the soliton propagation. (b) Example of the soliton reflection by a Fano-like defect. From Burioni *et al.*, 2005.

leads to a renormalization of the self-energy of the Fano state and consequently to an intensity-dependent shift of the resonance. Miroshnichenko, Mingaleev, *et al.* (2005) showed that the nonlinear Fano resonance exists for any value of the input intensity $|I|^2$ [see Fig. 10(c)]. Therefore, nonlinearity allows us to tune the location of the Fano resonance by changing the intensity of the input waves. In general, there exist up to three solutions of the cubic equation (17), which will result in bistable transmission [see Fig. 10(d)].

E. Resonant reflection of pulses and solitons

So far we have discussed the scattering of monochromatic plane waves. Consider a pulse instead, which is launched toward the scattering region. The narrower the pulse is in real space, the broader is its spectral decomposition in Fourier (plane-wave) space k, which is characterized by the maximum frequency ω_m and the spectral width $\Delta\omega$. Each pulse component in Fourier space k will scatter as discussed above. The spectral width $\Delta\omega$ has to be compared with the width of a Fano resonance Γ. If $\Delta\omega \ll \Gamma$, tuning ω_m into resonance with a Fano resonance will lead to an almost complete reflection of the pulse. If, on the contrary, $\Delta\omega \gg \Gamma$, only a narrow part of the spectral component of the pulse will be reflected, while the rest will be transmitted with a spectral hole "burned" into it.

If nonlinearities are added into the propagation channel, they lead to an interaction between the various plane waves constituting the pulse and may ultimately yield nondispersing solitons. Their scattering by Fano defects was studied as well (Miroshnichenko *et al.*, 2003; Burioni *et al.*, 2005, 2006; Wulf and Skalozub, 2005). There are two characteristic time scales important for the scattering of solitons. One of them is the time the soliton resides in the vicinity of the defect $\tau_{\rm rs}$, which is inversely proportional to its spectral width $\Delta\omega$ and the soliton velocity v. The second one is set by the nonlinearity. It is the time scale on which the plane waves that constitute the soliton interact with each other $\tau_{\rm int}$ (Miroshnichenko *et al.*, 2003). For fast-propagating solitons the residence time is much smaller than the interaction time $\tau_{\rm rs} \ll \tau_{\rm int}$. Then, during the scattering process the soliton can be considered as a set of noninteracting plane waves, and the above results of the pulse scattering apply (Miroshnichenko *et al.*, 2003; Burioni *et al.*, 2005, 2006); see Fig. 9(b). In the opposite case, when the residence time is much larger than the interaction time $\tau_{\rm rs} \gg \tau_{\rm int}$, the nonlinearity-induced mode-mode interaction becomes crucial during the scattering process. In general, a nonlinear interaction between many degrees of freedom (modes or plane waves) will lead to chaotic dynamics and consequently to a dephasing of individual plane waves. Therefore phase coherence will not be maintained during scattering, and interference effects will vanish. The Fano resonance should quickly deteriorate as the soliton parameters are tuned into the region of validity of the second case. This was numerically confirmed by Miroshnichenko *et al.* (2003).

F. Quadratic nonlinearities

Consider wave scattering in an array of channel waveguides with quadratic nonlinearity generated by periodic poling of several waveguides (Miroshnichenko, Kivshar, *et al.*, 2005). When the matching conditions are satisfied, the fundamental-frequency mode with frequency ω can parametrically generate a second-harmonic wave with frequency 2ω [see Fig. 11(a)], such that a structure with several poled waveguides may behave as a nonlinear defect with spatially confined quadratic nonlinearity (Iwanow *et al.*, 2004). The waveguide array can be described by a discrete model of weakly coupled linear waveguides with several waveguides having a quadratic nonlinear response (Iwanow *et al.*, 2004;

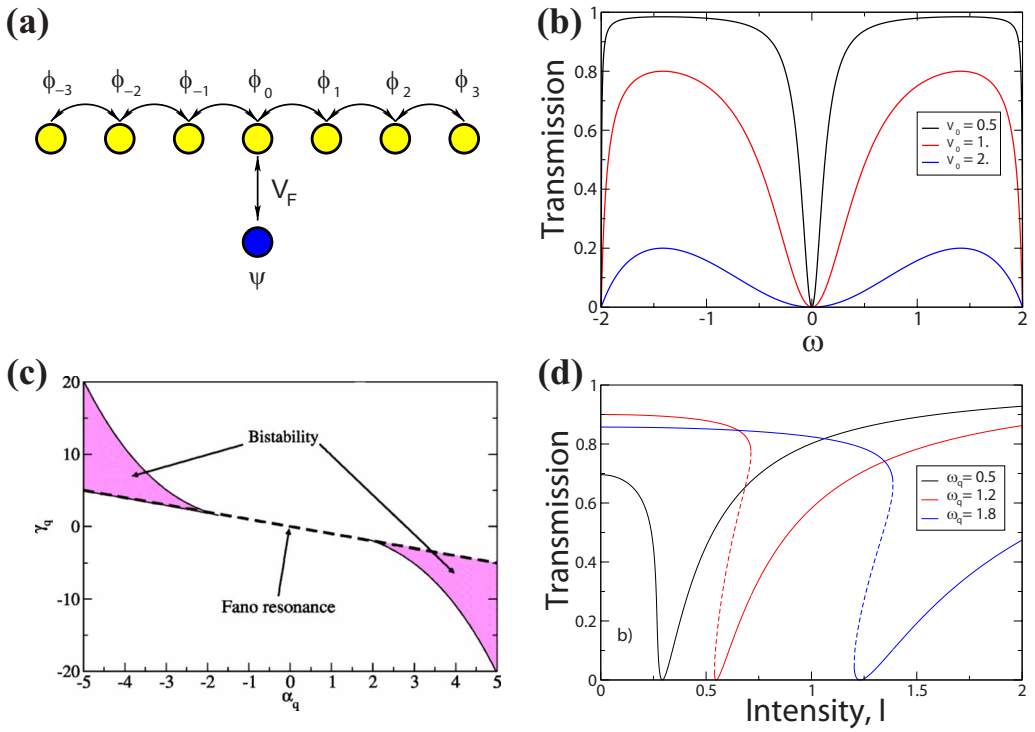

FIG. 10. (Color online) Fano-Anderson model as a discrete one-dimensional system with a single side-coupled Fano state defect. (a) The array of circles corresponds to a linear chains, and the isolated circle is the Fano state. Arrows indicate the coupling between different states. (b) Transmission coefficient [Eq. (10)] for various values of the coupling coefficient V_F. Other parameters are $C=1$, and $E_F=0$. (c) Areas of bistability of the nonlinear Fano resonance (dashed line) in the parameter space (α_k, γ_k). (d) Nonlinear transmission coefficient versus input intensity for various frequencies ω_k for $C=1$, $V_F=0.8$, $E_F=0$, and $\lambda=1$. Regions of bistability are indicated by dashed lines, corresponding to unstable solutions. Adapted from Miroshnichenko, Mingaleev, *et al.*, 2005.

Miroshnichenko, Kivshar, *et al.*, 2005), which is similar to the Fano-Anderson model [Eq. (4)]. The fundamental mode in this case can be considered as a continuum of propagating states, while the generated second harmonic can be either extended or effectively localized depending on the phase matching condition (Miroshnichenko, Kivshar, *et al.*, 2005). In the latter case, the excited second harmonic will act as a discrete state in the continuum, leading to the appearance of a Fano resonance in the transmission [see Fig. 11(b)]. Direct numerical simulation results of the Gaussian beam scattering are in good agreement with the plane-wave analysis [see Fig. 11(b)]. Figures 11(c) and 11(d) show the evolution of the fundamental and second harmonic of the Gaussian beam scattering at resonance. A part of the fundamental harmonic of the Gaussian beam is resonantly reflected by a single nonlinear defect [see Fig. 11(c)]. Since the spectral width of the Gaussian beam is larger than the width of the resonance, some part of the beam still propagates through the defect. During the scattering the second harmonic is resonantly excited [see Fig. 11(d)]. After the scattered beam parts leave the defect region, the second harmonic persists in a self-sustained form.

IV. MODELING: COMPLEX DYNAMICS

Several propagation paths and interference phenomena can be generated not only by imprinting complex geometries but also using complex dynamics. Nonlinear wave excitations, e.g., discrete solitons, when scattering small-amplitude waves, generate several propagation paths purely dynamically. The reason is that the scattering potentials are time dependent (in fact usually time periodic). The amplitude and the temporal period can be tuned by controlling the characteristics of the nonlinear excitations (Li and Reichl, 1999; Martinez and Reichl, 2001; Emmanouilidou and Reichl, 2002). Total resonant reflection has also been observed (Bagwell and Lake, 1992). This is because the time-periodic scattering potential generates several harmonics. In general, these harmonics will correspond to open and closed propagation channels. The presence of such dynamically generated channels is equivalent to a local increase in the spatial dimensionality, discussed in the previous section. In other words, each new channel generates an alternative pathway in which the scattering wave can propagate. The spectrum of excitations in each additional closed channel may contain discrete (localized) states, which happen to resonate with the continuum of the original open channel. As a result, Fano resonances can be expected, where the Fano state is the discrete state from a dynamically generated closed channel.

A. Scattering by discrete breathers

Discrete breathers (DBs) are known as time-periodic and spatially localized solutions of nonlinear wave equa-

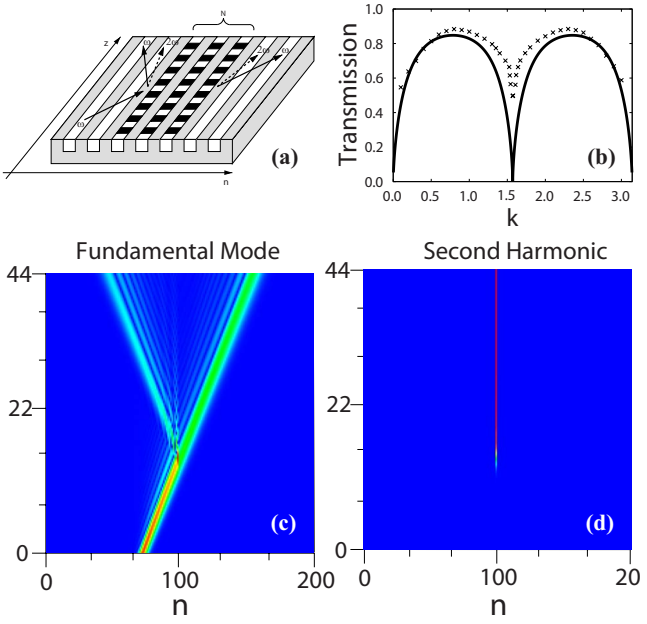

FIG. 11. (Color online) Light scattering in an array of channel waveguides with quadratic nonlinearity. (a) Schematic view of a one-dimensional array of channel waveguides with nonlinear defects, created by periodic poling. Arrows indicate the scattering process. (b) Comparison of the transmission coefficients of plane waves (solid line) and a Gaussian beam (crosses). Bottom: Example of the Gaussian beam scattering by a single nonlinear defect showing (c) the resonant reflection part of the beam at the fundamental frequency and (d) resonant excitation of the second harmonic. Adapted from Miroshnichenko, Kivshar, *et al.*, 2005.

tions on lattices (MacKay and Aubry, 1994; Aubry, 1997; Flach and Willis, 1998; Flach and Gorbach, 2008). They originate from a constructive interplay between nonlinearity and discreteness. DBs exist independent of the lattice dimension and do not rely on integrability properties. In return, these excitations cannot freely move through lattices. Therefore, they act as scattering centers for small-amplitude plane waves. By tuning the amplitude of the DB excitation, one tunes its temporal period and all other characteristics of the resulting time-periodic scattering potential. DBs have been detected and studied experimentally in interacting Josephson-junction networks (Binder *et al.*, 2000; Trías *et al.*, 2000), coupled nonlinear optical waveguides (Eisenberg *et al.*, 1998), lattice vibrations in crystals (Swanson *et al.*, 1999), antiferromagnetic structures (Schwarz *et al.*, 1999), micromechanical cantilever arrays (Sato *et al.*, 2003), Bose-Einstein condensates loaded on optical lattices (Eiermann *et al.*, 2004), and many others (Flach and Gorbach, 2008).

Resonant scattering of plane waves by DBs was studied and showed Fano resonances with zero transmission $T=0$ (Kim and Kim, 2000, 2001; Lee and Kim, 2000b; Flach, Miroshnichenko, and Fistul, 2003; Flach, Miroshnichenko, Fleurov, and Fistul, 2003; Miroshnichenko, Schuster, *et al.*, 2005). Below we demonstrate the concept using a particular example of wave scattering by DBs in the discrete nonlinear Schrödinger (DNLS) model (Flach, Miroshnichenko, Fleurov, and Fistul, 2003).

The equations of motion for the DNLS model are given by

$$i\dot{\Psi}_n = C(\Psi_{n+1} + \Psi_{n-1}) + |\Psi_n|^2\Psi_n, \tag{18}$$

where n is an integer labeling the lattice sites, Ψ_n is a complex scalar variable, and C describes the nearest-neighbor interaction (hopping) on the lattice. The last term in Eq. (18) is a cubic nonlinearity. For small-amplitude waves $\Psi_n(t)=\epsilon e^{i(\omega_k t-kn)}$, the dispersion relation

$$\omega_k = -2C\cos k \tag{19}$$

follows from Eq. (18).

The DNLS model supports DB solutions with a single harmonic,

$$\hat{\Psi}_n(t) = \hat{A}_n e^{-i\Omega_b t}, \quad \hat{A}_{|n|\to\infty} \to 0, \tag{20}$$

where the time-independent amplitude $\hat{A}_n$ can be taken real valued, and the breather frequency $\Omega_b \neq \omega_k$ is some function of the maximum amplitude $\hat{A}_0$. The spatial localization is given by an exponential law $\hat{A}_n \sim e^{-\lambda|n|}$ where $\cosh\lambda = |\Omega_b|/2C$. Thus the DB can be approximated by a single-site excitation if $|\Omega_b| \gg C$. In this case, the relation between the single-site amplitude $\hat{A}_0$ and Ω_b becomes $\Omega_b = \hat{A}_0^2$. In the following, the DB amplitudes for $n \neq 0$ will be neglected, i.e., $\hat{A}_{n\neq 0} \approx 0$, since $\hat{A}_{\pm 1} \approx (C/\Omega_b)\hat{A}_0 \ll A_0$.

We now perturb the breather solution with small fluctuations $\phi_n(t)$,

$$\Psi_n(t) = \hat{\Psi}_n(t) + \phi_n(t), \tag{21}$$

and substitute this ansatz into Eq. (18). Linearization in the small fluctuating perturbation leads to the following set of equations:

$$i\dot{\phi}_n = C(\phi_{n+1} + \phi_{n-1}) + \Omega_b\delta_{n,0}(2\phi_0 + e^{-2i\Omega_b t}\phi_0^*), \tag{22}$$

with $\delta_{n,m}$ the Kronecker symbol. The DB generates a scattering potential that consists of two parts: a static (dc) one, which depends on the breather intensity only $\sim\Omega_b = \hat{A}_0^2$, and a dynamical (ac) one, which depends periodically on time $\sim\Omega_b e^{-2i\Omega_b t}$. With the two-channel ansatz

$$\phi_n(t) = X_n e^{i\omega t} + Y_n^* e^{-i(2\Omega_b+\omega)t} \tag{23}$$

Eq. (22) is reduced to a set of algebraic equations for the complex channel amplitudes X_n and Y_n:

$$-\omega X_n = C(X_{n+1} + X_{n-1}) + \Omega_b\delta_{n,0}(2X_0 + Y_0), \tag{24}$$

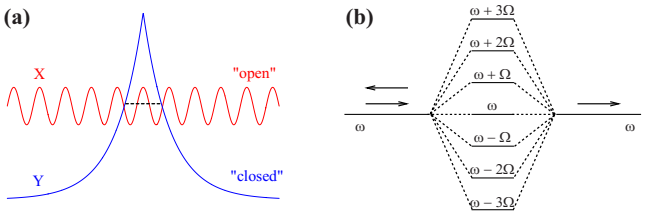

FIG. 12. (Color online) Time-periodic scattering potentials. (a) Schematic view of the open channel X and closed channel Y from Eqs. (24)–(26). The dashed line indicates the localized state of the closed channel Y inside the open channel X. (b) Schematic view of the virtual states, generated by a possibly infinite number of harmonics of the time-periodic scattering potential.

$$(2\Omega_b + \omega)Y_n = C(Y_{n+1} + Y_{n-1}) + \Omega_b \delta_{n,0}(2Y_0 + X_0). \tag{25}$$

For scattering problem the frequency ω should be chosen from the propagation band ω_k. As a result, the channel X_n supports extended waves, while the Y_n channel does not since the frequency $-(2\Omega_b+\omega_q)$ is outside the propagation band ω_k (Flach, Miroshnichenko, Fleurov, and Fistul, 2003); see Fig. 12(a). Therefore the scattering takes place with an open channel X_n which interacts with a closed channel Y_n.

Consider the more general set of equations

$$-\omega_k X_n = C(X_{n+1} + X_{n-1}) - \delta_{n,0}(V_x X_0 + V_a Y_0), \tag{26}$$

$$(\Omega + \omega_k)Y_n = C(Y_{n+1} + Y_{n-1}) - \delta_{n,0}(V_y Y_0 + V_a X_0), \tag{27}$$

which can be reduced to Eq. (24) with the parameters $\Omega=2\Omega_b$ and $V_x=V_y=2V_a=-2\Omega_b$. For $V_a=0$ the closed channel Y_n possesses exactly one localized eigenstate

$$Y_n = Ye^{-\lambda|n|}, \tag{28}$$

with eigenfrequency

$$\omega_L^{(y)} = -\Omega + \sqrt{V_y^2 + 4C^2}. \tag{29}$$

The transmission coefficient for the general case $V_a \neq 0$ (Flach, Miroshnichenko, Fleurov, and Fistul, 2003)

$$T = \frac{4\sin^2 k}{[2\cos k - a - d^2\eta/(2-b\eta)]^2 + 4\sin^2 k},$$
$$a = \frac{-\omega_k + V_x}{C}, \quad b = \frac{\Omega + \omega_k + V_y}{C}, \quad d = \frac{V_a}{C}. \tag{30}$$

From Eq. (30) it follows that the transmission coefficient vanishes when the condition

$$2 - b\eta = 0 \tag{31}$$

is satisfied, which is equivalent to requesting the resonance condition

$$\omega_k = \omega_L^{(y)}. \tag{32}$$

The conclusion is that total reflection takes place when a local mode, originating from the closed Y channel, resonates with the plane-wave spectrum ω_k of the open X channel. The resonance condition is not renormalized by the actual value of V_a. The existence of local modes that originate from the X channel for nonzero V_x and possibly resonate with the closed Y channel is evidently not of any relevance. The resonant total reflection is a Fano resonance, as it is unambiguously related to a local state resonating and interacting with a continuum of extended states. The fact that the resonance is independent of V_a is due to the local coupling between the Fano state (originating from the Y channel) and the open channel and originates from the approximative DB solution in the limit $|\Omega_b| \gg C$. Corrections to the DB solution will increase the range of coupling between the Fano state and the continuum and correspondingly lead to a renormalization of the resonance location (Flach, Miroshnichenko, Fleurov, and Fistul, 2003). Therefore we conclude that the resonance location is not significantly renormalized if the wavelength of the propagating wave is large compared to the extension of the space region where the coupling between a Fano state and a continuum occurs (Flach, Miroshnichenko, and Fistul, 2003).

If the closed channel is reduced to the localized discrete Fano state Y only, the equations for the amplitudes take the form

$$-\omega X_n = C(X_{n-1} + X_{n+1}) + V_a Y \delta_{n0},$$
$$-\omega Y = E_F Y - V_a X_0. \tag{33}$$

The different signs in front of the coupling between the chain and the Fano state are due to the fact that time-periodic scattering potentials correspond to eigenvalue problems with a symplectic propagator. In contrast, complex geometries [Eq. (6)] remain as unitary propagators. Remarkably, these differences in the symmetries of the underlying dynamical processes do not alter the final result of destructive interference and Fano resonances.

The above analysis leads to a recipe for finding the positions of resonances. One first calculates the localized states of closed channels decoupled from the open one (Flach, Miroshnichenko, and Fistul, 2003; Flach, Miroshnichenko, Fleurov, and Fistul, 2003). When the coupling is switched on again, Fano resonances will take place exactly at the eigenfrequencies of the localized states for weak coupling. For stronger coupling, the positions of the resonances will renormalize. In general, there is an infinite number of harmonics of the DB, which generate an infinite number of closed channels (Flach, Miroshnichenko, and Fistul, 2003; Flach, Miroshnichenko, Fleurov, and Fistul, 2003). The approach described above is rather generic and can be applied to the scattering through many types of oscillating barriers, self-induced (such as DBs) or parametrically driven (by external forces) (Bagwell and Lake, 1992; Li and Reichl, 1999; Boese *et al.*, 2000; Martinez and Reichl, 2001; Emman-

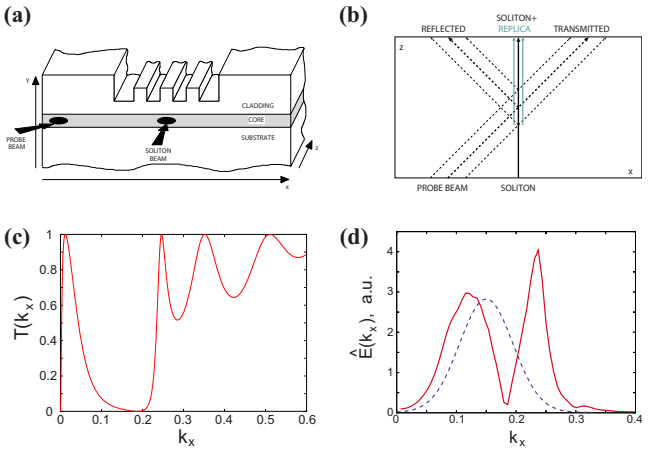

FIG. 13. (Color online) Light scattering by optical solitons. (a) Sketch of the scattering setup by an optical soliton in a one-dimensional waveguide array. The soliton beam is sent along the z axis, while the probe beam propagates in the x-z-plane at some angle to the soliton. (b) Top view of the scattering process (c) Transmission coefficient vs k_x for plane waves under oblique incidence. There is total suppression of the transmission near $k_x \approx 0.181$. (d) Fourier spectrum of the incident (dashed line) and transmitted (solid line) beams. The suppression of the resonant frequency [see (c)] in the spectrum is observed. Adapted from Flach *et al.*, 2005.

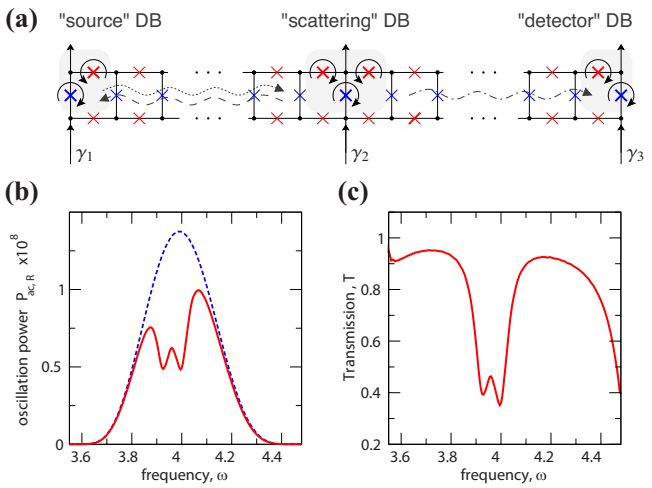

FIG. 14. (Color online) Plasmon scattering by discrete breathers in Josephson-junction ladders. (a) Schematic setup for the measurement of plasmon scattering with the use of controlled bias currents γ_i; (b) oscillating power $P_{\mathrm{ac},R}$ at the right end with (solid line) and without (dashed line) the DB; (c) transmission coefficient T, derived from (b) by using Eq. (34). Adapted from Miroshnichenko, Schuster, *et al.*, 2005.

ouilidou and Reichl, 2002; Kim, 2002; Longhi, 2006). All of them produce similar scattering potentials with an open and a number of closed channels for small-amplitude scattering waves.

B. Light scattering by optical solitons

The above concept of scattering by solitary excitations was applied to predict resonant light scattering by optical solitons in a slab waveguide with an inhomogeneous refractive index core (Flach *et al.*, 2005, 2006). The soliton is generated in a nonlinear planar waveguide by a laser beam injected into the slab along the z direction [see Fig. 13(a)]. The soliton beam is confined in the y direction by total internal reflection. The localization in the x direction is achieved by a balance between linear diffraction and an instantaneous Kerr-type nonlinearity. The analogy with the scattering problem discussed above by time-periodic potentials comes from the possibility of interpreting the spatial propagation along the z direction as an artificial time (Agrawal, 1995). Thus, the propagation constant of the soliton can be considered as the frequency of the breather. The evolution of the soliton envelope function satisfies the nonlinear Schrödinger equation, the continuum analog of Eq. (18) (Flach *et al.*, 2005). Analysis of the scattering problem is similar to that discussed above. Figure 13(c) shows the dependence of the transmission coefficient for oblique incident light for various k_x wave numbers. It results in a Fano resonance for plane waves at $k_x \approx 0.181$, where the transmission coefficient vanishes. This result has been confirmed by direct numerical simulations of a propagating small-amplitude wave packet scattered by the optical soliton (Flach *et al.*, 2006); see Fig. 13(b). The Fourier spectrum of the transmitted wave packet reveals that the resonant wave number $k_x \approx 0.181$ was filtered out from the initial wave packet [see Fig. 13(d)]. Such a spectral hole-burning effect can be used as a characteristic feature for the detection of the Fano resonance in an experimental setup.

C. Plasmon scattering in Josephson-junction ladders

Another theoretical prediction concerns the plasmon wave scattering by DBs in Josephson-junction ladders (JJLs). JJLs are formed by an array of small Josephson junctions that are arranged along the spars and rungs of a ladder [see Fig. 14(a)]. Each junction consists of two small, weakly coupled superconducting islands. The dynamical state of a junction is described by the phase difference $\phi(t)$ (Josephson phase) of the superconducting order parameters of two neighboring islands. When the difference does not vary in time, $\phi(t) = \mathrm{const}$, the junction is traversed by a superconducting current only, with zero voltage drop. Otherwise, the junction is traversed in addition by a resistive current component with a nonzero voltage drop $V \propto \dot{\phi}(t)$. It was observed experimentally that JJLs support dynamic localized states (DBs) (Binder *et al.*, 2000; Trías *et al.*, 2000). A discrete breather is characterized by a few junctions being in the resistive state $\langle \dot{\phi} \rangle \neq 0$ while the others reside in the superconducting state $\langle \dot{\phi} \rangle = 0$. The frequency of a DB is proportional to the average voltage drop across the resistive junctions $\Omega_b \propto \langle \dot{\phi} \rangle$. Miroshnichenko, Schuster, *et al.* (2005) proposed an experimental setup to measure Fano resonances in that transmission line. Small-

amplitude waves are generated in a JJL with open ends by local application of a time-periodic current $\gamma_1(t) = \gamma_{ac}\cos(\omega t)$. The local current acts as a local parametric drive. It excites edge junctions at a frequency ω. This tail extends into the ladder. To monitor the linear wave propagation in the system, the time-averaged oscillation power $P_{ac,n}=\langle \dot{\phi}_n^2 \rangle$ is measured. The transmission coefficient can be obtained by relating the oscillation power at the right boundary with and without an excited DB in the system,

$$T = \frac{P_{ac,R}(\text{with DB})}{P_{ac,R}(\text{without DB})}. \tag{34}$$

Figures 14(b) and 14(c) show the presence of resonant suppression of the transmission coefficient for particular frequencies ω. The analysis by Miroshnichenko, Schuster, *et al.* (2005) revealed that they correspond to Fano resonances, which originate from localized states of closed channels of the time-periodic scattering potential that is generated by the DB.

D. Matter-wave scattering in Bose-Einstein condensates

Over the last couple of years it has been shown that optical lattices, generated by counterpropagating laser beams and providing a periodic potential modulation for the atoms, introduce many interesting and potentially useful effects by modifying single-atom properties and enhancing correlations between atoms (Morsch and Oberthaler, 2006). Using about 1000 ^{87}Rb atoms in a quasi-one-dimensional optical lattice, Eiermann *et al.* (2004) obtained a spatially localized Bose-Einstein condensate (BEC) which is an experimental manifestation of a gap soliton or a discrete breather. The solitary state exists due to the atom-atom interaction, which can be tuned in various ways experimentally.

Vicencio *et al.* (2007) considered a BEC on a lattice, where interactions between atoms are present only in a localized region (see Fig. 15). Such a situation could be realized experimentally by combining optical lattices with atom-chip technology (Hänsel *et al.*, 2001; Ott *et al.*, 2001) or in optical microlens arrays (Dumke *et al.*, 2002). The system is described by the DNLS equation, a classical variant of the Bose-Hubbard model appropriate for a BEC in a periodic potential in the tight-binding limit (Morsch and Oberthaler, 2006). With interactions being present only on site number n_c, it follows that

$$i\frac{d\Psi_n}{dt} = -(\Psi_{n+1}+\Psi_{n-1}) - \gamma|\Psi_{n_c}|^2\Psi_{n_c}\delta_{n,n_c}, \tag{35}$$

where Ψ_n is the complex amplitude of the condensate field at site n and $-\gamma = U/J$ is the interaction strength on site n_c, J is the tunneling energy between the lattice sites, and U is the on-site interaction energy per atom.

Equation (35) supports a localized state $\Psi_n(t) = bx^{|n-n_c|}\exp(-iE_b t)$, where $x=-\frac{1}{2}(E_b+g)$ with $g=\gamma b^2$, b is the condensate amplitude, and $E_b=-(4+g^2)^{1/2}$ is the chemical potential.

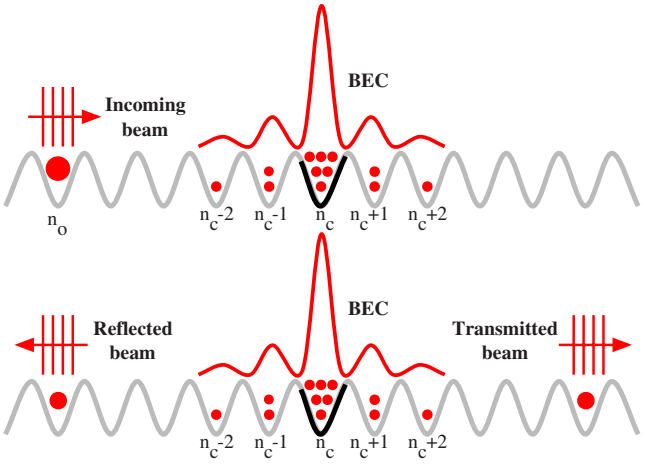

FIG. 15. (Color online) Scattering scheme in an optical lattice. The incoming, reflected, and transmitted beams of atoms are represented as plane waves. The atoms interact only around $n=n_c$, where the BEC is centered. From Vicencio *et al.*, 2007.

The scattering of propagating atomic matter waves with the energy $E_k=-2\cos k$ by this localized BEC was calculated analytically within the framework of the Bogoliubov–de Gennes equations (Vicencio *et al.*, 2007). The transmission $T(k)$ is shown in Fig. 16 for three values of g (solid curves). As g increases, the width and the position of the resonance increase. Furthermore, the more localized the BEC becomes, the more strongly it reflects the atom beam off resonance. By tuning the nonlinear parameter g, we can thus choose the amount of the beam that passes through the BEC. Off resonance (for larger values of k), we can select the percentage of the incoming beam that is transmitted for a defined quasimomentum. Therefore, the actual setup can be used as a 100% blockade or as a selective filter.

Analytical results have been confirmed by numerical simulation of Eq. (35) with a Gaussian atom beam profile. The results are shown in Fig. 16 by symbols for three different values of the parameter g. The agreement between theory and simulations is good.

V. LIGHT PROPAGATION IN PHOTONIC DEVICES

Optical microcavity structures are of great interest for device applications, and many of these structures in-

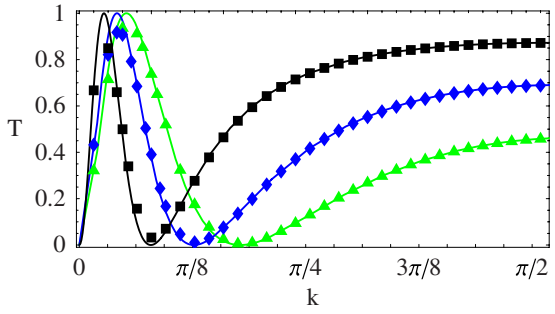

FIG. 16. (Color online) Transmission T vs momentum k. Lines, analytic solution; symbols, real time numerical simulations of Eq. (35) using wave packets for $g=0.36$ (line and boxes), $g=0.6$ (line and diamonds), and $g=0.9$ (line and triangles). From Vicencio *et al.*, 2007.

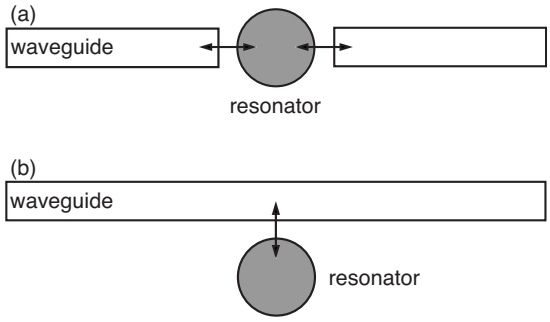

FIG. 17. Typical resonant structures. Schematic setup for (a) a waveguide directly coupled to a cavity and (b) a waveguide side-coupled to a cavity.

volve coupling of one or several cavities to a waveguide. Such waveguide-cavity systems can naturally exhibit Fano resonances with high quality factors, and they can be used for optical modulations and switching. The on-off switching functionality can be realized by shifting the resonant frequency either toward or away from the signal frequency.

The basic geometry of a waveguide-cavity system that demonstrates a sharp Fano resonance has been introduced and analyzed by Haus and Lai (1991) and Xu *et al.* (2000). It consists of a waveguide coupled to a cavity (or resonator). In general, two-port photonic devices based upon waveguide-resonator interaction can be presented in two geometries, as shown in Figs. 17(a) and 17(b). The first configuration is based on a direct-coupling geometry (Marin Soljačić and Joannopoulos, 2002), and the second geometry is a waveguide side coupled with a single-mode cavity (Xu *et al.*, 2000; Yanik, Fan, and Soljačić, 2003). Such structures are tunable by addition of cavities with nonlinear response or by employing an external control. Next, we review the basic properties of the simplest waveguide-cavity systems and discuss several generalizations, including all-optical switching structures based on the concepts of Fano resonances.

A. Green's function formalism

The Green's function approach (Mingaleev and Kivshar, 2002a, 2002b) allows us to obtain accurate results in comparison to the time-consuming direct numerical finite-difference time-domain (FDTD) simulations, even for rather complex geometries of the waveguide-cavity systems. To derive the corresponding equations, one takes the explicit temporal dependencies into account, which allows one to study the pulse propagation and scattering.

We consider a photonic crystal created by a periodic square lattice of infinite cylindrical rods parallel to the z axis. We neglect the material dispersion and assume the dielectric constant $\epsilon(\vec{r})$ to be periodic in two transverse directions, $\vec{r}=(x,y)$. The evolution of the E-polarized electric field propagating in the (x,y) plane is governed by the scalar wave equation

$$\nabla^2 E_z(\vec{r},\tau) - \frac{1}{c^2}\partial_\tau^2[\epsilon(\vec{r})E_z(\vec{r},\tau)] = 0, \tag{36}$$

where $\nabla^2=\partial_x^2+\partial_y^2$. We assume that the light field propagating in such structures can be separated into fast and slow components, $E_z(\vec{r},\tau)=e^{-i\omega\tau}E(\vec{r},\tau|\omega)$, where $E(\vec{r},\tau|\omega)$ is a slowly varying envelope of the electric field, i.e., $\partial_\tau^2 E(\vec{r},\tau|\omega) \ll \omega\partial_t E(\vec{r},\tau|\omega)$. This allows us to simplify Eq. (36) to the following form:

$$\left[\nabla^2 + \epsilon(\vec{r})\left(\frac{\omega}{c}\right)^2\right]E(\vec{r},\tau|\omega) \simeq -2i\epsilon(\vec{r})\frac{\omega}{c^2}\frac{\partial E(\vec{r},\tau|\omega)}{\partial\tau}. \tag{37}$$

Both the straight waveguide and the side-coupled cavity are created by introducing defect rods into a perfect two-dimensional periodic structure. Therefore, the dielectric constant can be represented as a sum of two components, describing the periodic and defect structures $\epsilon(\vec{r})=\epsilon_{\rm pc}+\delta\epsilon$. We employ the Green's function of the two-dimensional periodic structure without defects and rewrite Eq. (37) in the integral form

$$E(\mathbf{x},\tau|\omega) = \int d^2\mathbf{y}\, G(\mathbf{x},\mathbf{y}|\omega)\hat{L}E(\mathbf{y},\tau,\omega), \tag{38}$$

where we introduce the linear operator

$$\hat{L} = \left(\frac{\omega}{c}\right)^2\delta\epsilon(\vec{r}) + 2i\epsilon(\vec{r})\frac{\omega}{c^2}\frac{\partial}{\partial\tau} \tag{39}$$

and consider the time evolution of the slowly varying envelope as a perturbation to the steady state.

The defect rods introduced into the periodic structure can formally be described as follows:

$$\delta\epsilon(\vec{r}) = \sum_{n,m}[\delta\epsilon_{m,n}^{(0)} + \chi^{(3)}|E(\mathbf{x},\tau|\omega)|^2]\theta(\mathbf{x}-\mathbf{x}_{n,m}), \tag{40}$$

where we use the θ function to describe the position of a defect rod at site n, m, with $\theta(\mathbf{x})=1$ for $\mathbf{x}$ inside the defect rods and $\theta(\mathbf{x})=0$ otherwise. $\delta\epsilon_{m,n}^{(0)}$ is the variation of the dielectric constant of the defect rod (m,n). Importantly, this approach allows us to incorporate a nonlinear response in a straightforward manner, which is assumed to be of the Kerr type described by the term $\chi^{(3)}|E|^2$.

Substituting Eq. (40) into the integral equation (38) and assuming that the electric field does not change inside the dielectric rods, we can evaluate the integral at the right-hand side of Eq. (38) and derive a set of discrete nonlinear equations

$$i\sigma\frac{\partial}{\partial\tau}E_{n,m} - E_{n,m} + \sum_{k,l}J_{n-k,m-l}(\omega)(\delta\epsilon_{k,l}^{(0)} + \chi^{(3)}|E_{k,l}|^2)E_{k,l} = 0, \tag{41}$$

for the amplitudes of the electric field $E_{n,m}(\tau|\omega)=E(\mathbf{x}_{n,m},\tau|\omega)$ calculated at the defect rods. The parameters σ and $J_{k,l}(\omega)$ are determined using the corresponding integrals of the Green's function, where information about the photonic crystal dispersion is now hidden in their specific frequency dependencies, which can be

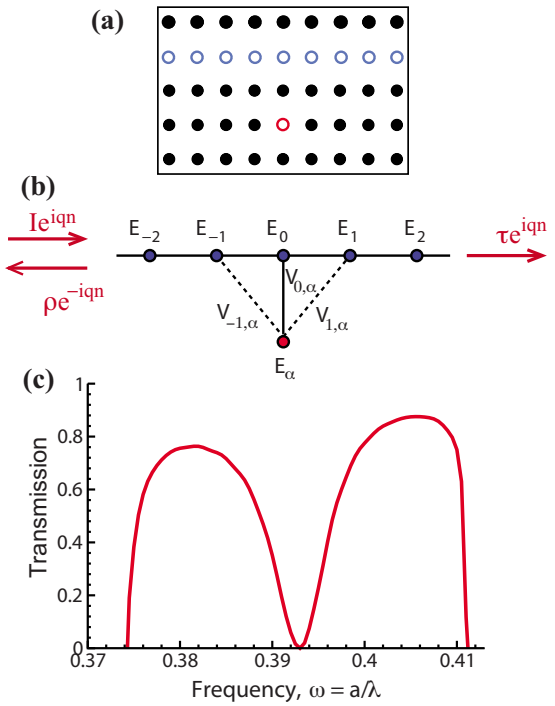

FIG. 18. (Color online) Modeling Fano resonances in photonic crystals. Schematic view of (a) photonic crystal waveguide with an isolated side-coupled cavity and (b) effective discrete system. (c) Typical profile of the Fano resonance.

found in Mingaleev and Kivshar (2001) and Mingaleev *et al.* (2006). In this way, the Green's function needs to be calculated only once for a given photonic structure, e.g., by employing the approach outlined by Ward and Pendry (1998), and then it can be used to study any photonic circuit in that structure.

For the simple system when the photonic crystal has a waveguide side coupled to a single defect [see Fig. 18(a)], the problem describes a discrete system studied earlier [see Fig. 18(b)], and the transmission shows a Fano resonance [see Fig. 18(c)], analyzed by Miroshnichenko, Mingaleev, *et al.* (2005) and Mingaleev *et al.* (2006).

In a general case, the effective interaction between defect rods is of long-range nature (Mingaleev *et al.*, 2000; Mingaleev and Kivshar, 2002b). However, the coupling strength decays exponentially with increasing distance, and as a result, for coupled-resonator optical waveguides, the specific discrete arrays with nearest-neighbor interactions (at $L=1$) already give a excellent agreement with direct FDTD simulations (Mingaleev and Kivshar, 2002b).

B. Defects in the waveguide

The two basic geometries shown in Figs. 17(a) and 17(b) can be further improved by placing partially reflecting elements into the waveguides (Fan, 2002; Khelif *et al.*, 2003). These elements allow creation of sharp and asymmetric response line shapes. In such systems, the transmission coefficient can vary from 0% to 100% in a

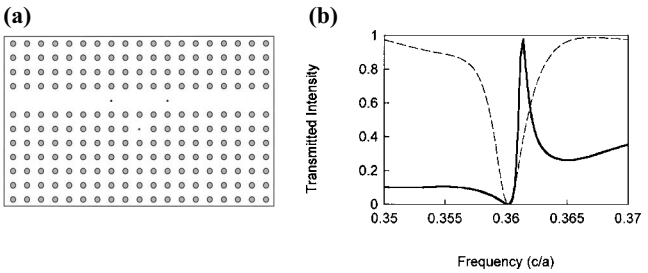

FIG. 19. Light propagation in a photonic crystal waveguide with a side-coupled cavity. (a) Photonic crystal waveguide formed by removing a single row of rods. Within the line defect there are two smaller rods. A point defect, created by reducing the radius of a single rod, is placed away from the waveguide. (b) Transmission spectra through the structure (a) with (solid) and without (dashed) the two defects in the waveguide. From Fan, 2002.

frequency range narrower than the full width of the resonance itself.

To illustrate the effect of defects, Fan (2002) simulated the response of the structure shown in Fig. 19(a) using a FDTD scheme with perfectly matched layer boundary conditions. A pulse is excited by a monopole source at one end of the waveguide. The transmission coefficient is then calculated by Fourier transforming the amplitude of the fields at the other end; it is shown as a solid line in Fig. 19(b). In comparison, the transmission spectrum for the same structure, but without the two small cylinders in the waveguide, is shown by a dashed line.

Importantly, no detailed tuning of either the resonant frequency or the coupling between the cavity and the waveguide is required to achieve asymmetric line shapes. Also, since the reflectivity of the partially reflecting elements need not to be large, the underlying physics here differs from that in typical coupled-cavity systems and resembles Fano resonances involving interference between a continuum and a discrete level.

C. Sharp bends

One of the most fascinating properties of photonic crystals is their ability to guide electromagnetic waves in narrow waveguides created by a sequence of line defects, including light propagation through extremely sharp waveguide bends with nearly perfect power transmission (Mekis *et al.*, 1996; Lin *et al.*, 1998). It is believed that the low-loss transmission through sharp waveguide bends in photonic crystals is one of the most promising approaches to combining several devices inside a compact nanoscale optical chip.

Interestingly, the transmission through sharp bends in photonic crystal waveguides can be reduced to a simple model with Fano resonances, where the waveguide bend hosts a specific localized defect. Miroshnichenko and Kivshar (2005b) derived effective discrete equations for two types of waveguide bends in two-dimensional photonic crystals and obtained exact analytical solutions for the resonant transmission and reflection.

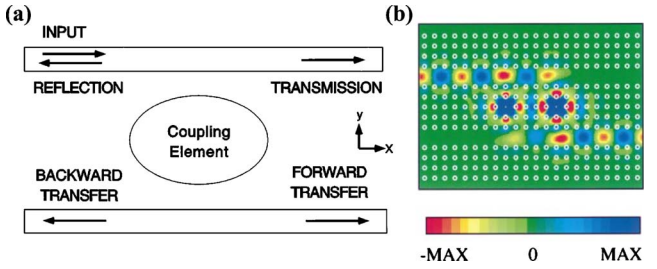

FIG. 20. (Color online) Add-drop filter. (a) Schematic diagram of two waveguides coupled through an element which supports a localized resonant state. (b) Electric field pattern of the photonic crystal at the resonant frequency. The white circles indicate the position of the rods. From Fan *et al.*, 1998.

D. Add-drop filters

Fano resonances can be employed for a variety of photonic devices based on resonant tunneling. In particular, if two waveguides interact through a coupling element which supports a localized mode, a channel add-drop filter can be realized via the resonant tunneling between the waveguides (Fan *et al.*, 1998, 1999; Soljačić *et al.*, 2003). The schematic diagram of a generic coupled system of this kind is shown in Fig. 20(a). At Fano resonance, the propagating state excites the resonant modes, which in turn decay into both waveguides. The transmitted signal in the first waveguide is made up of the directly propagating signal and the signal that originates from the second path which visits the coupling region. In order to achieve complete transfer from one waveguide to the other, these two signal components must interfere destructively. The reflected amplitude, on the other hand, originates entirely from the second path into the coupling region. Hence, at least two states in the coupling region are needed to also achieve destructive interference of backscattered waves in the first waveguide. With these conditions satisfied, one may resonantly transfer excitation from the first into the second waveguide.

This concept was developed by Fan *et al.* (1998) for the propagation of electromagnetic waves in a two-dimensional photonic crystal. To realize this concept, they used two photonic crystal waveguides and two coupled single-mode high-Q cavities, as shown in Fig. 20(b). The photonic crystal is made of a square lattice of high-index dielectric rods, and the waveguides are formed by removal of two rows of dielectric rods. The cavities are introduced between the waveguides by reduction of the radius of two rods. The resonant states have different symmetry. An accidental degeneracy, caused by an exact cancellation between the two coupling mechanisms, is enforced by reducing the dielectric constant of four specific rods in the photonic crystal. The cancellation could equally have been accomplished by reducing the size of the rods instead of their dielectric constant.

Figure 20(b) shows the field pattern at resonance. The quality factor is larger than 10^3. The backward-transferred signal is almost completely absent over the entire frequency range.

This type of four-port photonic crystal system can be employed for optical bistability, being particularly suitable for integration with other active devices on a chip (Soljačić *et al.*, 2003). A similar concept can be employed for the realization of all-optical switching action in a nonlinear photonic crystal cross-waveguide geometry with instantaneous Kerr nonlinearity. There the transmission of a signal can be reversibly switched on and off by a control input (Yanik *et al.*, 2003).

E. All-optical switching and bistability

A powerful principle that could be explored to implement all-optical transistors, switches, and logical gates is based on the concept of optical bistability. The use of photonic crystals enables the system to be of a size of the order of the wavelength of light, consume only a few milliwatts of power, and have a recovery and response time smaller than 1 ps. Several theoretical and experimental studies explored nonlinear Fano resonances for designing optimal bistable switching in nonlinear photonic crystals (Marin Soljačić and Joannopoulos, 2002; Mingaleev and Kivshar, 2002b; Cowan and Young, 2003; Yanik, Fan, and Soljačić, 2003; Mingaleev *et al.*, 2007, 2006; Maes *et al.*, 2008). A photonic crystal provides optimal control over the input and output and facilitates further large-scale optical integration.

The main idea of using the Fano resonance for all-optical switching and bistability is quite simple: One should introduce an element with nonlinear response and achieve nonlinearity-induced shifts of the resonant frequency, as discussed above for discrete models. Thus, by employing *nonlinear Fano resonances* we can achieve bistability in many of the device structures suggested on the photonic-crystal platform. For example, for the side-coupled geometry shown in Fig. 17(b), one could take advantage of the interference between the propagating wave inside the waveguide and the decaying wave from the cavity to greatly enhance achievable contrast ratio in the transmission between the two bistable states. This approach was realized by Yanik, Fan, and Soljačić (2003), who demonstrated that such a configuration can generate extremely high contrast between the bistable states in its transmission with low input power.

One of the great advantages in using nonlinear photonic crystal cavities is the enhancement of nonlinear optical processes, including nonlinear Fano resonance (Soljacic and Joannopoulos, 2004; Bravo-Abad *et al.*, 2007) (Fig. 21). Such an enhancement can be efficient in the regime of slow-light propagation that was demonstrated experimentally with the smallest achieved group velocity $c/1000$ (Notomi *et al.*, 2001; Gersen *et al.*, 2005; Jacobsen *et al.*, 2005; Vlasov *et al.*, 2005). Because of this success, the interest in slow-light applications based on photonic crystal waveguides is rapidly growing and posing problems of a design of different types of functional optical devices which would efficiently operate in the slow-light regime.

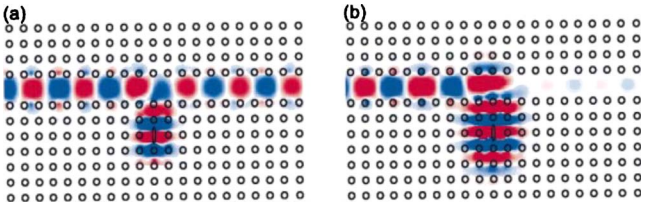

FIG. 21. (Color online) Electric field distributions in a photonic crystal for (a) high and (b) low transmission states. The same color scale is used for both panels. The black circles indicate the positions of the dielectric rods. From Yanik, Fan, and Soljačić, 2003.

Recently Mingaleev *et al.* (2007) studied the resonant transmission of light through a photonic crystal waveguide coupled to a nonlinear cavity and demonstrated how to modify the structure geometry for achieving bistability and all-optical switching at ultralow power in the slow-light regime. This can be achieved by placing a side-coupled cavity between two defects of a photonic crystal waveguide, assuming that all the defect modes and the cavity mode have the same symmetry. In this structure the quality factor grows inversely proportionally to the group velocity of light at the resonant frequency, and, accordingly, the power threshold required for all-optical switching vanishes as the square of the group velocity (see Fig. 22).

The numerically obtained dependence $Q(v_{gr}) \sim 1/v_{gr}$ is shown in Fig. 22(a), and it is in an excellent agreement with the theoretical predictions. Since the bistability threshold power of the incoming light in waveguide-cavity structures scales as $P_{th} \sim 1/Q^2$ (Mingaleev *et al.*, 2006), one observes a rapid diminishing of $P_{th} \sim v_g^2$ when the resonance frequency approaches the band edge, as shown in numerical calculations summarized in Figs. 22(b) and 22(c).

By now, several experimental observations of optical bistability enhanced through Fano interferences have been reported (Weidner *et al.*, 2007; Yang *et al.*, 2007). In particular, Yang *et al.* (2007) employed a high-Q cavity mode ($Q=30\,000$) in a silicon photonic crystal and demonstrated Fano-resonance-based bistable states and

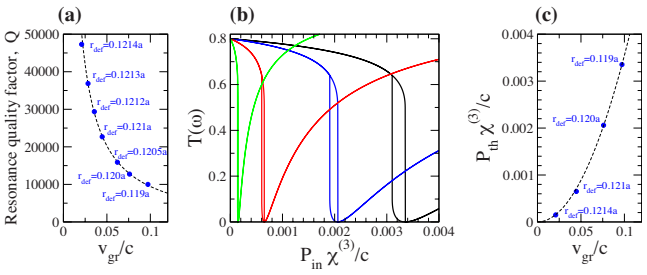

FIG. 22. (Color online) Ultralow all-optical switching in the slow-light regime. (a) Quality factor Q vs group velocity v_g at resonance for the waveguide-cavity structure. (b) Nonlinear bistable transmission at the frequencies with 80% of linear light transmission vs the incoming light power for different values of the rod radius. (c) Switch-off bistability threshold vs the group velocity at resonance. From Mingaleev *et al.*, 2007.

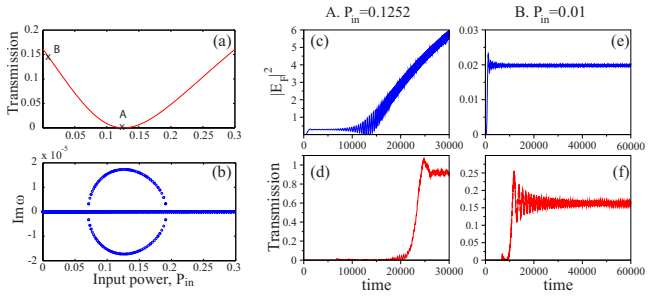

FIG. 23. (Color online) Dynamical instability of the nonlinear Fano resonance. (a) Nonlinear transmission coefficient and (b) imaginary part of eigenvalues of the stability problem vs input power. In the vicinity of the nonlinear Fano resonance the plane-wave excitation becomes dynamically unstable. Temporal evolution of (c) and (e) the field inside the side-coupled cavity and (d) and (f) the transmission coefficient for two different values of the input power values, indicated in (a). Near the resonance the dynamics of the field inside the nonlinear cavity yields a buildup of a modulation instability in time. Adapted from Miroshnichenko *et al.*, 2009.

switching with thresholds of 185 μW and 4.5 fJ internally stored cavity energy that might be useful for scalable optical buffering and logic.

It is important to note that the nonlinear Fano resonance shows dynamical instabilities with plane-wave excitations (Miroshnichenko, 2009a; Miroshnichenko *et al.*, 2009). Near the resonance the intensity of the scattered wave starts to grow in time, leading to modulational instability, while far from resonance it converges to a steady-state solution (see Fig. 23). However, as demonstrated by Miroshnichenko *et al.* (2009), this instability can be suppressed for temporal Gaussian pulse excitations, providing an effective method of recovering the bistable transmission.

F. Overlapping resonances

An important effect associated with the Fano resonances in double-resonator photonic structures can be linked to electromagnetically induced transparency (EIT) (Fleischhauer *et al.*, 2005). Coupled-resonator-induced transparency (CRIT) structures were introduced in 2004 (Maleki *et al.*, 2004; Smith *et al.*, 2004; Suh *et al.*, 2004), although early work (Opatrný and Welsch, 2001) already suggested the idea of a macroscopic double-resonator optical system exhibiting an EIT-like effect. Recently, the CRIT effect has been observed experimentally in a system of two interacting microresonators (glass spheres of about 400 μm in diameter) with whispering-gallery modes (Naweed *et al.*, 2005), in a cavity with at least two resonant modes (Franson and Hendrickson, 2006), in integrated photonic chips with two microring resonators (Xu *et al.*, 2006; Tomita *et al.*, 2009), and in planar metamaterials (Fedotov *et al.*, 2007; Papasimakis *et al.*, 2008, 2009; Papasimakis and Zheludev, 2009). Providing an efficiently tunable transparency on an optical chip, such CRIT devices are consid-

ered as a crucial step toward the development of integrated all-optical chips (Boyd and Gauthier, 2006).

To explain the origin of CRIT resonances, we characterize the light transmission by the transmission and reflection coefficients, which can be presented in the form

$$T(\omega) = \frac{\sigma^2(\omega)}{\sigma^2(\omega)+1}, \quad R(\omega) = \frac{1}{\sigma^2(\omega)+1}, \tag{42}$$

where the detuning function $\sigma(\omega)$ may have a quite different type of frequency dependence for different types of waveguide-cavity structure. Zero transmission (total reflection) corresponds to the condition $\sigma(\omega)=0$, while perfect transmission (zero reflection) corresponds to the condition $\sigma(\omega)=\pm\infty$.

For the waveguide-cavity structure shown in Fig. 17(b), we obtain (Mingaleev *et al.*, 2006)

$$\sigma(\omega) \simeq (\omega_\alpha - \omega)/\gamma_\alpha, \tag{43}$$

where ω_α is the eigenfrequency of the localized cavity mode of an isolated cavity α. The spectral width γ_α of the resonance is determined by the overlap integral between the cavity mode and the guided mode at the resonant frequency.

To find $\sigma(\omega)$ for the two-cavity structure, one can apply a variety of methods but the simplest approach is based on the transfer-matrix technique (Fan, 2002). When two cavities are separated by the distance $d=2\pi m/k(\omega_t)$, where $k(\omega)$ is the waveguide's dispersion relation, m is any integer number, and the frequency ω_t is defined below, and there is no direct coupling between the cavities, we obtain

$$\sigma(\omega) \simeq \frac{(\omega_\alpha - \omega)(\omega_\beta - \omega)}{\Gamma(\omega_t - \omega)}, \tag{44}$$

with the total resonance width $\Gamma=\gamma_\alpha+\gamma_\beta$ and the frequency of perfect transmission $\omega_t=(\gamma_\alpha\omega_\beta+\gamma_\beta\omega_\alpha)(\gamma_\alpha+\gamma_\beta)^{-1}$, lying between the two cavity frequencies ω_α and ω_β of zero transmission.

In the case when the cavities α and β are identical, we obtain a single-cavity resonance, and the only effect of using two cavities is the doubling of the spectral width $\Gamma=2\gamma_\alpha$ of the resonant reflection line, as shown in Fig. 25(a). However, introduction of even the smallest difference between two cavities leads to the opening of an extremely narrow resonant transmission line on the background of this broader reflection line, as shown in Fig. 25(c). Indeed, for slightly different cavities we may rewrite Eq. (44) in the vicinity of the resonant transmission frequency $\omega_t=\omega_\alpha+\delta\omega/2$ as $\sigma(\omega)\approx\Gamma_t/(\omega-\omega_t)$, with the linewidth $\Gamma_t=\delta\omega^2/8\gamma_\alpha$, which can easily be controlled by tuning the frequency difference $\delta\omega$. The quality factor of this transmission line $Q_t=\omega_t/2\Gamma_t \approx 4\gamma_\alpha\omega_\alpha/\delta\omega^2$ grows indefinitely when $\delta\omega$ vanishes. As mentioned, this effect is the all-optical analog of the electromagnetically induced transparency and is now often referred to as the effect of coupled-resonator-induced transparency (Smith *et al.*, 2004).

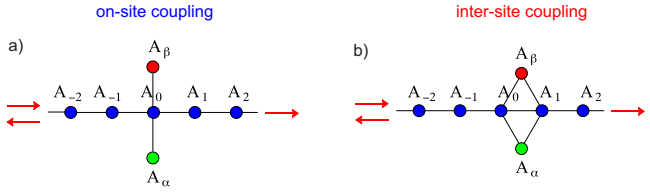

FIG. 24. (Color online) Two types of the geometries of a photonic crystal waveguide side-coupled to two nonlinear optical resonators. Light transmission and bistability are qualitatively different for (a) on-site and (b) intersite locations of the resonator along the waveguide. Adapted from Mingaleev *et al.*, 2008.

In contrast, the intercoupling between two cavities, as shown in Fig. 24(b), manifests itself as a qualitatively new effect of coupled-resonator-induced reflection (CRIR): for small detuning $\delta\omega=\omega_\beta-\omega_\alpha$, one of the resonant reflection frequencies shifts close to the perfect transmission frequency ω_t, producing a narrow resonant reflection line, as shown in Fig. 25(d). The frequency of this line is always close to the frequency ω_α of the cavity mode, while its spectral width is determined by the frequency difference $\delta\omega$, growing indefinitely as $\delta\omega$ vanishes (Landobasa, Mario, and Chin, 2006; Mingaleev *et al.*, 2008).

It should be emphasized that, despite such a qualitative difference in their spectral manifestations, both CRIT and CRIR effects have the same physical origin, which can be attributed to the Fano-Feshbach resonances (Feshbach, 1958, 1962; Mies, 1968) that are known to originate from the interaction of two or more resonances (e.g., two Fano resonances) in the overlapping regime, where the spectral widths of resonances are comparable to or larger than the frequency separation between them. In a general situation it leads to a drastic deformation of the transmission spectrum and the for-

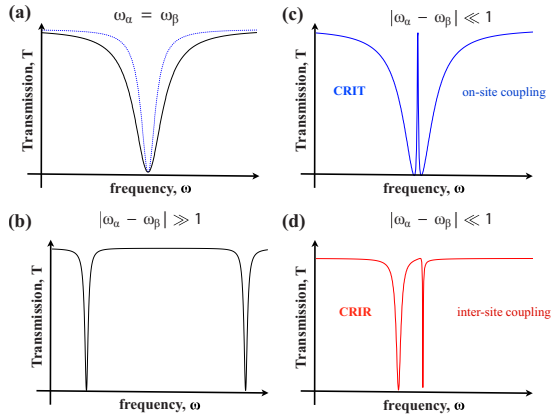

FIG. 25. (Color online) Overlapping Fano resonances. Typical transmission curves for four different cases. (a) Two identical side-coupled defects $\omega_\alpha=\omega_\beta$ (solid). Transmission for a single side-coupled cavity is shown by a dashed line. (b) Two side-coupled cavities with strongly detuned eigenfrequencies $|\omega_\alpha-\omega_\beta|\gg 1$. (c) and (d) Two side-coupled cavities with slightly detuned eigenfrequencies $|\omega_\alpha-\omega_\beta|\ll 1$ for (c) on-site coupling and (d) intersite coupling. From Mingaleev *et al.*, 2008.

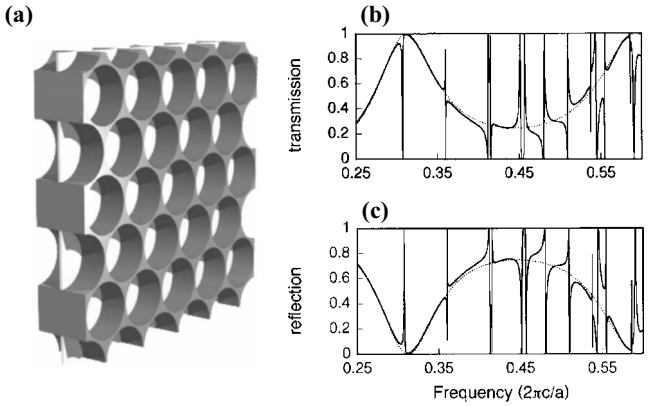

FIG. 26. Light scattering by photonic crystal slabs. (a) Geometry of the photonic crystal film. (b) Transmission and (c) reflection spectra. The solid lines are for the photonic crystal structure, and the dashed lines are for a uniform dielectric slab with a frequency-dependent dielectric constant. Adapted from Fan and Joannopoulos, 2002.

mation of additional resonances with sharp peaks. The Fano-Feshbach resonances are associated with a collective response of multipe interacting resonant degrees of freedom, and they occur frequently in quantum-mechanical systems (Magunov *et al.*, 2003; Raoult and Mies, 2004).

Finally, we discuss the interaction between two Fano resonances (Hino, 2001; Miroshnichenko, 2009c), which can be employed to stop and store light coherently, with an all-optical adiabatic and reversible pulse bandwidth compression process (Yanik and Fan, 2004; Yanik *et al.*, 2004). Such a process overcomes the fundamental bandwidth delay constraint in optics and can generate arbitrarily small group velocities for any light pulse with a given bandwidth, without any coherent or resonant light-matter interaction. The mechanism can be realized in a system consisting of a waveguide side coupled to tunable resonators, which generates a photonic band structure that represents a classical EIT analog (Yanik *et al.*, 2004; Maes *et al.*, 2005).

G. Guided resonances in photonic crystal slabs

Scattering of light by photonic crystal slabs leads to another class of Fano resonances associated with the presence of guided resonances in periodic structures. A photonic crystal slab consists of a two-dimensional periodic-index contrast introduced into a high-index guiding layer Fig. 26(a). Such modulated structures support in-plane guided modes that are completely confined by the slab without any coupling to external radiation. In addition to in-plane waveguiding, the slabs can also interact with external radiation in a complex and interesting way (Fan and Joannopoulos, 2002; Fan *et al.*, 2003; Koshino, 2003). Of particular importance is the presence of guided resonances in the structures. Guided resonances can provide an efficient way to channel light from within the slab to the external environment. In addition, guided resonances can significantly affect the transmission and reflection of external incident light, resulting in complex resonant line shapes which can be linked to Fano resonances.

Fan and Joannopoulos (2002) calculated the transmission and reflection coefficients at various k points for the structure shown in Fig. 26(a). The calculated spectra for s-polarized incident waves are shown in Figs. 26(b) and 26(c). The spectra consist of sharp resonant features superimposed upon a smoothly varying background. The background resembles Fabry-Perot oscillations when light interacts with a uniform dielectric slab. To clearly see this, the background is fitted to the spectra of a uniform slab, which are shown as dashed lines in Figs. 26(b) and 26(c). The uniform slab has the same thickness as the photonic crystal. Resonances can be described by employing the Fano-type formulas, with the effective dielectric constant as the only fitting parameter. The fitting agrees well with the numerical simulations [see also Koshino (2003)].

By introduction of a nonlinear layer into the slab with a periodic lateral structure, we can generate a bistable transmission for significant intensity ranges due to Fano resonances and achieve a strong frequency-dependent transparency variation related to the transfer via guided modes. A self-consistent simulation tool which allows for the computation of multivalued transmission was developed by Lousse and Vigneron (2004). It explained the peculiar shape of the hysteresis loops associated with nonlinear Fano resonances.

Complex resonant line shapes due to Fano resonances have been observed experimentally in several settings (Grillet *et al.*, 2006; Harbers *et al.*, 2007; Qiang *et al.*, 2008; Yang *et al.*, 2008; Chen *et al.*, 2009). In particular, Grillet *et al.* (2006) observed Fano resonances in the optical transmission spectrum of a chalcogenide glass photonic crystal membrane and first demonstrated the suppression of optical transmission by over 40 dB, the strongest reported so far, and a remarkable result for a dielectric structure with a thickness of only 330 nm. These results will allow further progress toward the engineering of very sharp resonances and, combined with the large intrinsic nonlinearity of the chalcogenide glasses, should allow for the observation of optical bistability in a photonic crystal mirror.

Recently it was experimentally demonstrated that the shape of the Fano resonance in light scattering by a high-Q planar photonic-crystal nanocavity can be controlled by variation of the waste of the Gaussian beam (Galli *et al.*, 2009). For a tightly focused beam with a spot diameter $d_1 \approx 2\ \mu$m, a strong asymmetric Fano resonance was observed with the asymmetry parameter $q_1 = -0.348$ [see Fig. 27(a)]. On the other hand, for a slightly defocused Gaussian beam with the spot diameter $d_2 \approx 10\ \mu$m, a symmetric Fano resonance was observed with $q_2 = -0.016$ [see Fig. 27(b)]. In this geometry, the light reflected from the nanocavity mimics the scattering through a discrete level, while the light reflected from the photonic crystal pattern can be considered as scattering to the continuum. The interference of these two reflected components leads to the Fano resonance.

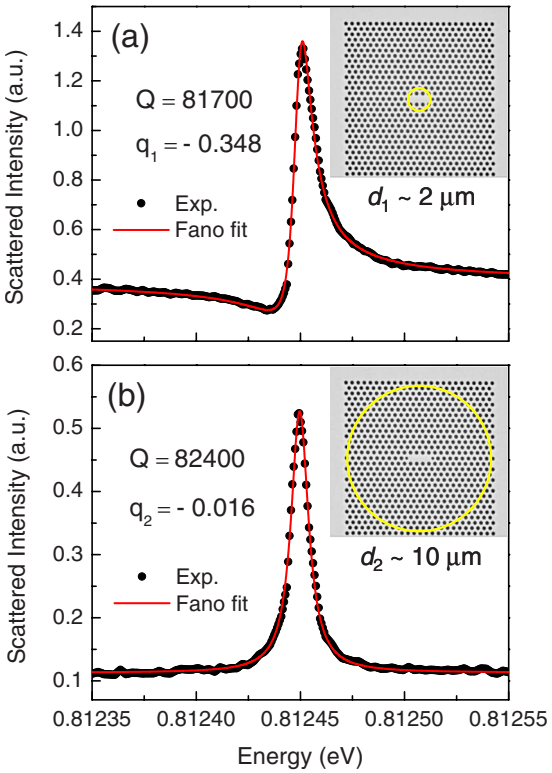

FIG. 27. (Color online) Measured scattering spectra (dots) and fitting by the Fano formula (solid lines) of a photonic crystal nanocavity for two different excitation conditions: (a) a tightly focused and (b) a slightly defocused laser beam of diameters d_1 and d_2, respectively, indicated by circles. Note that the actual profiles are inverted ones because of the use of cross-polarized detection. From Galli *et al.*, 2009.

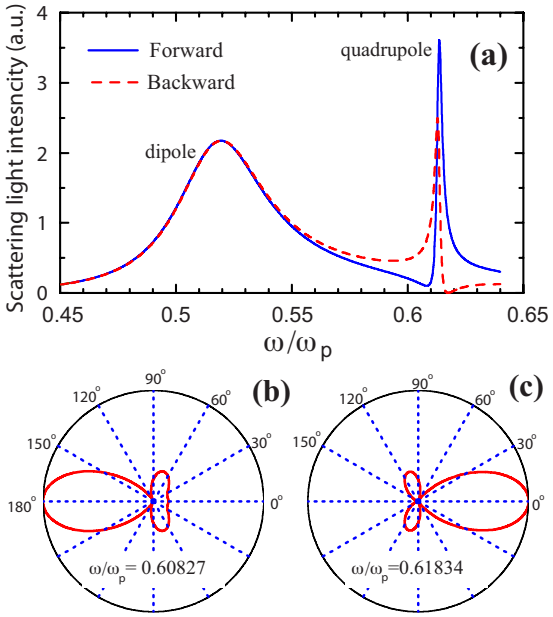

FIG. 28. (Color online) Exact Mie solution of the light scattering by a plasmonic nanoparticle. The radius of the nanoparticle is much smaller than the light wavelength $a/\lambda=0.083$. (a) Frequency dependence of the scattering light intensity in the vicinity of the dipole and quadrupole resonances. In the latter case both forward- (solid lines) and backward- (dashed lines) scattering profiles exhibit asymmetric Fano resonances. (b) and (c) The angular dependence of the light scattering in the vicinity of the quadrupole resonance. The plasmonic frequency is normalized to $\omega_p a/c=1$. Adapted from Luk'yanchuk *et al.*, 2008.

The variation in the Fano profile with increase of the excitation area can be understood as an enhancement of the scattering to the continuum, leading to a decrease in the asymmetry parameter q. Indeed, the variation in the asymmetry parameter $q_1/q_2\sim 22$ is proportional to the variation of the excitation areas $(d_2/d_1)^2\sim 25$. Thus, by changing the excitation conditions it is possible to tune the Fano resonance in the scattering by a photonic crystal nanocavity.

H. Light scattering by spherical nanoparticles

Light scattering by an obstacle is one of the fundamental problems of electrodynamics; see, e.g., the monographs by van der Hulst (1981), Bohren and Huffman (1998), and Born and Wolf (1999). It was first described by Lord Rayleigh and is characterized by a sharp increase in scattering intensity with increasing light frequency (Rayleigh, 1871a, 1871b, 1871c). It is used to explain why we can enjoy the blue sky during daytime (the intensely scattered blue component of the sunlight) and scarlet sunrises and sunsets at dawn and dusk (the weakly scattered red component). Rayleigh's studies were generalized by Gustav Mie, who obtained the complete analytical solution of Maxwell's equations for the scattering of electromagnetic radiation by a spherical particle valid for any ratio of diameter to wavelength (Mie, 1908).

A common assumption is that the general Mie solution transforms into that of Rayleigh when particles are small. However, recent studies of resonant scattering by small particles with weak dissipation rates (Bashevoy *et al.*, 2005; Tribelsky and Luk'yanchuk, 2006) revealed new and unexpected features, namely, giant optical resonances with an inverse hierarchy (the quadrupole resonance is much stronger than the dipole one, etc.), a complicated near-field structure with vortices, and unusual frequency and size dependencies, which allow such scattering to be called anomalous. Tribelsky *et al.* (2008) described that the physical picture of this anomalous scattering is analogous to the physics of Fano resonances. This analogy sheds new light on the phenomenon. It allows employment of the powerful methods developed in the theory of Fano resonances (such as the Feshbach-Fano partitioning theory) to describe resonant light scattering. It also easily explains certain features of the anomalous scattering and related problems, namely, sharp changes in the scattering diagrams upon small changes in ω (see Fig. 28). Tribelsky *et al.* (2008) analytically obtained an asymmetric profile of the resonance lines by analyzing the exact Mie solution of the light scattering by a spherical nanoparticle (Miroshnichenko *et al.*, 2008).

Figure 28 shows light scattering by a potassium colloidal nanoparticle immersed in a KCl crystal, calculated with a realistic dependence $\epsilon(\omega)$ and fitting actual experimental data (Luk'yanchuk *et al.*, 2008; Tribelsky *et al.*, 2008). A slight variation in the incident light frequency in the vicinity of the quadrupole resonance drastically changes the scattering pattern (see Fig. 28), resulting in asymmetric Fano-like profiles for intensities of the forward- and backward-scattered light. In this case, excited localized plasmons (polaritons) are equivalent to the discrete levels in Fano's approach, while the radiative decay of these excitations is similar to the tunneling to the continuum. In general, it may lead to a significant suppression of the scattering along any given direction (Miroshnichenko, 2009b). Note that, in accordance with the theoretical expression obtained from the Mie formula, the points of destructive interference for the forward and backward scattering lie on different sides of the corresponding resonant peaks.

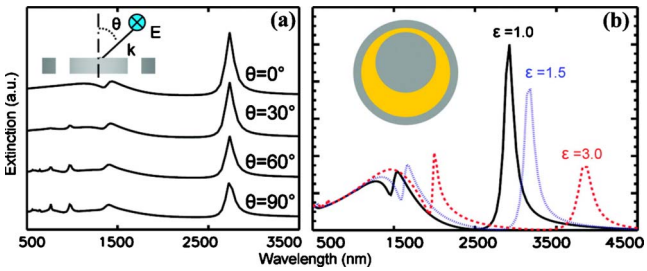

FIG. 29. (Color online) A metallic nanostructure consisting of a disk inside a thin ring supports superradiant and very narrow subradiant modes. Symmetry breaking in this structure enables a coupling between plasmon modes of differing multipolar order, resulting in a tunable Fano resonance: (a) extinction spectra as a function of incident angle θ; (b) the impact of filling the cavity with a dielectric material on the extinction spectrum or permittivity ϵ=1 (solid line), 1.5 (dashed line), and 3 (dotted line). Adapted from Hao *et al.*, 2008.

I. Plasmonic nanocavities and tunable Fano resonance

Recent progress in the fabrication and visualization of nanosized structures gave rise to the novel and rapidly emerging field of nanoplasmonics. The optical properties of metals are governed by coherent oscillations of conduction-band electrons, known as plasmons (Bohm and Pines, 1951). The interaction between light and metallic nanoparticles is dominated mostly by charge-density oscillations on the closed surfaces of the particles, called localized surface plasmon (LSP) resonances. The studies of LSPs in noble-metal nanoparticles, such as gold and silver, extended applications from various surface-enhanced spectroscopies (Moskovits, 1985) to novel nanometer optical devices and waveguides (Barnes *et al.*, 2003; Ozbay, 2006). One of the most important properties of LSPs is the possibility of strong spatial localization of the electron oscillations, combined with their high frequencies varying from uv to ir ranges. LSPs have the ability to strongly scatter, absorb, and squeeze light on nanometer scales, producing large enhancement of electromagnetic field amplitudes. Such unique properties of nanomaterials are essential for the development of novel material functions with potential technological and medical applications with specific optical, magnetic, and reactivity properties.

Plasmonic nanostructures can be considered as a physical realization of coupled oscillator systems at the nanoscale. The energies and linewidths of the LSPs depend mostly on the nanoparticle geometries, such as size and shape. Thus, the spectral tunability of LSPs has been widely investigated. As suggested by Hao *et al.* (2007), promising geometries for fine tuning are rings and disks. In such structures the dipolelike resonance can be tuned into the near-infrared region by changing the width of the metallic ring, for example. One important issue of nanoplasmonics is the effect of symmetry breaking, which allows us to excite higher-order multipolar modes, leading to larger electromagnetic field enhancements. Symmetry breaking can be easily achieved in metallic ring or disk cavity structures by displacement of the disk with respect to the center of the ring. The plasmon resonances of a ring or disk cavity system can be understood in terms of the interaction or hybridization of the single ring and disk cavity plasmons. This hybridization leads to a low-energy symmetric plasmon and high-energy antisymmetric plasmon (Hao *et al.*, 2007). The latter is superradiant, i.e., it strongly radiates, because disk and ring dipolar plasmons are aligned and oscillate in phase. The low-energy symmetric plasmon is subradiant because of opposite alignment of dipolar moments. It turns out that in a symmetry-broken structure the quadrupole ring resonance couples to the superradiant high-energy antisymmetric disk-ring dipole mode (Hao *et al.*, 2008). The direct coupling interferes with the dispersive coupling between the quadrupolar ring mode and the superradiant mode, resulting in a Fano resonance in the extinction spectrum (see Fig. 29). By variation of the incident angle, the shape of the Fano resonance can be altered from asymmetric to symmetric.

Other examples of nanoplasmonic structures supporting the asymmetric Fano resonance are metallic nanoshells near a metallic film (Le *et al.*, 2007) and heterogeneous dimers composed of gold and silver nanoparticles (Bachelier *et al.*, 2008). Both structures have a highly tunable plasmonic Fano resonance, accompanied by large local electric field enhancement (Hao *et al.*, 2009; Mirin *et al.*, 2009; Verellen *et al.*, 2009). Thus, the strong response of LSP resonances may be effectively used for biological and medical sensing applications.

A novel type of nonlinear Fano resonance has been found in hybrid molecules composed of semiconductor and metal nanoparticles (Zhang *et al.*, 2006). The latter support surface plasmons with a continuous spectrum, while the former support discrete interband excitations. Plasmons and excitons become strongly coupled via Förster energy transfer. At high light intensities, the absorption spectrum demonstrates a sharp asymmetric profile, which originates from the coherent interparticle Coulomb interaction and can be understood in terms of a nonlinear Fano resonance.

J. Extraordinary transmission of light through metallic gratings

Scattering by metallic gratings has been the subject of extensive research for over a century. One important early achievement of the optics of metallic gratings was the discovery and understanding of Wood's anomalies (Wood, 1902, 1935; Rayleigh, 1907). One type of anomaly is due to the excitation of surface plasmon-polaritons propagating on the metallic surface. Another is the diffraction anomaly when a diffracted order becomes tangential to the plane of the grating. It is characterized by a rapid variation in the diffracted order intensity, corresponding to the onset or disappearance of a particular spectral order (Wood, 1935). This resonant behavior of the Wood's anomaly can be understood in terms of the coupling of the incoming waves with the surface-bound states of periodic arrays (Fano, 1936, 1937, 1938, 1941; Hessel and Oliner, 1965; Neviere *et al.*, 1973; Magnusson and Wang, 1992). Thus, by considering a surface-bound state as a discrete level and scattered waves as a continuum, Wood's anomaly can be interpreted as a Fano resonance (Abdulhalim, 2009; Billaudeau *et al.*, 2009).

It was demonstrated that for a periodic thin-film metallic grating, formed from a two-dimensional array of holes, the transmitted fraction of incident light can exceed the open fraction of the array for certain wavelengths (Ebbesen *et al.*, 1998; Ghaemi *et al.*, 1998). The enhancement in the transmitted zero-order beam is reported to be several orders of magnitude larger than that from a pure metallic slab without holes. This phenomenon has been called extraordinary transmission through periodic arrays of subwavelength holes in metallic films.

The common understanding of extraordinary transmission is that it is due to a resonant excitation of surface plasmon polaritons by incoming radiation (Ghaemi *et al.*, 1998; van der Molen *et al.*, 2005). In addition to the resonant enhancement of the transmission, resonant suppression was observed as well. It was demonstrated that these transmission minima correspond exactly to loci of Wood's anomaly (Ghaemi *et al.*, 1998); see Fig. 30. According to experimental observations, each extraordinary transmission is accompanied by resonant suppression of transmission, resulting in asymmetric line shapes, which can be perfectly fitted by the Fano formula (de Abajo, 2007). Moreover, it was theoretically demonstrated by Spevak *et al.* (2009) that periodically modulated ultrathin metal films may exhibit resonant suppression of the transmittance, emphasizing the Wood's anomaly effect. Thus, the extraordinary resonant scattering of light by modulated metal films can be described in terms of the Fano resonance, revealing the interference nature of the phenomenon.

Kobyakov *et al.* (2009) suggested the use of active layers to simultaneously enhance both transmittance and reflectance at the resonance in subwavelength periodic planar bimetallic grating by excitation of gain-assisted surface plasmons.

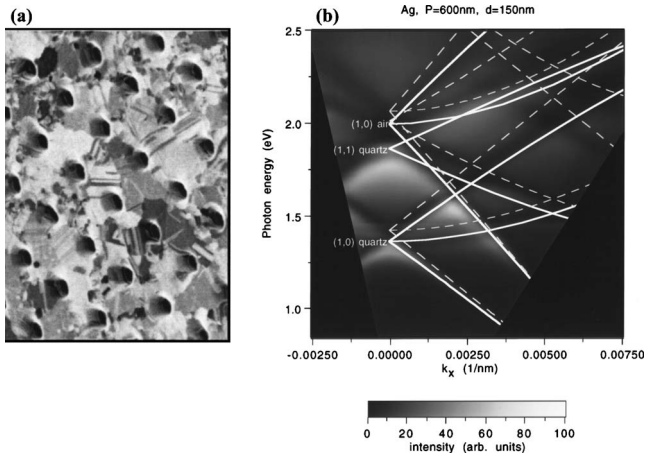

FIG. 30. Light scattering by metallic gratings. (a) Focused ion beam image of a two-dimensional hole array in a polycrystalline silver film. (b) Observed transmission intensity as a function of photon energy and k_x with predicted energy dispersion of surface plasmon-polaritons (solid) and loci of Wood's anomaly (dashed lines). From Ghaemi *et al.*, 1998.

K. Resonant four-wave-mixing-induced autoionization

Four-wave mixing involves the interaction of three laser beams to produce a nonlinear polarization via the cubic electric susceptibility $\chi^{(3)}$. The induced polarization acts as the source of a fourth coherent light beam, detected as the signal. Four-wave mixing can be considered as the formation of and scattering from laser-induced gratings. The grating is formed by two laser beams, called grating beams, with wave vector $\mathbf{k}_g$. The third probe beam with the wave vector $\mathbf{k}_p$ is then scattered off the laser-induced grating and produces the fourth scattered beam, which is detected as the four-wave-mixing signal. Because of energy conservation, the frequency of the signal beam must be equal to the frequency of the probe beam $\omega_s \equiv \omega_p$. Momentum conservation results in a phase-matching condition for the signal wave vector,

$$|\mathbf{k}_s| = |\mathbf{k}_{g_1} - \mathbf{k}_{g_2} + \mathbf{k}_p| = \omega_p/c, \tag{45}$$

and the Bragg-scattering angular condition,

$$\frac{\omega_p}{\omega_g} = \frac{\sin(\theta_g/2)}{\sin(\theta_{p-s}/2)}, \tag{46}$$

where θ_g is the angle between two grating beams and θ_{p-s} is the angle between the probe and signal beams (see Fig. 31).

In general, the four-wave-mixing process can take place in any material. When the frequency of the incident laser beams matches the transition resonances of the medium, a drastic enhancement of the signal intensity can be observed. Such processes are called resonant four-wave mixings (RFWMs), and they are used as spectroscopic and diagnostic tools for probing stable and transient molecular species. Armstrong and Wynne (1974) experimentally studied four-wave mixing involving an autoionizing resonance in an alkali-metal atomic

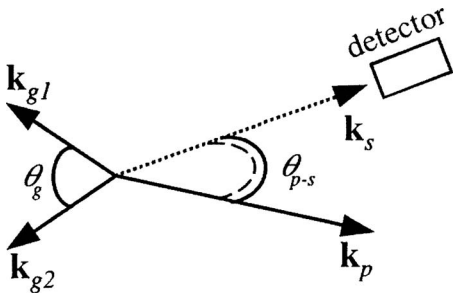

FIG. 31. Planar wave-vector diagram illustrating the phase-matching condition for RFWM. From Teodoro and McCormack, 1999.

vapor. In their experiment, a two-photon transition between two bound states of the metal was excited, followed by a single-photon absorption to the autoionizing level. The detected signal demonstrated a characteristic asymmetric response. Using the Fano formalism, they derived an expression for the line shape and fitted it with the Fano formula (Armstrong and Wynne, 1974), which allows the width and asymmetry parameter for the autoionizing states to be obtained (Armstrong and Beers, 1975; Crance and Armstrong, 1982a, 1982b; Agarwal and Lakshmi, 1983; Alber and Zoller, 1983; Haan and Agarwal, 1987; Meier *et al.*, 1995). Thus, this form of RFWM can be considered as one of the techniques to study autoionizing levels.

A double-resonance version of RFWM is called two-color RFWM (TCRFWM) and takes place when two optical fields have frequencies in resonance with two different transitions. It yields a variety of excitation schemes, which are useful for high-resolution spectroscopy. In Fig. 32 possible TCRFWM excitation schemes are shown, where the grating beams are in resonance with the lower transition and the probe is tuned to the upper transition [see Fig. 32(a)], and vice versa [see Fig. 32(b)]. Because of the presence of autoionizing states in the overall FWM process, in both cases TCRFWM exhibits asymmetric profiles, which can be approximated by the Fano formula [see Fig. 32(c)]. Unlike the Fano profile, the TCRFMW spectral lines have no exact zeros. This can be explained using the dephasing during nonlinear parametric conversions, which is a key difference from the usual Fano resonance case. Nevertheless, TCRFMW provides an efficient way to coherently control the signal line shape (McCormack *et al.*, 1998).

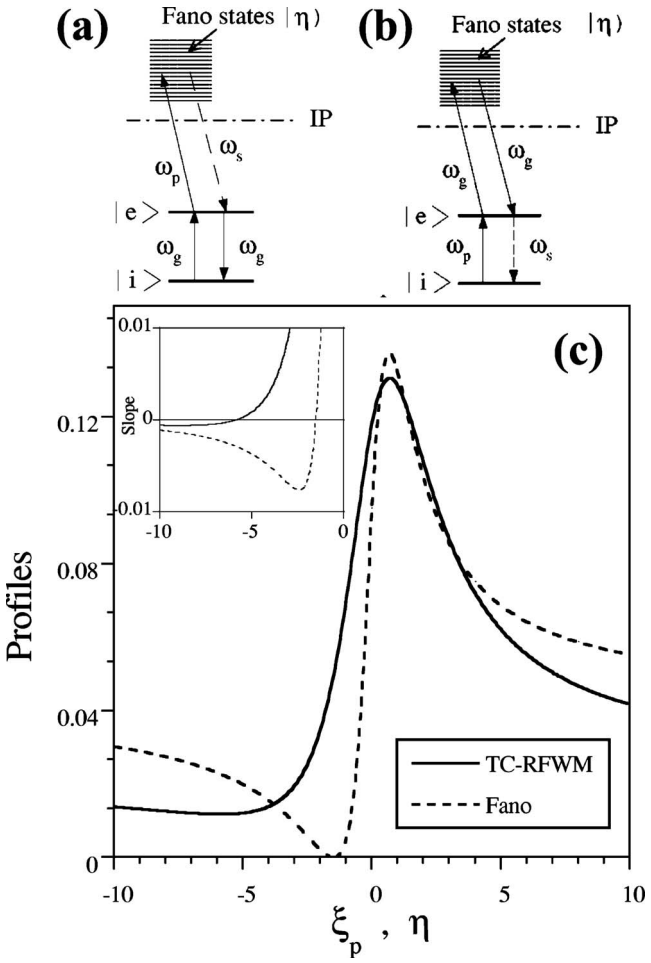

FIG. 32. Two-color resonant four-wave mixing. (a) Nonparametric and (b) parametric TCRFWM process. The autoionizing level (Fano state) above the ionization potential is indicated by $|\eta\rangle$. $|i\rangle$ and $|e\rangle$ are ground and intermediate states, respectively. (c) TCRFWM and Fano profiles. Inset: the slopes of two profiles. Note the separation between the slope zeros which correspond to profile minima. From Teodoro and McCormack, 1998.

VI. CHARGE TRANSPORT THROUGH QUANTUM DOTS

In recent decades, charge transport through quantum dots (QDs) has been extensively studied both theoretically and experimentally (Altshuler *et al.*, 1991; Kastner, 1992; Koch and Lübbig, 1992; Reimann and Manninen, 2002; Katsumoto, 2007; Hanson *et al.*, 2007). One of the reasons for that interest is the further miniaturization of electronic device components. A comprehensive picture of a large variety of underlying physical phenomena has emerged [see, e.g., Alhassid (2000) and Aleiner *et al.* (2002), and references therein]. The finite size of the dot is responsible for a dense but discrete set of single-particle levels. Confinement of electrons in small quantum dots leads to the necessity of taking into account their Coulomb repulsion. As a result, at temperatures below the charging energy the Coulomb blockade emerges (Alhassid, 2000; Aleiner *et al.*, 2002). At even lower temperatures, the phase coherence of the excitations in the quantum dot is preserved during scattering, and additional interference phenomena appear, depending on the coupling strength to the leads. In view of the enormous literature available, we introduce the main physics and focus on results that are directly related to the finding of destructive interferences and Fano resonances.

A. From a single-electron transistor to quantum interference

A quantum dot is a small confinement region for electrons (typically almost two dimensional) with leads

coupled to it. The manufacturing of a large variety of geometries is easily possible. In the simplest case, two leads are used, and a voltage V is applied, resulting in a current of electrons which enter the dot through one lead and eventually exit into the second lead. Various gate voltages can be additionally applied, e.g., V_g, which controls the energy of the electrons in the dot relative to the leads, and others which control the strength of the coupling between the leads and the dot. Here we consider only situations where the applied voltage V between the two leads is small so that the energy eV is smaller than all other relevant energy scales. This is also called the equilibrium case, at variance with the nonequilibrium case, which is also frequently studied.

Consider a closed dot with linear size L, when the leads are decoupled. If one neglects the contribution from Coulomb interaction, the spectrum of many-body states in a quantum dot can be obtained from the solution of the single-particle problem. The single-particle level spacing is given by $\Delta_{sp}=\pi\hbar^2/m^*L^2$ (Alhassid, 2000). The effective mass of an electron in GaAs is rather low: $m^*=0.067m_e$ (Alhassid, 2000). For $L=100$ nm one obtains $\Delta_{sp}\approx 2$ K, while for $L=500$ nm the spacing is reduced to $\Delta_{sp}\approx 90$ mK. Addition of one electron to the closed dot therefore leads to an energy increase of the order of Δ_{sp}. Now take the Coulomb interaction into account. If the number of electrons in the dot is N, then the charging energy of adding one additional electron is $E_c\sim Ne^2/L$. Therefore, for large values of N and not too small values of L, $E_c\gg\Delta_{sp}$. Note that typical dot sizes are of the order 100 nm–1 μm. N can vary greatly, with values $N\sim 10^2$–10^3. Characteristic values of the charging energy are in the range $E_c\sim 100$–400 K (12–50 meV). Therefore, for all practical purposes, $E_c\gg\Delta_{sp}$.

The number of electrons in a quantum dot is defined by minimizing the energy of the dot with respect to N. This energy is given by (Alhassid, 2000)

$$E(N)=-NeV_g+N^2e^2/2C, \tag{47}$$

where C is the total capacitance between the dot and its surroundings. Apart from special values of the gate voltage, there will be a given electron number N with the smallest energy, and changing the number of electrons will cost an amount of about one charging energy E_c. For particular values of the gate voltage $V_g^{(n)}$, however, degeneracies between $E(N)$ and $E(N+1)$ appear.

Consider the experimental geometry shown in Fig. 33. If the coupling to the leads is weak enough and the temperature $kT<E_c$, the Coulomb blockade regime sets in. As long as $V_g\neq V_g^{(n)}$, the charging energy prevents lead electrons from entering the dot, and the conductance G is practically zero. However, when $V_g=V_g^{(n)}$, a degeneracy sets in between N- and $(N+1)$-electron states on the dot. Therefore, electrons can pass through the dot one by one, and the conductance takes the universal value $G=2e^2/h$ (here the factor 2 accounts for spin degeneracy). Note that the Coulomb interaction is treated in a mean-field-type way; therefore no phase coherence of the dot electrons is required.

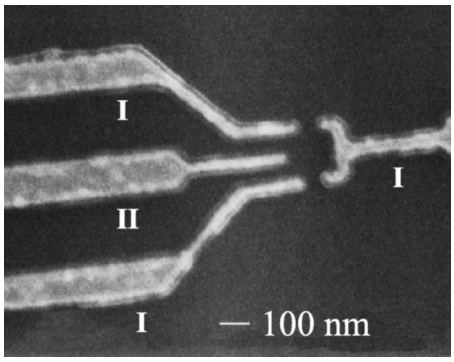

FIG. 33. Electron micrograph of a single-electron transistor based on a GaAs/AlGaAs heterostructure. The split gates (I) define the tunnel barriers and the additional gate electrode (II) adjusts the potential energy on the quantum dot. From Göres *et al.*, 2000.

On further temperature decrease, the phase coherence of the dot electrons becomes essential [see, e.g., Ji *et al.* (2000) and Aikawa *et al.* (2004a, 2004b)]. Note that the typical electron mean free path can be of the order of 10 μm, one to two orders of magnitude larger than the dot size. It may also be possible to reduce *decoherence* effects within some suitable range by *increasing* the coupling of the dot to the leads, which may lead to a shorter residence time of electrons inside the dot and therefore to less scattering. With the option of having several channels that electrons can use to pass through the dot, phase coherence will lead to interference effects and therefore to possible Fano resonances.

If a magnetic field is added, orbital and spin effects have to be considered as well. The Zeeman energy $E_Z=g\mu_BH$ sets another temperature scale. Depending on the Landé factor g, which can vary strongly from sample to sample, the corresponding Zeeman energy E_Z is on the order of 100–200 mK for $B=1$ T. If electrons are allowed to traverse the dot along different paths, an Aharonov-Bohm phase shift ϕ occurs because of the nonzero magnetic flux penetrating the area S enclosed by them (Altshuler *et al.*, 1980): $\phi=(e/h)BS$. With $S=L^2$ we find for $L=100$ nm that $\phi/2\pi=0.38\ B/T$, and for $L=1$ μm that $\phi/2\pi=38\ B/T$.

Therefore, for $L=100$ nm and $B=1$ T, it follows that $E_Z\ll\Delta_{sp}$. Then at low temperatures $kT<E_Z$ of the order of $T\sim 50$–100 mK and at a magnetic field $B\sim 1$ T, the Coulomb-blockaded dot has a well-defined spin: either $|S_z|=1/2$ or $S_z=0$. By changing the gate voltage and reaching the next degeneracy $E(N)=E(N+1)$, an electron with a well-defined spin is allowed to enter the dot—either spin up or spin down. The allowed spin value alternates as one tunes the gate voltage further to the next degeneracy. If the phase coherence of electrons is preserved during the scattering, one may again expect interference phenomena—but this time, depending on the chosen value of V_g, only electrons with spin up (spin down) will interfere along different channels. Increase in

the coupling to the leads may cause spin-selective destructive interference for a given spin species, while the other spin species freely passes through. The orbital effect of the magnetic field leads to an additional phase shift of the order of 0.8π, independent of applied gate voltages.

For $L=1$ μm the single-particle spacing $\Delta_{sp}\approx 20$ mK. Therefore at $B=1$ T it follows that $E_Z \gg \Delta_{sp}$. Then at temperatures $T\sim 50-100$ mK the Coulomb-blockaded dot is magnetized, but electrons that enter the dot can have any spin, preventing spin-selective destructive interference. The orbital effect of the magnetic field is large, with a 2π phase shift every 25 mT upon change in the magnetic field.

Before proceeding, we mention related studies of the Kondo effect in transport through quantum dots. In the Coulomb blockade, the number of electrons on the dot is well defined and either even or odd. Assuming a ground state only, the total electronic spin is either 1/2 (odd number of electrons) or zero (even number). In the absence of a magnetic field and for odd numbers of electrons, the whole dot could be viewed as some magnetic impurity with spin 1/2, which scatters conduction electrons passing from one lead to another. That calls for an analogy with the well-known Kondo effect that is observed in the low-temperature properties of the conductivity of electrons in metals with magnetic impurities (Hewson, 1993). The resistivity in metals usually drops with decrease in temperature since the number of phonons, which are responsible for electron scattering due to electron-phonon interaction, decreases. At around 30 K a minimum in the resistivity appears for some metals, and subsequently the resistivity increases again with further decrease in the temperature. This increase is caused by scattering of electrons by magnetic impurities and originates from an exchange interaction of the conductance-electron spin with the spin of the magnetic impurity. The exchange interaction sets an energy and temperature scale (the Kondo temperature T_K), which is typically of the order of $T_K \sim 100$ mK–1 K, similar to the Zeeman energy of an electronic spin 1/2 in a magnetic field of 1 T. For temperatures $T<T_K$, the impurity spin is screened by a cloud of renormalized conduction electrons. The Kondo temperature depends sensitively on the coupling strength (hybridization) Γ between the conduction electrons and the magnetic impurities. For weak coupling, T_K is exponentially small in $-1/\Gamma$. This analogy led to the idea to observe the Kondo effect in the conductance of electrons through quantum dots. For that, low temperatures have to be used, and the coupling of the leads to the dot has to be increased (in order to increase T_K). An enormous number of theoretical studies have been performed (Aleiner *et al.*, 2002). Experimental results showed a deviation from the Coulomb-blockade regime for strong lead-dot coupling (see below). The relation to theoretical models based on Kondo mechanisms is still debated [see, e.g., Ji *et al.* (2000) and Aleiner *et al.* (2002)].

B. From Coulomb blockade to Fano resonances

A number of experimental studies reported on the observation of Coulomb blockade in various quantum dot realizations on the basis of AlGaAs heterostructures (Cronenwett *et al.*, 1998; Goldhaber-Gordon, Göres, *et al.*, 1998; Goldhaber-Gordon, Shtrikman, *et al.*, 1998; Schmid *et al.*, 1998; Göres *et al.*, 2000; Goldhaber-Gordon *et al.*, 2001; Kobayashi *et al.*, 2002). The charging energies are in the range $E_c\sim 100-300$ K. Temperatures were as low as 30 mK; applied magnetic fields up to 1 T and higher. Therefore, the Zeeman energy E_Z is two to three orders of magnitude lower than the charging energy E_c. The Coulomb blockade is usually observed in the case of weak coupling between the leads and the dot. In Fig. 34 the results of Göres *et al.* (2000) are shown, which correspond to the setup in Fig. 33. For weak lead-dot coupling [Fig. 34(c)] the Coulomb-blockade regime is observed (temperatures are around 100 mK, and the drain-source voltage $V_{ds}\approx 5$ μV$\ll V_g$). With increasing coupling the sharp peak structure is smeared out [Fig. 34(b)], which has been discussed in relation to the Kondo effect. With further increase in the coupling, Fano resonances are observed in the strong-coupling case [Fig. 34(a)]. A fitting yields asymmetry parameters $q=-0.03$ and -0.99 for the center and right resonances, respectively. Note that also the peaks in Fig. 34(c) separating Coulomb blockades with different numbers of electrons on the dot are clearly asymmetric. They also studied the temperature and weak magnetic field dependence of the Fano profiles in the strong-coupling regime for even larger absolute values of the gate voltage, shown in Fig. 35.

The fitting of the resonances in Fig. 35(a) yields an almost linear decrease in the linewidth Γ with temperature, reaching values of 2 meV at 100 mK. The depth of the Fano resonance increases with decreasing temperature, making the Fano resonance sharper and deeper at low temperatures. The Fano resonances show very strong dependence on the value of the weak applied magnetic field [Fig. 35(b)]. Note that the largest applied fields are at 50 mT, which corresponds to a Zeeman energy on the order of 10 mK or less.

The origin of the observed Fano resonances is interference of electrons along several channels (paths) traversing the quantum dot. When the lead-dot coupling is weak, the background conductance is very small [see Fig. 34(c)]. An asymmetric line shape is still observed. The Fano resonance (dip) may either be hard to detect with that background or simply absent since essentially only one path is active. Another possibility is that the antiresonance is extremely narrow (weak coupling to a dot state). Since the Fano resonances are well observed at large lead-dot coupling, phase coherence of electrons passing through the dot is therefore established and is further increased with reduction in temperature.

The dramatic change of the resonance shape at weak magnetic fields is attributed to a suppression of the coupling into the dot states (Göres *et al.*, 2000). That leads to an enhancement of the asymmetry parameter q and

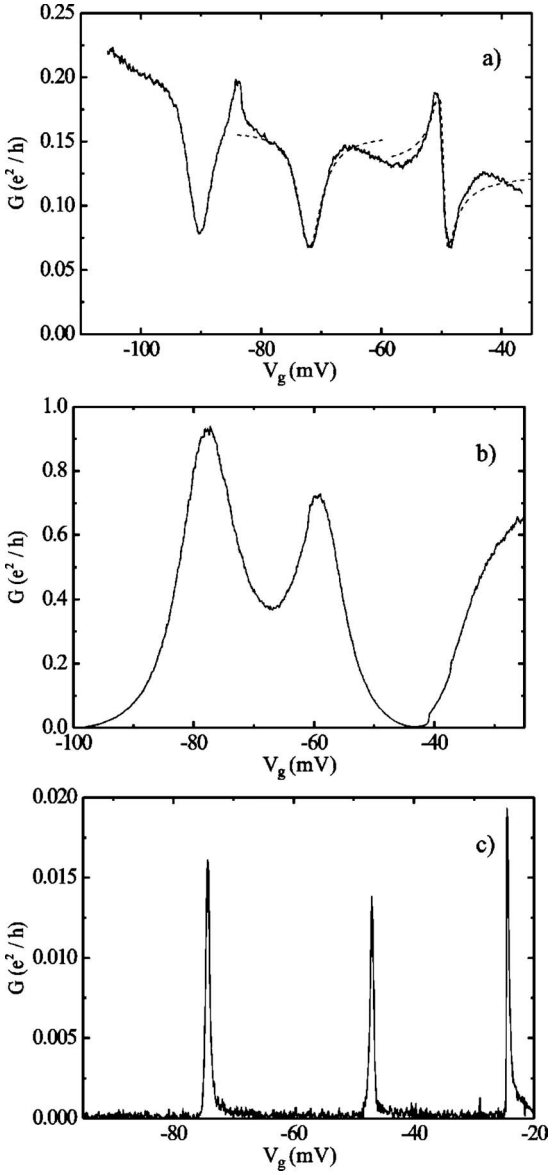

FIG. 34. Conductance vs gate voltage. Comparison of conductance measurements in the (a) Fano regime, (b) intermediate regime, and (c) Coulomb-blockade regime. From (c) to (a) the lead-dot coupling increases. Fits to the Fano formula (1) are shown for the center and right resonances in (a). The respective asymmetry parameters are $q=-0.03$ and -0.99. From Göres *et al.*, 2000.

correspondingly to a shifting of the Fano resonance (dip) out of the window of available gate voltages. An alternative explanation of loss of phase coherence of the traversing electrons does not account for the extremely low-field scale at which the change occurs (Göres *et al.*, 2000). In a similar way, one can exclude orbital Aharonov-Bohm effects, since the expected phase shifts are of the order of $\phi \leqslant 0.12$.

C. From Fano to Aharonov-Bohm interferometers

In the experiments described above, the quantum dot design allowed control of essentially only the lead-dot

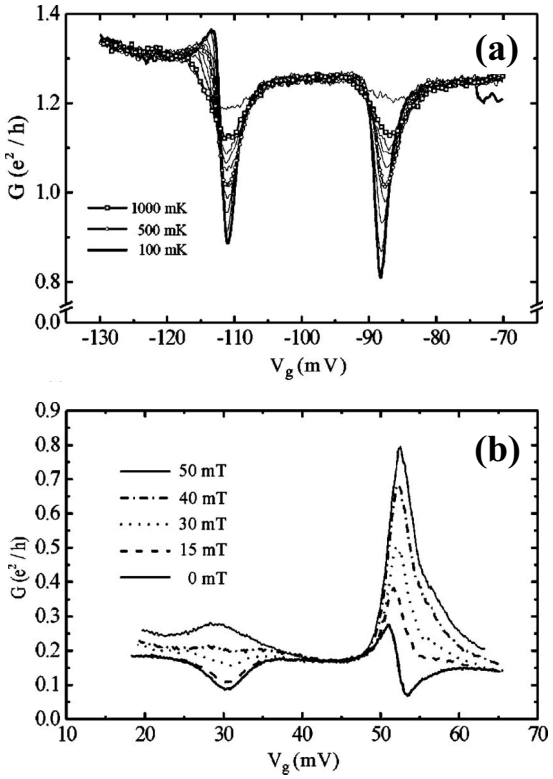

FIG. 35. Conductance vs gate voltage. (a) Temperature dependence of the conductance for two Fano resonances. (b) Conductance as a function of the gate voltage for various magnetic fields applied perpendicular to the two-dimensional electron gas. Adapted from Göres *et al.*, 2000.

coupling. To further advance in the tunability of Fano resonances with quantum dots, interferometer devices have been manufactured. In addition to a small quantum dot, which can be traversed by electrons, a second region (second dot, additional channel, or additional arm) is coupled in a controlled way. Therefore, the coupling to a second channel can be tuned systematically. Of course there may already be several channels involved in the traversing of electrons through the primary dot.

Impressive results were obtained by Johnson *et al.* (2004) in designing a tunable Fano interferometer, which consists of a quantum dot and an additional tunnel-coupled channel (see Fig. 36). A sequence of several Fano resonances was observed and well fitted with the Fano formula (1). Moreover, Johnson *et al.* (2004) performed careful fittings of various resonance shapes as shown in Fig. 37. In Fig. 37(a) another set of resonances is observed. Upon variation in the gate voltage, the asymmetry of the resonance shape clearly changes, as also seen in Fig. 37(e). In addition, the linewidth Γ is changing [Fig. 37(d)]. In another gate voltage window [Fig. 37(f)] these changes are even more drastic. Indeed, the fit yields a change of the sign of q with V_g [Fig. 37(g)]. Note that according to Eq. (1), at $q=0$ a symmetric resonant reflection, with no resonant transmission, is predicted. Indeed, around the value $V_g \approx -1900$ mV the conductance in Fig. 37(f) shows a dip only.

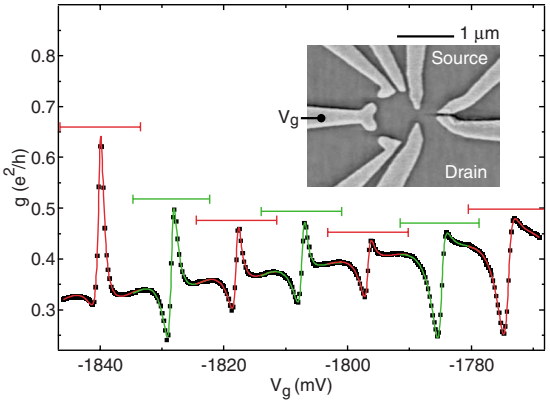

FIG. 36. (Color online) Channel conductance data (squares) and fits (curves) vs gate voltage in the Fano regime. Bars show fitting ranges. Inset: scanning electron microscope image of a similar sample. From Johnson *et al.*, 2004.

Yet another step was taken by Kobayashi *et al.* (2002) with a qualitatively similar geometry but an additional magnetic field penetrating the interferometer area and turning it into an Aharonov-Bohm (AB) device (see Fig. 38). The currents through the quantum dot and the additional arm (channel) can be controlled independently. Magnetic fields were around 1 T. With the arm switched off, a series of Coulomb-blockade peaks is observed (see Fig. 39).

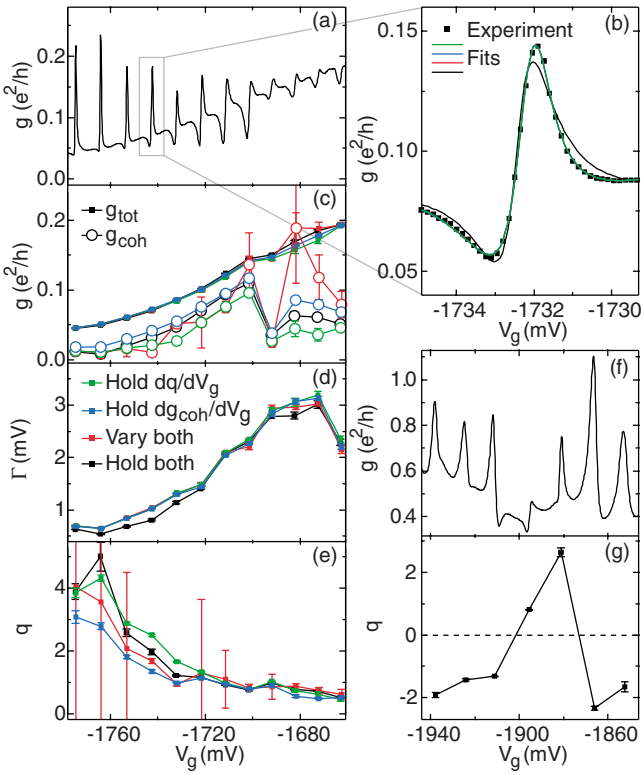

FIG. 37. (Color online) Tunable Fano interferometer. (a) Experimental data with 12 Fano resonances. (b) Fits of one resonance using different fitting parameters. (c)–(e) g_{tot}, g_{coh}, Γ, and q from (a). (f) Data exhibiting reversals of q. (g) Extracted q values. From Johnson *et al.*, 2004.

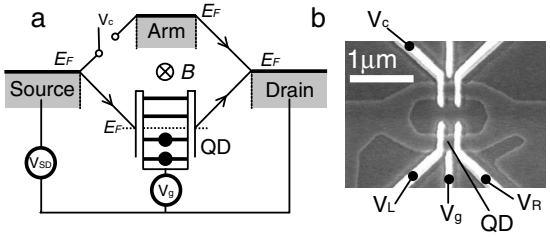

FIG. 38. An Aharonov-Bohm ring with an embedded QD in one of its arms. (a) Schematic representation of the experimental setup. (b) Scanning electron micrograph of the fabricated device. From Kobayashi *et al.*, 2002.

When the arm is made transmittable, clear interference effects are observed through asymmetric Fano line shapes (see Fig. 39). In that system, the discrete level and the continuum are spatially separated, allowing us to control Fano interference via the magnetic field piercing the ring, as shown in Fig. 40. The line shape changes periodically with the AB period ~3.8 mT, which agrees with the expected value using the ring dimension (Kobayashi *et al.*, 2002). As the magnetic field B is swept, an asymmetric line shape with negative q continuously changes to a symmetric one and then to an asymmetric one with positive q. Kobayashi *et al.* (2002) argued that, because of the breaking of time-reversal symmetry in the presence of a magnetic field, the matrix elements defining q are not real as usually assumed, but complex, therefore leading to complex q values. This confirms theoretical investigations for the noninteracting single-particle AB interferometer case (Aharony *et al.*, 2002, 2003; Entin-Wohlman, Aharony, Imry, and Levinson, 2002; Entin-Wohlman, Aharony, Imry, Levinson, and Schiller, 2002; de Guevara *et al.*, 2003; Orellana *et al.*, 2004; Sasada and Hatano, 2005; Malyshev *et al.*, 2006; Gong, Zheng, Liu, Lü, *et al.*, 2008). Note that the discussion above assumed one or several resonances but only one open channel. It has been generalized to the case of one resonance and several open channels, e.g., in Nockel and Stone (1994).

D. Correlations

An enormous amount of theoretical literature is available on various facets of the conductance properties of

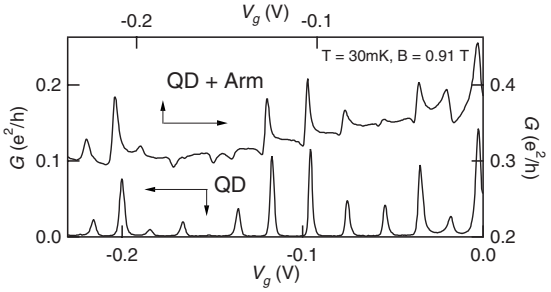

FIG. 39. Coulomb oscillation at V_c=−0.12 V with the arm pinched off and asymmetric Coulomb oscillation at V_c=−0.086 V with the arm transmissible. Here T=30 mK and B=0.91 T. Adapted from Kobayashi *et al.*, 2002.

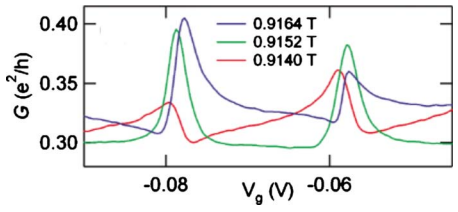

FIG. 40. (Color online) Control of the Fano resonance via magnetic field. Conductance of (a) two Fano peaks at 30 mK and selected magnetic fields, (b) one Fano peak vs V_g and B, (c) same as (b) but for larger windows of V_g variations. The white line represents the AB phase as a function of V_g. From Kobayashi *et al.*, 2002.

quantum dots. We discuss some of these results below. We remind the reader about some characteristic scales. The Coulomb energy (charging energy) of quantum dots is of the order of 50 meV (380 K). The Kondo temperature in a typical metal with magnetic impurities is of the order of 10 μeV (100 mK), comparable to the Zeeman energy of a spin-1/2 electron in a magnetic field of around 1 T. Therefore, when it is operating at temperatures of the order of the Zeeman energy, the charge on a typical quantum dot is extremely well fixed by the number of electrons. The next question is whether a conductance electron, when penetrating the quantum dot, is able to efficiently interact with an excess spin-1/2 particle for odd electron numbers or whether it will usually follow a path that avoids strong exchange interaction. These, partly open, issues make it sometimes hard to judge the relevance of many theories.

The simplest model, which retains the effect of Coulomb interactions and correlations, uses exactly one level from the quantum dot, adds links to leads (left and right), and takes the Coulomb interaction of spin-up and spin-down electrons into account—but only on the dot [see Fig. 41(a)]. Within that frame we study the ballistic transport into and out of the dot. The leads can also be viewed as analogs of detectors in the asymptotic region of a scattering experiment. The resulting Hamiltonian has the following form:

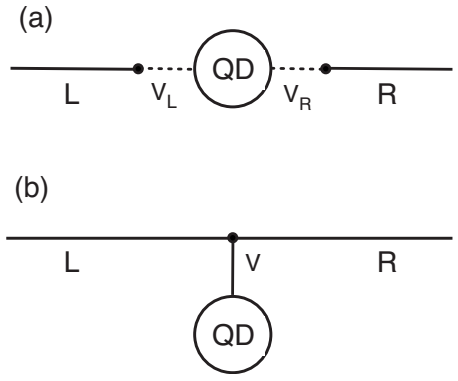

FIG. 41. Typical resonant structures with quantum dots. Schematic representation of (a) a serial model of leads and a quantum dot [Eqs. (48) and (49)], and (b) a T-shaped model of leads and a side-coupled quantum dot [Eq. (50)].

$$H_s = H_D + H_W, \quad H_D = \epsilon_d \sum_\sigma n_\sigma + U n_\uparrow n_\downarrow, \tag{48}$$

$$H_W = \sum_{k\sigma r} \epsilon_{kr} c^\dagger_{k\sigma r} c_{k\sigma r} + (V_r c^\dagger_{k\sigma r} d_\sigma + \text{H.c.}). \tag{49}$$

Here $n_\sigma = d^\dagger_\sigma d_\sigma$ measures the number of electrons on the quantum dot level, which interact with each other with strength U. The left and right leads are denoted by $r = L(R)$. The level energy ϵ_d is measured from the Fermi energy of the leads. The lead states are chosen in the momentum representation. All fermionic creation and annihilation operators c, $c^\dagger$, d, $d^\dagger$ obey the standard anticommutation relations.

E. Interference

There are many ways to incorporate interference and multiple paths in order to reach Fano resonances. One of the simplest ones is a T-shaped scheme, which is a small change of the above model by *side coupling* the quantum dot to the quantum wire (leads) [see Fig. 41(b)]:

$$H_T = -t \sum_{n,\sigma} (c^\dagger_{n,\sigma} c_{n-1,\sigma} + c^\dagger_{n,\sigma} c_{n+1,\sigma}) + \sum_\sigma \epsilon_{d,\sigma} n_\sigma + \sum_\sigma (V d^\dagger_\sigma c_{0,\sigma} + V^\star c^\dagger_{0,\sigma} d_\sigma) + U n_\uparrow n_\downarrow. \tag{50}$$

The lead states are chosen in the coordinate representation. Interference is possible because electrons can directly pass from the left to the right but can also visit the side dot and exit again. These two paths are enough for destructive interference.

Another possibility is to extend the serial dot scheme [Eqs. (48) and (49)] by adding a direct path (arm) for electrons to transit from the left to the right leads (Hofstetter *et al.*, 2001):

$$H_{\text{AB}} = H_s + H_a, \quad H_a = \sum_{kq\sigma} W e^{i\phi} c^\dagger_{k\sigma R} c_{q\sigma L} + \text{H.c.} \tag{51}$$

The phase ϕ models a magnetic flux which is encompassed by the loop of the direct path and the path via the quantum dot.

The Hamiltonians (48)–(50) belong to the class of Anderson Hamiltonians (Anderson, 1961). Thus the thermodynamic properties of both models are similar, e.g., the average number of (spin-up and spin-down) electrons on the dot $\langle n_\sigma \rangle$. However, the transport properties depend crucially on the chosen geometry (Kobayashi *et al.*, 2004; Luo *et al.*, 2004). Note that a change in the dot level ϵ_d is qualitatively similar a variation of the gate voltage of a quantum dot. The dot level is capable of accepting at most one spin-up and one spin-down electron.

Wiegmann and Tsvelick (1983) obtained analytical results for $\langle n_\sigma \rangle$ assuming a linearized spectrum of lead electrons, which is not a crucial constraint, as long as the lead electron bands are partially filled (ideally at half filling), and as long as the temperature is much smaller

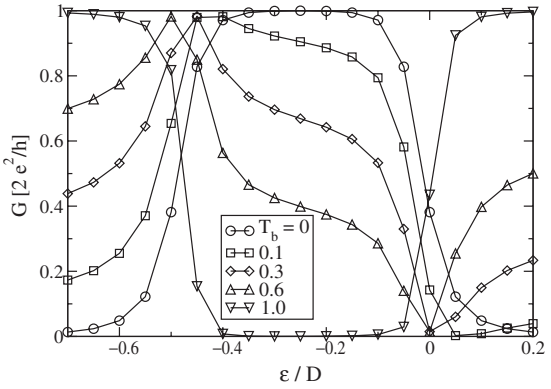

FIG. 42. Conductance as a function of ϵ_d for different values of background transmission T_b. The AB phase $\phi=0$. From Hofstetter *et al.*, 2001.

than the distance from the Fermi energy to the band edges. In addition, there exist various numerical methods to compute $\langle n_\sigma \rangle$ approximately.

With standard scattering matrix approaches, as well as use of the Friedel sum rule (Langreth, 1966; Hewson, 1993), the conductance of the serial dot scheme [Eqs. (48) and (49)] at zero temperature can be expressed as follows (Glazman and Raikh, 1988; Ng and Lee, 1988):

$$g_\sigma = \left(\frac{2V_L V_R}{V_L^2 + V_R^2} \right)^2 \sin^2 \pi \langle n_\sigma \rangle. \tag{52}$$

Hofstetter *et al.* (2001) studied Fano resonances in transport through the AB interferometer model [Eq. (51)] at zero temperature. The schematic view of the AB interferometer is similar to Fig. 38(a). For zero AB phase $\phi=0$ and the direct path switched off, $W=0$, there are three states of a Coulomb blockade to be expected upon variation in the gate voltage ϵ_d: the dot contains either zero, one, or two electrons, with sharp transitions between them. We recall again that the empty dot is almost nonconducting (Coulomb energy too large), and so is the dot filled with two electrons (Pauli principle). When there is one electron on the dot, a second can enter while the first leaves. Despite application of a magnetic field, the model of Eq. (51) is invariant under spin reversal (because the bare dot levels are not Zeeman slit). This may not be easy to achieve in an experiment. Therefore, when there is one electron on the dot, it can have either spin up or spin down, and on average $\langle n_\sigma \rangle = 1/2$ in that case. For $\epsilon_d > 0$ (the Fermi energy is placed at zero) the dot is empty, and the conductance is zero. When $-U < \epsilon_d < 0$, one electron can enter the dot but not two. Then additional electrons can tunnel through, giving maximal conductance. Finally, for $\epsilon_d < -U$, two electrons occupy the dot, and the conductance is zero again. This broad region of almost perfect conductance is due to spin-exchange processes on the quantum dot level and can therefore be related to the Kondo effect discussed above. Indeed, in Fig. 42 this is observed for $T_b=0$, with $T_b = 4x/(1+x)^2$ being the background transmission probability, where $x = \pi^2 W^2 N_L N_R$ and $N_{L,R}$ is the density of states in the left (right) lead. With increasing T_b the curves change dramatically. Most importantly, a Fano resonance appears in the studied energy window, qualitatively similar to experimental observations (Kobayashi *et al.*, 2002; Sato *et al.*, 2005). For the model considered the resonance location is shifting toward $-U/2$, and its width tends to $-U$ as T_b further increases (Fig. 42). A variation in the AB phase ϕ in some intermediate-T_b regime yields the possibility of changing the sign of the asymmetry parameter q.

F. Spin filters

When a magnetic field is applied to the AB interferometer setup in Fig. 38(a), it is reasonable to also consider its action on the quantum dot region itself, which leads to a Zeeman splitting of the dot level. This is incorporated in the side dot model [Eq. (50)] by specifying

$$\epsilon_{d,\uparrow} = \epsilon_d + \Delta/2, \quad \epsilon_{d,\downarrow} = \epsilon_d - \Delta/2, \tag{53}$$

where Δ is the Zeeman energy up to which the single-particle level is slit for spin-down and spin-up electrons. It is easy to incorporate the AB phase shift as well, as we discuss below.

For $U=0$ Eq. (50) is reduced to the Fano-Anderson model [Eq. (6)], and the transmission is computed within the one-particle picture for an electron moving at the Fermi energy ϵ_F:

$$-\epsilon_F \phi_i = t(\phi_{n-1} + \phi_{n+1}) + V^\star \varphi \delta_{n0}, \tag{54}$$

$$-\epsilon_F \varphi = -\epsilon_{d,\sigma} \varphi + V \phi_0, \tag{55}$$

where ϕ_n refers to the amplitude of a single particle at site n in the conducting channel and φ is the amplitude at the side dot. With the help of the Friedel sum rule (Langreth, 1966; Hewson, 1993), one arrives at (Torio *et al.*, 2004)

$$g_\sigma = \cos^2 \pi \langle n_\sigma \rangle. \tag{56}$$

This relation has a geometric origin and actually holds for arbitrary U (at zero temperatures). For a nonzero magnetic field $\Delta \gg \Gamma$ the two Fano resonances for spin-up and spin-down electrons are energetically separated. Therefore, the current through the channel is completely polarized at $\epsilon_F = \epsilon_{d,\uparrow}$ and $\epsilon_F = \epsilon_{d,\downarrow}$. The AB phase can be easily included into the model [Eq. (50)] similar to Eq. (51). Remarkably, it will not change the position of the resonances [cf. also Eq. (9)] since the position of the Fano resonance is entirely determined by the matching condition between the dot level(s) and the Fermi energy.

The spin filter obtained will operate at temperatures $kT \ll \Delta$. For a field of a few tesla that implies temperatures below 100 mK. While that is possible in principle, two more problems appear. First, to control such a spin filter, one would have to control the gate voltage on the scale of μeV (because the spin-polarized Fano resonances are separated in the gate voltage by the same amount of the Zeeman energy). Second, as discussed, Coulomb interactions have to be taken into account.

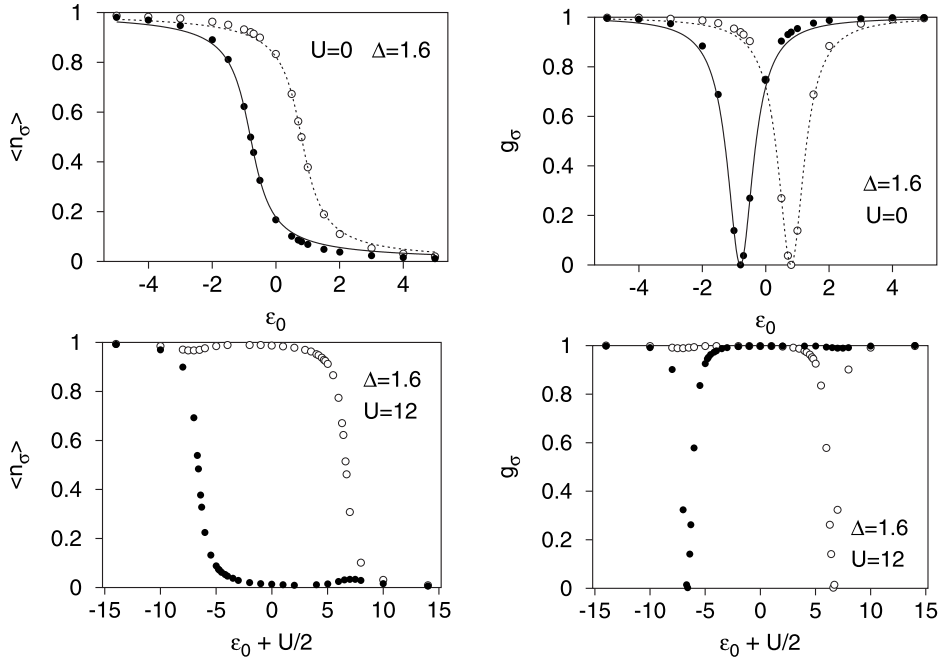

FIG. 43. Spin filter with Fano dot. Left plots: $\langle n_\sigma \rangle$ vs ϵ_d for a finite splitting $\Delta=1.6$, $U=0$ (top) and $U=12$ (bottom). The black (white) dots represent the numerical results for the spin-up (spin-down) occupation number. Right plots: g_σ vs ϵ_d for finite splitting $\Delta=1.6$, $U=0$ (top), and $U=12$ (bottom). The conductance is computed numerically for spin-up (black dots) and spin-down (white dots) electrons. The solid and dashed lines on the top figures represent the exact results of Eq. (56). Adapted from Torio *et al.*, 2004.

For nonzero U and Δ, the results for the mean number of particles on the dot and for the spin-resolved conductance, have been obtained by Torio *et al.* (2004), and are shown in Fig. 43. The main outcome is that the presence of a strong Coulomb interaction shifts the two Fano resonances for spin-up and spin-down electrons further apart. Therefore, the current through the channel is completely polarized at $\epsilon_F=\epsilon_{d,\uparrow}+U$ and $\epsilon_F=\epsilon_{d,\downarrow}$. For $U\gg\Delta$ the distance between the two spin-polarized Fano resonances is of the order of the charging energy (and not the Zeeman energy). At the same time, the Kondo regime is completely suppressed. For $\epsilon_F<\epsilon_{d,\downarrow}$, the dot level is empty, and electrons pass directly from the left to the right lead (background transmission). For $\epsilon_F=\epsilon_{d,\downarrow}$ the dot is opened for spin-down electrons. A Fano resonance appears, and its width is determined solely by $\Gamma=2|V|^2/|v_F|$, where $v_F=d\epsilon/dq|\epsilon_F$ is the Fermi velocity. For $\epsilon_{d,\downarrow}<\epsilon_F<\epsilon_{d,\uparrow}+U$ the dot level is filled with one spin-down electron and does not contribute to the conductance, leading to direct transmission from left to right leads. For $\epsilon_F=\epsilon_{d,\uparrow}+U$ the dot is opened for spin-up electrons. A Fano resonance appears, with the same width as in the previous case. Finally, for $\epsilon_F>\epsilon_{d,\uparrow}+U$, the dot is filled with two electrons and does not contribute to the conductance, leading to direct transmission from left to right leads.

For typical quantum dots with $L\approx100$ nm and $B\approx1$ T, the spin filter effect is expected to be active for temperatures below 100 mK, with a distance between the spin-polarized Fano resonances on the order of 20–50 meV. To observe it, one needs to monitor experimentally the spin-resolved flow of electrons with a spatial resolution smaller than the dot dimension.

G. Perspectives

Gurvitz and Levinson (1993) obtained resonant reflection and transmission within a generalized description of a conducting channel (with several transverse modes) with a single impurity.

Extensions of the theoretical models in order to include many dot levels were performed by Stefanski *et al.* (2004) for very large (0.1 eV) charging energies. Two dots with rather small charging energies (1 meV) were discussed by Stefanski (2003). Some considered the limit $U\to\infty$ (Kang and Shin, 2000; Bulka and Stefanski, 2001; Kang *et al.*, 2001). It remains to be clarified whether such models can be used to discuss temperature effects on transport properties through quantum dots.

Lee and Bruder (2006) extended the spin filter model by inclusion of spin-orbit interactions and extension of the side dot into a side ring with many levels. Song *et al.* (2003) discussed a possible realization of the spin filter in an open quantum dot. Estimates of Kondo temperatures and general temperature effects were discussed by Aligia and Salguero (2004). Lobos and Aligia (2008) included Rashba spin-orbit coupling into the consideration of AB interferometers [see also Sanchez and Serra (2006), Chi *et al.* (2007), Serra and Sánchez (2007), and Gong, Zheng, Liu, Kariuki *et al.* (2008)]. Spin inversion devices in a quasi-two-dimensional semiconductor waveguide under sectionally constant magnetic fields and

spin-orbit interactions were discussed by Cardoso and Pereyra (2008).

Experimental progress was reported by Neel *et al.* (2007) through the contact of the tip of a low-temperature scanning tunneling microscope with individual cobalt atoms adsorbed on Cu(100), where Fano resonances have been observed.

Single-molecule devices have attracted attention recently. In these devices one sandwiches various molecules between gold electrodes and studies their conductance properties. Impressive Fano resonances (with the background transmission dropping by several orders of magnitude) were reported recently by Finch *et al.* (2009). The additional influence of Andreev reflection at low temperatures, when the metallic contacts turn superconducting, was studied by Kormányos *et al.* (2009).

Since Fano resonances rely on the phase coherence of electrons traversing the structure along different paths, several have investigated the influence of phonons on decoherence in quantum dots (Pastawski *et al.*, 2002; Torres *et al.*, 2006). Clerk *et al.* (2001) studied the possibility of extracting phase-decoherence properties from measurements on the q factor of the Fano resonance.

During recent decades, carbon nanotubes have been studied extensively because of their unconventional properties (Saito *et al.*, 1998). For applications to nanoscale electronic devices, researchers have fabricated various forms of carbon nanotubes to engineer their physical properties, including new morphologies such as X- and T-shaped junctions (Terrones *et al.*, 2000). These developments offer interesting opportunities for studying phase-coherent transport in novel geometries. Carbon nanotubes are excellent objects for observing phase-coherence phenomena and Fano effects, and there are many theoretical studies and experimental signatures of the Fano effect in different types of carbon nanotube (Kim *et al.*, 2003, 2005; Yi *et al.*, 2003; Babic and Schonenberger, 2004; Zhang *et al.*, 2004; Hu *et al.*, 2006; Zhang and Chandrasekhar, 2006). In particular, Fano resonances are pronounced in the transport properties of multiply connected carbon nanotubes where a single tube branches into two smaller arms which then merge into one. Both π-bonding and π^*-bonding (π-antibonding) electron transport channels show resonant Fano tunneling through discrete energy levels in the finite arms (Kim *et al.*, 2005).

There are many other systems where Fano resonances have been observed and studied in detail, e.g., for resonant phonon transport caused by nonlocal interaction between two crystalline media in the presence of a weakly bounded intermediate layer (Kosevich, 1997, 2008; Kosevich *et al.*, 2008) or the generalized concept of Mach-Zhender-Fano interferometry in photonic structures (Miroshnichenko and Kivshar, 2009; Wang *et al.*, 2009).

VII. CONCLUSIONS

This review offers a bird's-eye view of Fano resonances in various physical systems. All examples presented here share the same basic feature—coexistence of resonant and nonresonant paths for the scattering waves to propagate. This results in constructive and destructive interference phenomena and asymmetric line shapes, first quantitatively described by Ugo Fano. It turns out to be a common situation in any complex system describing wave propagation, either on a classical footing or on a quantum-mechanical one. This makes the Fano resonance a very generic phenomenon. The characteristic fingerprints of the Fano resonance are usually assumed to be related to an asymmetric profile of a cross section or transmission as a function of some relevant control parameters. A detailed study of the problem shows that symmetric profiles are allowed as well, and therefore a Fano resonance is indicating its presence whenever a resonant suppression of forward scattering (transmission) is observed. This is intimately related to the presence of a quasibound state resonantly interacting with a continuum of scattering states. The pinning down of such a bound state may or may not be an obvious undertaking, depending on the given physical setting. In particular, such quasibound states can be generated by geometrical means and in more complicated settings by many-body interactions. We focused here on the study of Fano resonances in light propagation through artificial nanoscale optical devices and in charge transport through quantum dots. Several other potential applications were discussed as well, touching such areas as superconductivity and Bose-Einstein condensates in optical lattices, among others.

Despite the Fano resonance being caused by interference, we should point out that it is quite different from other interference phenomena, such as, for instance, double-slit experiments or weak localization in disordered media (Gantmakher, 2005). The latter two share the common feature of interference between two open channels (or broad continua), represented by the similar diffraction patterns of the slits in the first case and the identical length of the two counterpropagating paths along a loop in the second. The phase of a scattering wave varies relatively slowly along a continuum. Therefore, for nearly identical continua the phase accumulation during propagation along two paths will be practically the same. Constructive or destructive interference takes place when the sum of these two phases becomes equal to zero or π, and, in general, they are well separated from each other. In the case of a Fano resonance the situation is quite different. Along the discrete-level path, the phase undergoes sharp variations (in comparison with the continuum) with a consequent change of its sign. It results in a very strong asymmetric profile where constructive and destructive interferences are located close to each other. Several detailed examples considered in this review demonstrate that systems which support Fano resonance can be mapped onto the Fano-Anderson model [Eq. (3)]. This model is very simple and provides us with a core understanding of the phenomenon. It can be considered as a guideline for explanation of the Fano resonance in a particular system.

ACKNOWLEDGMENTS

We thank A. Dyugaev, Yu. Ovchinnikov, M. Rybin, and M. Titov for useful discussions and careful reading of parts of the paper. The work was supported by the Australian Research Council through the Discovery and Centre of Excellence projects.

REFERENCES

Abdulhalim, I., 2009, "Optimized guided mode resonant structure as thermooptic sensor and liquid crystal tunable filter," Chin. Opt. Lett. **7**, 667–670.

Agarwal, G. S., and P. A. Lakshmi, 1983, "Effect of spontaneous emission and recombination on the four-wavemixing profiles involving autoionizing resonances," Phys. Rev. A **28**, 3430–3437.

Agrawal, G., 1995, *Nonlinear Fiber Optics* (Academic, San Diego).

Aharony, A., O. Entin-Wohlman, B. I. Halperin, and Y. Imry, 2002, "Phase measurement in the mesoscopic Aharonov-Bohm interferometer," Phys. Rev. B **66**, 115311.

Aharony, A., O. Entin-Wohlman, and Y. Imry, 2003, "Measuring the transmission phase of a quantum dot in a closed interferometer," Phys. Rev. Lett. **90**, 156802.

Aikawa, H., K. Kobayashi, A. Sano, S. Katsumoto, and Y. Iye, 2004a, "Interference effect in multilevel transport through a quantum dot," J. Phys. Soc. Jpn. **73**, 3235–3238.

Aikawa, H., K. Kobayashi, A. Sano, S. Katsumoto, and Y. Iye, 2004b, "Observation of "partial coherence" in an Aharonov-Bohm interferometer with a quantum dot," Phys. Rev. Lett. **92**, 176802.

Alber, G., and P. Zoller, 1983, "Harmonic generation and multiphoton ionization near an autoionizing resonance," Phys. Rev. A **27**, 1373–1388.

Aleiner, I. L., P. W. Brouwer, and L. I. Glazman, 2002, "Quantum effects in Coulomb blockade," Phys. Rep. **358**, 309–440.

Aleshkin, V. Y., A. V. Antonov, L. V. Gavrilenko, and V. I. Gavrilenko, 2007, "Fano resonance study in impurity photocurrent spectra of bulk GaAs and GaAs quantum wells doped with shallow donors," Phys. Rev. B **75**, 125201.

Alhassid, Y., 2000, "The statistical theory of quantum dots," Rev. Mod. Phys. **72**, 895–968.

Aligia, A. A., and L. A. Salguero, 2004, "Magnetotransport through a quantum wire side coupled to a quantum dot," Phys. Rev. B **70**, 075307.

Altshuler, B. L., D. Khmel'nitzkii, A. I. Larkin, and P. A. Lee, 1980, "Magnetoresistance and Hall effect in a disordered two-dimensional electron gas," Phys. Rev. B **22**, 5142–5153.

Altshuler, B. L., P. A. Lee, and R. A. Webb, 1991, *Mesoscopic Phenomena in Solids* (Springer/North-Holland, Amsterdam).

Anderson, P. W., 1961, "Localized magnetic states in metals," Phys. Rev. **124**, 41–53.

Aoki, K., H. Yamawaki, and M. Sakashita, 1996, "Observation of Fano interference in high-pressure ice VII," Phys. Rev. Lett. **76**, 784–786.

Armstrong, J. A., and J. J. Wynne, 1974, "Autoionizing states of Sr studied by the generation of tunable vacuum uv radiation," Phys. Rev. Lett. **33**, 1183–1185.

Armstrong, L., and B. L. Beers, 1975, "Comment concerning the study of autoionizing states using parametric generation," Phys. Rev. Lett. **34**, 1290–1291.

Armstrong, L., C. E. Theodosiou, and M. J. Wall, 1978, "Interference between radiative emission and autoionization in the decay of excited states of atoms," Phys. Rev. A **18**, 2538–2549.

Aubry, S., 1997, "Breathers in nonlinear lattices: Existence, linear stability, and quantization," Physica D **103**, 201–250.

Auger, P., 1925a, "Sur l'effet photoélectrique composé," J. Phys. Radium **6**, 205–208.

Auger, P., 1925b, "Sur les rayons secondaires produit dans un gal par des rayons," Compt. Rend. **180**, 65–68.

Auger, P., 1926, Ann. Phys. (Paris) **6**, 183.

Babić, B., and C. Schonenberger, 2004, "Observation of Fano resonances in single-wall carbon nanotubes," Phys. Rev. B **70**, 195408.

Bachelier, G., I. Russier-Antoine, E. Benichou, C. Jonin, N. D. Fatti, F. Vallée, and P.-F. Brevet, 2008, "Fano profiles induced by near-field coupling in heterogeneous dimers of gold and silver nanoparticles," Phys. Rev. Lett. **101**, 197401.

Bagwell, P. F., and R. K. Lake, 1992, "Resonances in transmission through an oscillating barrier," Phys. Rev. B **46**, 15329–15336.

Bandopadhyay, S., B. Dutta-Roy, and H. S. Mani, 2004, "Understanding the Fano resonance through toy models," Am. J. Phys. **72**, 1501–1507.

Bandrauk, A. D., and J. P. Laplante, 1976, "Fano line shapes in predissociation," J. Chem. Phys. **65**, 2602–2608.

Bar-Ad, S., P. Kner, M. V. Marquezini, S. Mukamel, and D. S. Chemla, 1997, "Quantum confined fano interference," Phys. Rev. Lett. **78**, 1363–1366.

Barnes, W. L., A. Dereux, and T. W. Ebbesen, 2003, "Surface plasmon subwavelength optics," Nature (London) **424**, 824–830.

Bärnthaler, A., S. Rotter, F. Libisch, J. Burgdörfer, S. Gehler, U. Kuhl, and H.-J. Stöckmann, 2010, "Probing decoherence through Fano resonances," Phys. Rev. Lett. **105**, 056801.

Bashevoy, M., V. Fedotov, and N. Zheludev, 2005, "Optical whirlpool on an absorbing metallic nanoparticle," Opt. Express **13**, 8372–8379.

Bechstedt, F., and K. Peuker, 1975, "Theory of interference between electronic and phonon Raman scattering," Phys. Status Solidi B **72**, 743–752.

Becker, U., T. Prescher, E. Schmidt, B. Sonntag, and H. E. Wetzel, 1986, "Decay channels of the discrete and continuum Xe 4*d* resonances," Phys. Rev. A **33**, 3891–3899.

Belitsky, V. I., A. Cantarero, M. Cardona, C. Trallero-Giner, and S. T. Pavlov, 1997, "Feynman diagrams and Fano interference in light scattering from doped semiconductors," J. Phys.: Condens. Matter **9**, 5965–5976.

Bell, M. I., R. N. Tyte, and M. Cardona, 1973, "Resonant Raman scattering in GaP in the $E0-E0+[\mathrm{Delta}]0$ region," Solid State Commun. **13**, 1833–1837.

Beutler, H., 1935, "Über absorptionsserien von argon, krypton und xenon zu termen zwischen den beiden ionisierungsgrenzen $^2P_3^{2/0}$ und $^2P_1^{2/0}$," Z. Phys. A **93**, 177–196.

Bhatia, A. K., and A. Temkin, 1984, "Line-shape parameters for ^1P Feshbach resonances in He and Li^+," Phys. Rev. A **29**, 1895–1900.

Bianconi, A., 2003, "Ugo Fano and shape resonances," AIP Conf. Proc. **652**, 13–18.

Billaudeau, C., S. Collin, F. Pardo, N. Bardou, and J.-L. Pelouard, 2009, "Tailoring radiative and nonradiative losses of thin nanostructured plasmonic waveguides," Opt. Express **17**, 3490–3499.

Binder, P., D. Abraimov, A. V. Ustinov, S. Flach, and Y. Zolotaryuk, 2000, "Observation of breathers in Josephson lad-

ders," Phys. Rev. Lett. **84**, 745–748.
Bloch, I., J. Dalibard, and W. Zwerger, 2008, "Many-body physics with ultracold gases," Rev. Mod. Phys. **80**, 885–964.
Boese, D., M. Lischka, and L. E. Reichl, 2000, "Resonances in a two-dimensional electron waveguide with a single δ-function scatterer," Phys. Rev. B **61**, 5632–5636.
Bohm, D., and D. Pines, 1951, "A collective description of electron interactions: I. Magnetic interactions," Phys. Rev. **82**, 625–634.
Bohren, C. F., and D. R. Huffman, 1998, *Absorption and Scattering of Light by Small Particles* (Wiley, New York).
Born, M., and E. Wolf, 1999, *Principles of Optics* (Cambridge University Press, UK).
Bortchagovsky, E. G., and U. C. Fischer, 2003, "Transmission spectra of systems with thin films: classical analog of the Fano effect," Proc. SPIE **5064**, 47–61.
Boyd, R. W., and D. J. Gauthier, 2006, "Photonics: Transparency on an optical chip," Nature (London) **441**, 701–702.
Bravo-Abad, J., A. Rodriguez, P. Bermel, S. G. Johnson, J. D. Joannopoulos, and M. Soljacic, 2007, "Enhanced nonlinear optics in photonic-crystal microcavities," Opt. Express **15**, 16161–16176.
Breit, G., and E. Wigner, 1936, "Capture of slow neutrons," Phys. Rev. **49**, 519–531.
Bułka, B. R., and P. Stefanski, 2001, "Fano and Kondo resonance in electronic current through nanodevices," Phys. Rev. Lett. **86**, 5128–5131.
Burioni, R., D. Cassi, P. Sodano, A. Trombettoni, and A. Vezzani, 2005, "Propagation of discrete solitons in inhomogeneous networks," Chaos **15**, 043501.
Burioni, R., D. Cassi, P. Sodano, A. Trombettoni, and A. Vezzani, 2006, "Topological filters and high-pass/low-pass devices for solitons in inhomogeneous networks," Phys. Rev. E **73**, 066624.
Cardona, M., 1983, Ed., *Light Scattering in Solids* (Springer, Heidelberg).
Cardona, M., F. Cerdeira, and T. A. Fjeldly, 1974, "Sign of the Raman tensor of diamond and zinc-blende-type semiconductors," Phys. Rev. B **10**, 3433–3435.
Cardoso, J. L., and P. Pereyra, 2008, "Spin inversion devices operating at Fano antiresonances," EPL **83**, 38001.
Cerdeira, F., T. A. Fjeldly, and M. Cardona, 1973a, "Effect of free carriers on zone-center vibrational modes in heavily doped *p*-type Si. II. Optical modes," Phys. Rev. B **8**, 4734–4745.
Cerdeira, F., T. A. Fjeldly, and M. Cardona, 1973b, "Interaction between electronic and vibronic Raman scattering in heavily doped silicon," Solid State Commun. **13**, 325–328.
Chakrabarti, A., 2006, "Electronic transmission in a model quantum wire with side-coupled quasiperiodic chains: Fano resonance and related issues," Phys. Rev. B **74**, 205315.
Chandrasekhar, M., J. B. Renucci, and M. Cardona, 1978, "Effects of interband excitations on Raman phonons in heavily doped *n*-Si," Phys. Rev. B **17**, 1623–1633.
Chen, L., Z. Qiang, H. Yang, H. Pang, Z. Ma, and W. Zhou, 2009, "Polarization and angular dependent transmissions on transferred nanomembrane Fano filters," Opt. Express **17**, 8396–8406.
Chergui, M., N. Schwentner, and V. Chandrasekharan, 1991, "Fano profiles on multiphonon continua in electronic transitions of matrix-isolated NO," Phys. Rev. Lett. **66**, 2499–2502.
Chi, F., J.-L. Liu, and L.-L. Sun, 2007, "Fano-Rashba effect in a double quantum dot Aharonov-Bohm interferometer," J. Appl. Phys. **101**, 093704.
Clark, C. W., 2001, "Obituary: Ugo Fano 1912–2001," Nature (London) **410**, 164.
Clerk, A. A., X. Waintal, and P. W. Brouwer, 2001, "Fano resonances as a probe of phase coherence in quantum dots," Phys. Rev. Lett. **86**, 4636–4639.
Connerade, J. P., 1998, *Highly Excited Atoms* (Cambridge University Press, Cambridge, England).
Cotting, R., J. R. Huber, and V. Engel, 1994, "Interference effects in the photodissociation of FNO," J. Chem. Phys. **100**, 1040–1048.
Cowan, A. R., and J. F. Young, 2003, "Optical bistability involving photonic crystal microcavities and Fano line shapes," Phys. Rev. E **68**, 046606.
Crance, M., and L. Armstrong, 1982a, "Fluorescence induced by resonant multiphoton ionisation near an autoionising state," J. Phys. B **15**, 3199–3210.
Crance, M., and L. Armstrong, 1982b, "Four-wave mixing under double-resonance conditions," J. Phys. B **15**, 4637–4646.
Cronenwett, S. M., T. H. Oosterkamp, and L. P. Kouwenhoven, 1998, "A tunable Kondo effect in quantum dots," Science **281**, 540–544.
Davis, L. C., and L. A. Feldkamp, 1977, "Interaction of many discrete states with many continua," Phys. Rev. B **15**, 2961–2969.
de Abajo, F. J. G., 2007, "*Colloquium:* Light scattering by particle and hole arrays," Rev. Mod. Phys. **79**, 1267–1290.
de Guevara, M. L. L., F. Claro, and P. A. Orellana, 2003, "Ghost Fano resonance in a double quantum dot molecule attached to leads," Phys. Rev. B **67**, 195335.
dell'Orto, T., M. D. Ventra, J. Almeida, C. Coluzza, and G. Margaritondo, 1995, "Evidence for a photocurrent Fano resonance in an artificial nanostructure," Phys. Rev. B **52**, R2265–R2268.
Dixit, S. N., and P. Lambropoulos, 1979, "Line-profile considerations of resonant multiphoton ionization," Phys. Rev. A **19**, 1576–1579.
Druger, S. D., 1977, "Coupling-strength incoherence and the absorption line shape of an isolated resonance in a large molecule," J. Chem. Phys. **67**, 3249–3255.
Dumke, R., T. Müther, M. Volk, W. Ertmer, and G. Birkl, 2002, "Interferometer-type structures for guided atoms," Phys. Rev. Lett. **89**, 220402.
Ebbesen, T., H. Lezec, H. Ghaemi, T. Thio, and P. Wolf, 1998, "Extraordinary optical transmission through sub-wavelength hole arrays," Nature (London) **391**, 667–669.
Efimov, V. N., 1970, "Energy levels arising from resonant two-body forces in a three-body system," Phys. Lett. B **33**, 563–564.
Efimov, V. N., 1971, "Weakly-bound states of three resonantly interacting particles," Sov. J. Nucl. Phys. **12**, 589–595.
Eichmann, U., T. F. Gallagher, and R. M. Konik, 2003, "Fano line shapes reconsidered: Symmetric photoionization peaks from pure continuum excitation," Phys. Rev. Lett. **90**, 233004.
Eiermann, B., T. Anker, M. Albiez, M. Taglieber, P. Treutlein, K.-P. Marzlin, and M. K. Oberthaler, 2004, "Bright Bose-Einstein gap solitons of atoms with repulsive interaction," Phys. Rev. Lett. **92**, 230401.
Eisenberg, H. S., Y. Silberberg, R. Morandotti, A. R. Boyd, and J. S. Aitchison, 1998, "Discrete spatial optical solitons in waveguide arrays," Phys. Rev. Lett. **81**, 3383–3386.
Emmanouilidou, A., and L. E. Reichl, 2002, "Floquet scattering and classical-quantum correspondence in strong time-

periodic fields," Phys. Rev. A **65**, 033405.
Entin-Wohlman, O., A. Aharony, Y. Imry, and Y. Levinson, 2002, "The Fano effect in Aharonov-Bohm interferometers," J. Low Temp. Phys. **126**, 1251–1273.
Entin-Wohlman, O., A. Aharony, Y. Imry, Y. Levinson, and A. Schiller, 2002, "Broken unitarity and phase measurements in Aharonov-Bohm interferometers," Phys. Rev. Lett. **88**, 166801.
Esry, B. D., and C. H. Greene, 2006, "Quantum physics: A menage a trois laid bare," Nature (London) **440**, 289–290.
Fan, S., 2002, "Sharp asymmetric line shapes in side-coupled waveguide-cavity systems," Appl. Phys. Lett. **80**, 908–910.
Fan, S., and J. D. Joannopoulos, 2002, "Analysis of guided resonances in photonic crystal slabs," Phys. Rev. B **65**, 235112.
Fan, S., W. Suh, and J. D. Joannopoulos, 2003, "Temporal coupled-mode theory for the Fano resonance in optical resonators," J. Opt. Soc. Am. A **20**, 569–572.
Fan, S., P. R. Villeneuve, J. D. Joannopoulos, and H. A. Haus, 1998, "Channel drop tunneling through localized states," Phys. Rev. Lett. **80**, 960–963.
Fan, S., P. R. Villeneuve, J. D. Joannopoulos, M. J. Khan, C. Manolatou, and H. A. Haus, 1999, "Theoretical analysis of channel drop tunneling processes," Phys. Rev. B **59**, 15882–15892.
Fano, U., 1935, "Sullo spettro di assorbimento dei gas nobili presso il limite dello spettro d'arco," Nuovo Cimento **12**, 154–161.
Fano, U., 1936, "Some theoretical considerations on anomalous diffraction gratings," Phys. Rev. **50**, 573.
Fano, U., 1937, "On the anomalous diffraction gratings. II," Phys. Rev. **51**, 288.
Fano, U., 1938, "Zur theorie der intensitätsanomalien der beugung," Ann. Phys. **424**, 393–443.
Fano, U., 1941, "The theory of anomalous diffraction gratings and of quasistationary waves on metallic surfaces (Sommerfeld's waves)," J. Opt. Soc. Am. **31**, 213–222.
Fano, U., 1961, "Effects of configuration interaction on intensities and phase shifts," Phys. Rev. **124**, 1866–1878.
Fano, U., 1964, "Exclusion of parity unfavored transitions in forward scattering collisions," Phys. Rev. **135**, B863–B864.
Fano, U., 1965, "Interaction between configurations with several open shells," Phys. Rev. **140**, A67–A75.
Fano, U., 1970, "Quantum defect theory of l uncoupling in H_2 as an example of channel-interaction treatment," Phys. Rev. A **2**, 353–365.
Fano, U., 1977, "Effects of configuration interaction on intensities and phase shifts," Citation Classics **27**, 219 (July 4).
Fano, U., and J. W. Cooper, 1965, "Line profiles in the far-uv absorption spectra of the rare gases," Phys. Rev. **137**, A1364–A1379.
Fano, U., and J. W. Cooper, 1968, "Spectral distribution of atomic oscillator strengths," Rev. Mod. Phys. **40**, 441–507.
Fano, U., and C. M. Lee, 1973, "Variational calculation of R matrices: Application to Ar photoabsorption," Phys. Rev. Lett. **31**, 1573–1576.
Fedotov, V. A., M. Rose, S. L. Prosvirnin, N. Papasimakis, and N. I. Zheludev, 2007, "Sharp trapped-mode resonances in planar metamaterials with a broken structural symmetry," Phys. Rev. Lett. **99**, 147401.
Feneuille, S., S. Liberman, J. Pinard, and A. Taleb, 1979, "Observation of Fano profiles in photoionization of rubidium in the presence of a dc field," Phys. Rev. Lett. **42**, 1404–1406.
Feshbach, H., 1958, "Unified theory of nuclear reactions," Ann. Phys. (N.Y.) **5**, 357–390.
Feshbach, H., 1962, "A unified theory of nuclear reactions. II," Ann. Phys. (N.Y.) **19**, 287–313.
Finch, C. M., V. M. García-Suárez, and C. J. Lambert, 2009, "Giant thermopower and figure of merit in single-molecule devices," Phys. Rev. B **79**, 033405.
Flach, S., V. Fleurov, A. Gorbach, and A. Miroshnichenko, 2006, "Resonant light-light interaction in slab waveguides: Angular filters and spectral hole burning," Proc. SPIE **5975**, 297–306.
Flach, S., V. Fleurov, A. V. Gorbach, and A. E. Miroshnichenko, 2005, "Resonant light scattering by optical solitons," Phys. Rev. Lett. **95**, 023901.
Flach, S., and A. V. Gorbach, 2008, "Discrete breathers: Advances in theory and applications," Phys. Rep. **467**, 1–116.
Flach, S., A. E. Miroshnichenko, and M. V. Fistul, 2003, "Wave scattering by discrete breathers," Chaos **13**, 596–609.
Flach, S., A. E. Miroshnichenko, V. Fleurov, and M. V. Fistul, 2003, "Fano resonances with discrete breathers," Phys. Rev. Lett. **90**, 084101.
Flach, S., and C. R. Willis, 1998, "Discrete breathers," Phys. Rep. **295**, 181–264.
Fleischhauer, M., A. Imamoglu, and J. P. Marangos, 2005, "Electromagnetically induced transparency: Optics in coherent media," Rev. Mod. Phys. **77**, 633–673.
Franson, J. D., and S. M. Hendrickson, 2006, "Optical transparency using interference between two modes of a cavity," Phys. Rev. A **74**, 053817.
Fransson, J., and A. V. Balatsky, 2007, "Exchange interaction and Fano resonances in diatomic molecular systems," Phys. Rev. B **75**, 153309.
Friedl, B., C. Thomsen, and M. Cardona, 1990, "Determination of the superconducting gap in $R\mathrm{Ba}_2\mathrm{Cu}_3\mathrm{O}_{7-\delta}$," Phys. Rev. Lett. **65**, 915–918.
Friedrich, H., and D. Wintgen, 1985a, "Interfering resonances and bound states in the continuum," Phys. Rev. A **32**, 3231–3242.
Friedrich, H., and D. Wintgen, 1985b, "Physical realization of bound states in the continuum," Phys. Rev. A **31**, 3964–3966.
Galli, M., S. L. Portalupi, M. Belotti, L. C. Andreani, L. O'Faolain, and T. F. Krauss, 2009, "Light scattering and Fano resonances in high-Q photonic crystal nanocavities," Appl. Phys. Lett. **94**, 071101.
Gantmakher, V. F., 2005, *Electrons and Disorder in Solids* (Clarendon, Oxford).
Ganz, J., M. Raab, H. Hotop, and J. Geiger, 1984, "Changing the Beutler-Fano profile of the Ne(ns') autoionizing resonances," Phys. Rev. Lett. **53**, 1547–1550.
Gersen, H., T. J. Karle, R. J. P. Engelen, W. Bogaerts, J. P. Korterik, N. F. van Hulst, T. F. Krauss, and L. Kuipers, 2005, "Real-space observation of ultraslow light in photonic crystal waveguides," Phys. Rev. Lett. **94**, 073903.
Ghaemi, H. F., T. Thio, D. E. Grupp, T. W. Ebbesen, and H. J. Lezec, 1998, "Surface plasmons enhance optical transmission through subwavelength holes," Phys. Rev. B **58**, 6779–6782.
Glazman, L. I., and M. E. Raikh, 1988, "Resonant Kondo transparency of a barrier with quasilocal impurity states," JETP Lett. **47**, 452–455.
Glutsch, S., 2002, "Optical absorption of the Fano model: General case of many resonances and many continua," Phys. Rev. B **66**, 075310.
Goldhaber-Gordon, D., J. Göres, M. A. Kastner, H. Shtrik-

man, D. Mahalu, and U. Meirav, 1998, "From the Kondo regime to the mixed-valence regime in a single-electron transistor," Phys. Rev. Lett. **81**, 5225–5228.
Goldhaber-Gordon, D., J. Göres, H. Shtrikman, D. Mahalu, U. Meirav, and M. A. Kastner, 2001, "The Kondo effect in a single-electron transistor," J. Mater. Sci. Eng. B **84**, 17–21.
Goldhaber-Gordon, D., H. Shtrikman, D. Mahalu, D. Abusch-Magder, U. Meirav, and M. A. Kastner, 1998, "Kondo effect in a single-electron transistor," Nature (London) **391**, 156–159.
Gong, W., Y. Zheng, Y. Liu, F. N. Kariuki, and T. Lü, 2008, "Fano effect in a T-shaped double quantum dot structure in the presence of Rashba spin-orbit coupling," Phys. Lett. A **372**, 2934–2940.
Gong, W., Y. Zheng, Y. Liu, and T. Lü, 2008, "A Feynman path analysis of the Fano effect in electronic transport through a parallel double quantum dot structure," Physica E **40**, 618–626.
Göres, J., D. Goldhaber-Gordon, S. Heemeyer, M. A. Kastner, H. Shtrikman, D. Mahalu, and U. Meirav, 2000, "Fano resonances in electronic transport through a single-electron transistor," Phys. Rev. B **62**, 2188–2194.
Grillet, C., D. Freeman, B. Luther-Davies, S. Madden, R. McPhedran, D. J. Moss, M. J. Steel, and B. J. Eggleton, 2006, "Characterization and modeling of Fano resonances in chalcogenide photonic crystal membranes," Opt. Express **14**, 369–376.
Grupp, M., R. Walser, W. P. Schleich, A. Muramatsu, and M. Weitz, 2007, "Resonant Feshbach scattering of fermions in one-dimensional optical lattices," J. Phys. B **40**, 2703–2718.
Gurvitz, S. A., and Y. B. Levinson, 1993, "Resonant reflection and transmission in a conducting channel with a single impurity," Phys. Rev. B **47**, 10578–10587.
Haan, S. L., and G. S. Agarwal, 1987, "Stability of dressed states against radiative decay in strongly coupled bound-continuum transitions," Phys. Rev. A **35**, 4592–4604.
Hänsel, W., P. Hommelhoff, T. W. Hänsch, and J. Reichel, 2001, "Bose-Einstein condensation on a microelectronic chip," Nature (London) **413**, 498–501.
Hanson, R., L. P. Kouwenhoven, J. R. Petta, S. Tarucha, and L. M. K. Vandersypen, 2007, "Spins in few-electron quantum dots," Rev. Mod. Phys. **79**, 1217–1265.
Hao, F., P. Nordlander, M. T. Burnett, and S. A. Maier, 2007, "Enhanced tunability and linewidth sharpening of plasmon resonances in hybridized metallic ring/disk nanocavities," Phys. Rev. B **76**, 245417.
Hao, F., P. Nordlander, Y. Sonnefraud, P. V. Dorpe, and S. A. Maier, 2009, "Tunability of subradiant dipolar and Fano-type plasmon resonances in metallic ring/disk cavities: Implications for nanoscale optical sensing," ACS Nano **3**, 643–652.
Hao, F., Y. Sonnefraud, P. van Dorpe, S. A. Maier, N. J. Halas, and P. Nordlander, 2008, "Symmetry breaking in plasmonic nanocavities: Subradiant LSPR sensing and a tunable Fano resonance," Nano Lett. **8**, 3983–3988.
Harbers, R., S. Jochim, N. Moli, R. F. Mahrt, D. Erni, J. A. Hoffnagle, and W. D. Hinsberg, 2007, "Control of Fano line shapes by means of photonic crystal structures in a dye-doped polymer," Appl. Phys. Lett. **90**, 201105.
Harmin, D. A., 1985, "Asymmetry of field-induced shape resonances in hydrogen," Phys. Rev. A **31**, 2984–2990.
Hase, M., J. Demsar, and M. Kitajima, 2006, "Photoinduced Fano resonance of coherent phonons in zinc," Phys. Rev. B **74**, 212301.
Haus, H. A., and Y. Lai, 1991, "Narrow-band distributed feedback reflector. design," J. Lightwave Technol. **9**, 754–760.
Heinzmann, U., J. Kessler, and J. Lorenz, 1970, "Wavelength dependence of the Fano effect," Phys. Rev. Lett. **25**, 1325.
Heller, D. F., and S. Mukamel, 1979, "Theory of vibrational overtone line shapes of polyatomic molecules," J. Chem. Phys. **70**, 463–472.
Hessel, A., and A. A. Oliner, 1965, "A new theory of Wood's anomalies on optical gratings," Appl. Opt. **4**, 1275–1297.
Hewson, A. C., 1993, *The Kondo Problem to Heavy Fermions* (Cambridge University Press, Cambridge, England).
Hino, K.-i., 2001, "Overlap structure of Fano-resonance profiles of excitons in a semiconductor quantum well," Phys. Rev. B **64**, 075318.
Hino, K.-i., and N. Toshima, 2005, "Spectral modulation of exciton Fano resonance due to Zener breakdown in strongly biased superlattices," Phys. Rev. B **71**, 205326.
Hofstetter, W., J. Konig, and H. Schoeller, 2001, "Kondo correlations and the Fano effect in closed Aharonov-Bohm interferometers," Phys. Rev. Lett. **87**, 156803.
Holfeld, C. P., F. Loser, M. Sudzius, K. Leo, D. M. Whittaker, and K. Kohler, 1998, "Fano resonances in semiconductor superlattices," Phys. Rev. Lett. **81**, 874–877.
Hopfield, J. J., P. J. Dean, and D. G. Thomas, 1967, "Interference between intermediate states in the optical properties of nitrogen-doped gallium phosphide," Phys. Rev. **158**, 748–755.
Hu, F., H. Yang, X. Yang, and J. Dong, 2006, "Electronic transport and Fano resonance in carbon nanotube ring systems," Phys. Rev. B **73**, 235437.
Iwanow, R., R. Schiek, G. I. Stegeman, T. Pertsch, F. Lederer, Y. Min, and W. Sohler, 2004, "Observation of discrete quadratic solitons," Phys. Rev. Lett. **93**, 113902.
Jacobsen, R., A. Lavrinenko, L. Frandsen, C. Peucheret, B. Zsigri, G. Moulin, J. Fage-Pedersen, and P. Borel, 2005, "Direct experimental and numerical determination of extremely high group indices in photonic crystal waveguides," Opt. Express **13**, 7861–7871.
Janzén, E., G. Grossmann, R. Stedman, and H. G. Grimmeiss, 1985, "Fano resonances in chalcogen-doped silicon," Phys. Rev. B **31**, 8000–8012.
Jevons, W., and A. G. Shenstone, 1938, "Spectroscopy: I. Atomic spectra," Rep. Prog. Phys. **5**, 210–227.
Ji, Y., M. Heiblum, D. Sprinza, D. Mahalu, and H. Shtrikman, 2000, "Phase evolution in a Kondo-correlated system," Science **290**, 779–783.
Jin, K.-j., and S. J. Xu, 2007, "Fano resonance in the luminescence spectra of donor bound excitons in polar semiconductors," Appl. Phys. Lett. **90**, 032107.
Jin, K.-j., J. Zhang, Z.-h. Chen, G.-z. Yang, Z. H. Chen, X. H. Shi, and S. C. Shen, 2001, "Phonon-induced photoconductive response in doped semiconductors," Phys. Rev. B **64**, 205203.
Joe, Y. S., A. M. Satanin, and C. S. Kim, 2006, "Classical analogy of Fano resonances," Phys. Scr. **74**, 259–266.
Johnson, A. C., C. M. Marcus, M. P. Hanson, and A. C. Gossard, 2004, "Coulomb-modified Fano resonance in a one-lead quantum dot," Phys. Rev. Lett. **93**, 106803.
Kang, K., S. Y. Cho, J.-J. Kim, and S.-C. Shin, 2001, "Anti-Kondo resonance in transport through a quantum wire with a side-coupled quantum dot," Phys. Rev. B **63**, 113304.
Kang, K., and S.-C. Shin, 2000, "Mesoscopic Kondo effect in an Aharonov-Bohm ring," Phys. Rev. Lett. **85**, 5619–5622.
Kastner, M. A., 1992, "The single-electron transistor," Rev. Mod. Phys. **64**, 849–858.

Katsumoto, S., 2007, "Coherence and spin effects in quantum dots," J. Phys.: Condens. Matter **19**, 233201.
Kessler, J., and J. Lorenz, 1970, "Experimental verification of the Fano effect," Phys. Rev. Lett. **24**, 87–88.
Khelif, A., B. Djafari-Rouhani, J. O. Vasseur, and P. A. Deymier, 2003, "Transmission and dispersion relations of perfect and defect-containing waveguide structures in photonic band gap materials," Phys. Rev. B **68**, 024302.
Kim, B., and K. Yoshihara, 1993, "Multichannel quantum interference in the predissociation of Cs_2: Observation of q-reversal in a complex resonance," J. Chem. Phys. **99**, 1433–1435.
Kim, G., S. B. Lee, T.-S. Kim, and J. Ihm, 2005, "Fano resonance and orbital filtering in multiply connected carbon nanotubes," Phys. Rev. B **71**, 205415.
Kim, J., J.-R. Kim, J.-O. Lee, J. W. Park, H. M. So, N. Kim, K. Kang, K.-H. Yoo, and J.-J. Kim, 2003, "Fano resonance in crossed carbon nanotubes," Phys. Rev. Lett. **90**, 166403.
Kim, S. W., 2002, "Floquet scattering in parametric electron pumps," Phys. Rev. B **66**, 235304.
Kim, S. W., and S. Kim, 2000, "The structure of eigenmodes and phonon scattering by discrete breathers in the discrete nonlinear Schrödinger chain," Physica D **141**, 91–103.
Kim, S. W., and S. Kim, 2001, "Fano resonances in translationally invariant nonlinear chains," Phys. Rev. B **63**, 212301.
Kleinpoppen, H., and M. McDowell, 1976, Eds., *Electron and Photointeraction with Atoms (Festschrift for Professor Ugo Fano)* (Plenum, New York).
Kobayashi, K., H. Aikawa, S. Katsumoto, and Y. Iye, 2002, "Tuning of the Fano effect through a quantum dot in an Aharonov-Bohm interferometer," Phys. Rev. Lett. **88**, 256806.
Kobayashi, K., H. Aikawa, S. Katsumoto, and Y. Iye, 2003, "Mesoscopic Fano effect in a quantum dot embedded in an Aharonov-Bohm ring," Phys. Rev. B **68**, 235304.
Kobayashi, K., H. Aikawa, A. Sano, S. Katsumoto, and Y. Iye, 2004, "Fano resonance in a quantum wire with a side-coupled quantum dot," Phys. Rev. B **70**, 035319.
Kobyakov, A., A. R. Zakharian, K. M. Gundu, and S. A. Darmanyan, 2009, "Giant optical resonances due to gain-assisted Bloch surface plasmons," Appl. Phys. Lett. **94**, 151111.
Koch, H., and H. Lübbig, 1992, Eds., *Single Electron Tunneling and Mesoscopic Devices*, Springer Series in Electronics and Photonics Vol. 31 (Springer, Berlin).
Kokoouline, V., C. Drag, P. Pillet, and F. Masnou-Seeuws, 2002, "Lu-Fano plot for interpretation of the photoassociation spectra," Phys. Rev. A **65**, 062710.
Kolorenč, P., V. Brems, and J. Horacek, 2005, "Computing resonance positions, widths, and cross sections via the Feshbach-Fano R-matrix method: Application to potential scattering," Phys. Rev. A **72**, 012708.
Kormányos, A., I. Grace, and C. J. Lambert, 2009, "Andreev reflection through Fano resonances in molecular wires," Phys. Rev. B **79**, 075119.
Kosevich, Y. A., 1997, "Capillary phenomena and macroscopic dynamics of complex two-dimensional defects in crystals," Prog. Surf. Sci. **55**, 1–57.
Kosevich, Y. A., 2008, "Multichannel propagation and scattering of phonons and photons in low-dimension nanostructures," Phys. Usp. **51**, 839–859.
Kosevich, Y. A., A. Feher, and E. S. Syrkin, 2008, "Resonance absorption, reflection, transmission of phonons, and heat transfer through interface between two solids," Low Temp. Phys. **34**, 575–582.
Koshino, K., 2003, "Analytic approach to the optical response of one-dimensional photonic crystal slabs," Phys. Rev. B **67**, 165213.
Kraemer, T., M. Mark, P. Waldburger, J. G. Danzl, C. Chin, B. Engeser, A. D. Lange, K. Pilch, A. Jaakkola, H.-C. Nägerl, and R. Grimm, 2006, "Evidence for Efimov quantum states in an ultracold gas of caesium atoms," Nature (London) **440**, 315–318.
Kroner, M., A. O. Govorov, S. Remi, B. Biedermann, S. Seidl, A. Badolato, P. M. Petroff, W. Zhang, R. Barbour, B. D. Gerardot, R. J. Warburton, and K. Karrai, 2008, "The nonlinear Fano effect," Nature (London) **451**, 311–314.
Landobasa, Y., S. D. Mario, and M. K. Chin, 2006, "Asymmetric Fano resonance and bistability for high extinction ratio, large modulation depth, and low power switching," Opt. Express **14**, 12770–12781.
Langreth, D. C., 1966, "Friedel sum rule for Anderson's model of localized impurity states," Phys. Rev. **150**, 516–518.
Le, F., N. Z. Lwin, N. J. Halas, and P. Nordlander, 2007, "Plasmonic interactions between a metallic nanoshell and a thin metallic film," Phys. Rev. B **76**, 165410.
Lebech, M., J. C. Houver, D. Dowek, and R. R. Lucchese, 2006, "Molecular frame photoelectron emission in the presence of autoionizing resonances," Phys. Rev. Lett. **96**, 073001.
Lee, C.-W., 1998, "Identification of the Beutler-Fano formula in eigenphase shifts and eigentime delays near a resonance," Phys. Rev. A **58**, 4581–4592.
Lee, J. D., J. Inoue, and M. Hase, 2006, "Ultrafast Fano resonance between optical phonons and electron-hole pairs at the onset of quasiparticle generation in a semiconductor," Phys. Rev. Lett. **97**, 157405.
Lee, M., and C. Bruder, 2006, "Spin filter using a semiconductor quantum ring side coupled to a quantum wire," Phys. Rev. B **73**, 085315.
Lee, S., and B. Kim, 2000a, "Direct evaluation of the asymmetry parameters for isolated resonances," J. Phys. B **33**, 3441–3448.
Lee, S.-S., and S. Kim, 2000b, "Phonon scattering by breathers in the discrete nonlinear Schrödinger chain," Int. J. Mod. Phys. B **14**, 1903–1914.
Lewis, B. R., S. T. Gibson, P. O'Keeffe, T. Ridley, K. P. Lawley, and R. J. Donovan, 2001, "Observation of completely destructive quantum interference between interacting resonances in molecular predissociation," Phys. Rev. Lett. **86**, 1478–1481.
Ley, L., R. Karcher, and R. L. Johnson, 1984, "Localized states at the conduction-band edge of amorphous silicon nitride detected by resonance photoemission," Phys. Rev. Lett. **53**, 710–713.
Li, W., and L. E. Reichl, 1999, "Floquet scattering through a time-periodic potential," Phys. Rev. B **60**, 15732–15741.
Limonov, M. F., A. I. Rykov, S. Tajima, and A. Yamanaka, 1998, "Raman scattering study on fully oxygenated $YBa_2Cu_3O_7$ single crystals: x-y anisotropy in the superconductivity-induced effects," Phys. Rev. Lett. **80**, 825–828.
Limonov, M. F., S. Tajima, and A. Yamanaka, 2000, "Phononic and electronic Raman spectroscopy of the pseudogap state in underdoped $YBa_2Cu_3O_{7-x}$," Phys. Rev. B **62**, 11859–11863.
Lin, S. Y., E. Chow, V. Hietala, P. R. Villeneuve, and J. D. Joannopoulos, 1998, "Experimental demonstration of guiding and bending of electromagnetic waves in a photonic crystal,"

Science **282**, 274–276.
Lobos, A. M., and A. A. Aligia, 2008, "Effects of interactions in transport through Aharonov-Bohm-Casher interferometers," Phys. Rev. Lett. **100**, 016803.
Longhi, S., 2006, "Transmission and localization control by ac fields in tight-binding lattices with an impurity," Phys. Rev. B **73**, 193305.
Lousse, V., and J. P. Vigneron, 2004, "Use of Fano resonances for bistable optical transfer through photonic crystal films," Phys. Rev. B **69**, 155106.
Luk'yanchuk, B. S., T. C. Chong, L. P. Shi, M. I. Tribelsky, Z. B. Wang, L. Li, C.-W. Qiu, C. J. R. Sheppard, and J. H. Wu, 2008, IEEE PhotonicsGlobal@Singapore (IPGS) **1&2**, 187.
Luo, H. G., T. Xiang, X. Q. Wang, Z. B. Su, and L. Yu, 2004, "Fano resonance for Anderson impurity systems," Phys. Rev. Lett. **92**, 256602.
MacKay, R. S., and S. Aubry, 1994, "Proof of existence of breathers for time-reversible or Hamiltonian networks of weakly coupled oscillators," Nonlinearity **7**, 1623–1643.
Maeda, K., K. Ueda, T. Namioka, and K. Ito, 1992, "High-resolution measurement of Beutler-Fano profiles for autoionizing Rydberg series of Xe," Phys. Rev. A **45**, 527–530.
Maes, B., P. Bienstman, and R. Baets, 2005, "Switching in coupled nonlinear photonic-crystal resonators," J. Opt. Soc. Am. B **22**, 1778–1784.
Maes, B., P. Bienstman, and R. Baets, 2008, "Symmetry breaking with coupled Fano resonances," Opt. Express **16**, 3069–3076.
Magidson, V., and R. Beserman, 2002, "Fano-type interference in the Raman spectrum of photoexcited Si," Phys. Rev. B **66**, 195206.
Magnusson, R., and S. S. Wang, 1992, "New principle for optical filters," Appl. Phys. Lett. **61**, 1022–1024.
Magunov, A. I., I. Rotter, and S. I. Strakhova, 2003, "Fano resonances in the overlapping regime," Phys. Rev. B **68**, 245305.
Mahan, G., 1993, *Many-Particle Physics* (Plenum, New York).
Maleki, L., A. B. Matsko, A. A. Savchenkov, and V. S. Ilchenko, 2004, "Tunable delay line with interacting whispering-gallery-moderesonators," Opt. Lett. **29**, 626–628.
Malyshev, A. V., P. A. Orellana, and F. Dominguez-Adame, 2006, "Quantum electron splitter based on two quantum dots attached to leads," Phys. Rev. B **74**, 033308.
Margulis, V. A., and M. A. Pyataev, 2004, "Fano resonances in a three-terminal nanodevice," J. Phys.: Condens. Matter **16**, 4315–4323.
Marinho, R. R. T., O. Bjorneholm, S. L. Sorensen, I. Hjelte, S. Sundin, M. Bassler, S. Svensson, and A. N. de Brito, 2001, "Interference between direct and resonant channels in near-resonance photoemission in argon," Phys. Rev. A **63**, 032514.
Marin Soljačić, S. G. J. Y. F., Mihai Ibanescu, and J. D. Joannopoulos, 2002, "Optimal bistable switching in nonlinear photonic crystals," Phys. Rev. E **66**, 055601.
Martinez, D. F., and L. E. Reichl, 2001, "Transmission properties of the oscillating delta-function potential," Phys. Rev. B **64**, 245315.
Mazumdar, I., A. R. P. Rau, and V. S. Bhasin, 2006, "Efimov states and their Fano resonances in a neutron-rich nucleus," Phys. Rev. Lett. **97**, 062503.
McCormack, E. F., F. D. Teodoro, J. M. Grochocinski, and S. T. Pratt, 1998, "Dynamics of Rydberg states of nitric oxide probed by two-color resonant four-wave-mixing spectroscopy," J. Chem. Phys. **109**, 63–71.
Mehlhorn, W., 1998, "70 years of Auger spectroscopy: A historical perspective," J. Electron Spectrosc. Relat. Phenom. **93**, 1–15.
Meier, T., A. Schulze, P. Thomas, H. Vaupel, and K. Maschke, 1995, "Signatures of Fano resonances in four-wave-mixing experiments," Phys. Rev. B **51**, 13977–13986.
Meijerink, A., and G. Blasse, 1989, "Fano antiresonance in the excitation spectra of the luminescence of divalent europium," Phys. Rev. B **40**, 7288–7291.
Mekis, A., J. C. Chen, I. Kurland, S. Fan, P. R. Villeneuve, and J. D. Joannopoulos, 1996, "High transmission through sharp bends in photonic crystal waveguides," Phys. Rev. Lett. **77**, 3787–3790.
Menéndez, J., and M. Cardona, 1985, "Interference effects: A key to understanding forbidden Raman scattering by LO phonons in GaAs," Phys. Rev. B **31**, 3696–3704.
Mie, G., 1908, "Beiträge zur optik trüber medien: Speziell kolloidaler metallösungen," Ann. Phys. **330**, 337–445.
Mies, F. H., 1968, "Configuration interaction theory: Effects of overlapping resonances," Phys. Rev. **175**, 164–175.
Mingaleev, S. F., and Y. S. Kivshar, 2001, "Self-trapping and stable localized modes in nonlinear photonic crystals," Phys. Rev. Lett. **86**, 5474–5477.
Mingaleev, S. F., and Y. S. Kivshar, 2002a, "Effective equations for photonic-crystal waveguides and circuits," Opt. Lett. **27**, 231–233.
Mingaleev, S. F., and Y. S. Kivshar, 2002b, "Nonlinear transmission and light localization in photonic-crystal waveguides," J. Opt. Soc. Am. B **19**, 2241–2249.
Mingaleev, S. F., Y. S. Kivshar, and R. A. Sammut, 2000, "Long-range interaction and nonlinear localized modes in photonic crystal waveguides," Phys. Rev. E **62**, 5777–5782.
Mingaleev, S. F., A. E. Miroshnichenko, and Y. S. Kivshar, 2007, "Low-threshold bistability of slow light in photonic-crystal waveguides," Opt. Express **15**, 12380–12385.
Mingaleev, S. F., A. E. Miroshnichenko, and Y. S. Kivshar, 2008, "Coupled-resonator-induced reflection in photonic-crystal waveguide structures," Opt. Express **16**, 11647–11659.
Mingaleev, S. F., A. E. Miroshnichenko, Y. S. Kivshar, and K. Busch, 2006, "All-optical switching, bistability, and slow-light transmission in photonic crystal waveguide-resonator structures," Phys. Rev. E **74**, 046603.
Mirin, N. A., K. Bao, and P. Nordlander, 2009, "Fano resonances in plasmonic nanoparticle aggregates," J. Phys. Chem. A **113**, 4028–4034.
Miroshnichenko, A. E., 2009a, "Instabilities and quasilocalized states in nonlinear Fano-like systems," Phys. Lett. A **373**, 3586–3590.
Miroshnichenko, A. E., 2009b, "Non-Rayleigh limit of the Lorenz-Mie solution and suppression of scattering by spheres of negative refractive index," Phys. Rev. A **80**, 013808.
Miroshnichenko, A. E., 2009c, "Nonlinear Fano-Feshbach resonances," Phys. Rev. E **79**, 026611.
Miroshnichenko, A. E., S. Flach, A. V. Gorbach, B. S. Luk'yanchuk, Y. S. Kivshar, and M. I. Tribelsky, 2008, "Fano resonances: A discovery that did not happen 100 years ago," Opt. Photonics News **19**, 48.
Miroshnichenko, A. E., S. Flach, and B. Malomed, 2003, "Resonant scattering of solitons," Chaos **13**, 874–879.
Miroshnichenko, A. E., Y. Kivshar, C. Etrich, T. Pertsch, R. Iliew, and F. Lederer, 2009, "Dynamics and instability of nonlinear Fano resonances in photonic crystals," Phys. Rev. A **79**, 013809.

Miroshnichenko, A. E., and Y. S. Kivshar, 2005a, "Engineering Fano resonances in discrete arrays," Phys. Rev. E **72**, 056611.
Miroshnichenko, A. E., and Y. S. Kivshar, 2005b, "Sharp bends in photonic crystal waveguides as nonlinear Fano resonators," Opt. Express **13**, 3969–3976.
Miroshnichenko, A. E., and Y. S. Kivshar, 2009, "Mach-Zehnder-Fano interferometer," Appl. Phys. Lett. **95**, 121109.
Miroshnichenko, A. E., Y. S. Kivshar, R. A. Vicencio, and M. I. Molina, 2005, "Fano resonance in quadratic waveguide arrays," Opt. Lett. **30**, 872–874.
Miroshnichenko, A. E., S. F. Mingaleev, S. Flach, and Y. S. Kivshar, 2005, "Nonlinear Fano resonance and bistable wave transmission," Phys. Rev. E **71**, 036626.
Miroshnichenko, A. E., M. Schuster, S. Flach, M. V. Fistul, and A. V. Ustinov, 2005, "Resonant plasmon scattering by discrete breathers in Josephson-junction ladders," Phys. Rev. B **71**, 174306.
Misochko, O., M. Hase, K. Ishioka, and M. Kitajima, 2005, "Fano interference with the alternating asymmetry parameter in time-domain experiments," JETP Lett. **82**, 426–430.
Misochko, O. V., K. Kisoda, K. Sakai, and S. Nakashima, 2000, "Dynamics of low-frequency phonons in the $YBa_2Cu_3O_{7-x}$ superconductor studied by time- and frequency-domain spectroscopies," Phys. Rev. B **61**, 4305–4313.
Morsch, O., and M. Oberthaler, 2006, "Dynamics of Bose-Einstein condensates in optical lattices," Rev. Mod. Phys. **78**, 179–215.
Moskovits, M., 1985, "Surface-enhanced spectroscopy," Rev. Mod. Phys. **57**, 783–826.
Mourokh, L. G., V. I. Puller, A. Y. Smirnov, and J. P. Bird, 2005, "Readout of single spins via Fano resonances in quantum point contacts," Appl. Phys. Lett. **87**, 192501.
Naweed, A., G. Farca, S. I. Shopova, and A. T. Rosenberger, 2005, "Induced transparency and absorption in coupled whispering-gallery microresonators," Phys. Rev. A **71**, 043804.
Néel, N., J. Kröger, L. Limot, K. Palotas, W. A. Hofer, and R. Berndt, 2007, "Conductance and Kondo effect in a controlled single-atom contact," Phys. Rev. Lett. **98**, 016801.
Neviere, M., R. Petit, and M. Cadilhac, 1973, "About the theory of optical grating coupler-waveguide systems," Opt. Commun. **8**, 113–117.
Ng, T. K., and P. A. Lee, 1988, "On-site Coulomb repulsion and resonant tunneling," Phys. Rev. Lett. **61**, 1768–1771.
Nöckel, J. U., and A. D. Stone, 1994, "Resonance line shapes in quasi-one-dimensional scattering," Phys. Rev. B **50**, 17415–17432.
Notomi, M., K. Yamada, A. Shinya, J. Takahashi, C. Takahashi, and I. Yokohama, 2001, "Extremely large group-velocity dispersion of line-defect waveguides in photonic crystal slabs," Phys. Rev. Lett. **87**, 253902.
Nussenzweig, A., E. E. Eyler, T. Bergeman, and E. Pollack, 1990, "Line shapes of ionizing Stark resonances in helium," Phys. Rev. A **41**, 4944–4957.
Nygaard, N., R. Piil, and K. Mølmer, 2008a, "Two-channel Feshbach physics in a structured continuum," Phys. Rev. A **78**, 023617.
Nygaard, N., R. Piil, and K. Mølmer, 2008b, "Feshbach molecules in a one-dimensional optical lattice," Phys. Rev. A **77**, 021601.
Oliveira, L. N., and J. W. Wilkins, 1985, "Fano antiresonances in x-ray absorption spectroscopy," Phys. Rev. B **32**, 696–707.
Opatrný, T., and D.-G. Welsch, 2001, "Coupled cavities for enhancing the cross-phase-modulation in electromagnetically induced transparency," Phys. Rev. A **64**, 023805.
Orellana, P. A., M. L. L. de Guevara, and F. Claro, 2004, "Controlling Fano and Dicke effects via a magnetic flux in a two-site Anderson model," Phys. Rev. B **70**, 233315.
Ott, H., J. Fortagh, G. Schlotterbeck, A. Grossmann, and C. Zimmermann, 2001, "Bose-Einstein condensation in a surface microtrap," Phys. Rev. Lett. **87**, 230401.
Ozbay, E., 2006, "Plasmonics: Merging photonics and electronics at nanoscale dimensions," Science **311**, 189–193.
Pálffy, A., Z. Harman, and W. Scheid, 2007, "Quantum interference between nuclear excitation by electron capture and radiative recombination," Phys. Rev. A **75**, 012709.
Papasimakis, N., V. A. Fedotov, N. I. Zheludev, and S. L. Prosvirnin, 2008, "Metamaterial analog of electromagnetically induced transparency," Phys. Rev. Lett. **101**, 253903.
Papasimakis, N., Y. H. Fu, V. A. Fedotov, S. L. Prosvirnin, D. P. Tsai, and N. I. Zheludev, 2009, "Metamaterial with polarization and direction insensitive resonant transmission response mimicking electromagnetically induced transparency," Appl. Phys. Lett. **94**, 211902.
Papasimakis, N., and N. Zheludev, 2009, "Metamaterial-induced transparency: Sharp Fano resonances and slow light," Opt. Photonics News **20**, 22–27.
Pastawski, H. M., L. E. F. F. Torres, and E. Medina, 2002, "Electron-phonon interaction and electronic decoherence in molecular conductors," Chem. Phys. **281**, 257–278.
Patthey, F., M.-H. Schaffner, W.-D. Schneider, and B. Delley, 1999, "Observation of a Fano resonance in photoemission," Phys. Rev. Lett. **82**, 2971–2974.
Piao, G., R. A. Lewis, and P. Fisher, 1990, "Fano resonances in the absorption spectrum of singly ionised zinc in germanium," Solid State Commun. **75**, 835–838.
Pichl, L., H. Nakamura, and J. Horacek, 2000, "Complete reflection in two-state crossing and noncrossing potential systems," J. Chem. Phys. **113**, 906–918.
Qiang, Z., H. Yang, L. Chen, H. Pang, Z. Ma, and W. Zhou, 2008, "Fano filters based on transferred silicon nanomembranes on plastic substrates," Appl. Phys. Lett. **93**, 061106.
Ramaker, D. E., and D. M. Schrader, 1974, "Multichannel configuration-interaction theory: Application to some resonances in helium," Phys. Rev. A **9**, 1980–1991.
Raoult, M., and F. H. Mies, 2004, "Feshbach resonance in atomic binary collisions in the Wigner threshold law regime," Phys. Rev. A **70**, 012710.
Rau, A. R. P., 2004, "Perspectives on the Fano resonance formula," Phys. Scr. **69**, C10–C13.
Rayleigh, L., 1871a, "On the light from the sky: Its polarization and color," Philos. Mag. **41**, 107–120.
Rayleigh, L., 1871b, "On the light from the sky: Its polarization and color," Philos. Mag. **41**, 274–279.
Rayleigh, L., 1871c, "On the scattering of light by small particles," Philos. Mag. **41**, 447–451.
Rayleigh, L., 1907, "On the dynamical theory of gratings," Proc. R. Soc. London, Ser. A **79**, 399–416.
Redner, S., 2004, "Citation statistics from more than a century of physical review," e-print arXiv:physics/0407137.
Reimann, S. M., and M. Manninen, 2002, "Electronic structure of quantum dots," Rev. Mod. Phys. **74**, 1283–1342.
Rice, O. K., 1933, "Predissociation and the crossing of molecular potential energy curves," J. Chem. Phys. **1**, 375–389.
Roney, P. L., 1994a, "Theory of spectral line shape: I. Formulation and line coupling," J. Chem. Phys. **101**, 1037–1049.

Roney, P. L., 1994b, "Theory of spectral line shape: II. Collision time theory and the line wing," J. Chem. Phys. **101**, 1050–1060.
Roney, P. L., 1995, "Theory of spectral line shape: III. The Fano operator from near to far wing," J. Chem. Phys. **102**, 4757–4771.
Rotter, S., F. Libisch, J. Burgdörfer, U. Kuhl, and H.-J. Stöckmann, 2004, "Tunable Fano resonances in transport through microwave billiards," Phys. Rev. E **69**, 046208.
Saito, R., G. Dresselhaus, and M. S. Dresselhaus, 1998, *Physical Properties of Carbon Nanotubes* (Imperial College Press, London).
Sánchez, D., and L. Serra, 2006, "Fano-Rashba effect in a quantum wire," Phys. Rev. B **74**, 153313.
Sánchez, I., and F. Martin, 1994, "Hidden Fano interferences in the resonant photoionization of He-like ions," Phys. Rev. A **49**, 5116–5119.
Sarrazin, M., J.-P. Vigneron, and J.-M. Vigoureux, 2003, "Role of Wood anomalies in optical properties of thin metallic films with a bidimensional array of subwavelength holes," Phys. Rev. B **67**, 085415.
Sasada, K., and N. Hatano, 2005, "Quantum interference effect of resonant transport in nano-scale systems," Physica E **29**, 609–613.
Sato, M., H. Aikawa, K. Kobayashi, S. Katsumoto, and Y. Iye, 2005, "Observation of the Fano-Kondo antiresonance in a quantum wire with a side-coupled quantum dot," Phys. Rev. Lett. **95**, 066801.
Sato, M., B. E. Hubbard, A. J. Sievers, B. Ilic, D. A. Czaplewski, and H. G. Craighead, 2003, "Observation of locked intrinsic localized vibrational modes in a micromechanical oscillator array," Phys. Rev. Lett. **90**, 044102.
Schmid, J., J. Weis, K. Eberl, and K. v. Klitzing, 1998, "A quantum dot in the limit of strong-coupling to reservoirs," Physica B **256-258**, 182–185.
Schwarz, U. T., L. Q. English, and A. J. Sievers, 1999, "Experimental generation and observation of intrinsic localized spin wave modes in an antiferromagnet," Phys. Rev. Lett. **83**, 223–226.
Seaton, M. J., 1966, "Quantum defect theory: I. General formulation," Proc. Phys. Soc. London **88**, 801–814.
Serra, L., and D. Sánchez, 2007, "The Fano-Rashba effect," J. Phys.: Conf. Ser. **61**, 1037–1041.
Siegner, U., M.-A. Mycek, S. Glutsch, and D. S. Chemla, 1995, "Quantum interference in the system of Lorentzian and Fano magnetoexciton resonances in GaAs," Phys. Rev. B **51**, 4953–4961.
Simonian, A. W., A. B. Sproul, Z. Shi, and E. Gauja, 1995, "Observation of Fano resonance in heavily doped *p*-type silicon at room temperature," Phys. Rev. B **52**, 5672–5674.
Simpson, J. A., and U. Fano, 1963, "Classification of resonances in the electron scattering cross section of Ne and He," Phys. Rev. Lett. **11**, 158–159.
Smirnov, B. M., 2003, *Physics of Atoms and Ions* (Springer, New York).
Smith, D. D., H. Chang, K. A. Fuller, A. T. Rosenberger, and R. W. Boyd, 2004, "Coupled-resonator-induced transparency," Phys. Rev. A **69**, 063804.
Smith, K., D. E. Golden, S. Ormonde, B. W. Torres, and A. R. Davies, 1973, "Theoretical model for resonances in *e*-He scattering near 60 eV," Phys. Rev. A **8**, 3001–3011.
Soljačić, M., and J. D. Joannopoulos, 2004, "Enhancement of nonlinear effects using photonic crystals," Nature Mater. **3**, 211–219.
Soljačić, M., C. Luo, J. D. Joannopoulos, and S. Fan, 2003, "Nonlinear photonic crystal microdevices for optical integration," Opt. Lett. **28**, 637–639.
Song, J. F., Y. Ochiai, and J. P. Bird, 2003, "Fano resonances in open quantum dots and their application as spin filters," Appl. Phys. Lett. **82**, 4561–4563.
Spevak, I. S., A. Y. Nikitin, E. V. Bezuglyi, A. Levchenko, and A. V. Kats, 2009, "Resonantly suppressed transmission and anomalously enhanced light absorption in periodically modulated ultrathin metal films," Phys. Rev. B **79**, 161406.
Stefanski, P., 2003, "Quantum dots as scatterers in electronic transport: interference and correlations," Solid State Commun. **128**, 29–34.
Stefański, P., A. Tagliacozzo, and B. R. Bułka, 2004, ""Fano versus Kondo resonances in a multilevel "semiopen" quantum dot," Phys. Rev. Lett. **93**, 186805.
Stillinger, F. H., and D. R. Herrick, 1975, "Bound states in the continuum," Phys. Rev. A **11**, 446–454.
Sturm, K., W. Schulke, and J. R. Schmitz, 1992, "Plasmon-Fano resonance inside the particle-hole excitation spectrum of simple metals and semiconductors," Phys. Rev. Lett. **68**, 228–231.
Suh, W., Z. Wang, and S. Fan, 2004, "Temporal coupled-mode theory and the presence of nonorthogonal modes in lossless multimode cavities," IEEE J. Quantum Electron. **40**, 1511–1518.
Swanson, B. I., J. A. Brozik, S. P. Love, G. F. Strouse, A. P. Shreve, A. R. Bishop, W.-Z. Wang, and M. I. Salkola, 1999, "Observation of intrinsically localized modes in a discrete low-dimensional material," Phys. Rev. Lett. **82**, 3288–3291.
Syage, J. A., and J. E. Wessel, 1987, "Antiresonance in autoionizing Rydberg series of naphthalene," J. Chem. Phys. **87**, 6207–6209.
Taylor, D. P., and P. M. Johnson, 1993, "Resonance enhanced multiphoton ionization photoelectron spectra of CO_2: III. Autoionization dominates direct ionization," J. Chem. Phys. **98**, 1810–1816.
Teodoro, F. D., and E. F. McCormack, 1998, "Theoretical treatment of quasibound resonances in two-color resonant four-wave-mixing spectroscopy," Phys. Rev. A **57**, 162–173.
Teodoro, F. D., and E. F. McCormack, 1999, "State-selective quantum beat spectroscopy via coherent control of Liouville-pathway interference in two-colour resonant four-wave mixing," J. Phys. B **32**, 4389–4404.
Terrones, M., H. Terrones, F. Banhart, J.-C. Charlier, and P. M. Ajayan, 2000, "Coalescence of single-walled carbon nanotubes," Science **288**, 1226–1229.
Tomita, M., K. Totsuka, R. Hanamura, and T. Matsumoto, 2009, "Tunable Fano interference effect in coupled-microsphere resonator-induced transparency," J. Opt. Soc. Am. B **26**, 813–818.
Tong, P., B. Li, and B. Hu, 1999, "Wave transmission, phonon localization, and heat conduction of a one-dimensional Frenkel-Kontorova chain," Phys. Rev. B **59**, 8639–8645.
Torio, M. E., K. Hallberg, S. F. A. E. Miroshnichenko, and M. Titov, 2004, "Spin filters with Fano dots," Eur. Phys. J. B **37**, 399–403.
Torres, L. E. F. F., H. M. Pastawski, and E. Medina, 2006, "Antiresonances as precursors of decoherence," EPL **73**, 164–170.
Trías, E., J. J. Mazo, and T. P. Orlando, 2000, "Discrete breathers in nonlinear lattices: Experimental detection in a Joseph-

son array," Phys. Rev. Lett. **84**, 741–744.
Tribelsky, M. I., S. Flach, A. E. Miroshnichenko, A. V. Gorbach, and Y. S. Kivshar, 2008, "Light scattering by a finite obstacle and Fano resonances," Phys. Rev. Lett. **100**, 043903.
Tribelsky, M. I., and B. S. Luk'yanchuk, 2006, "Anomalous light scattering by small particles," Phys. Rev. Lett. **97**, 263902.
Ueda, K., 1987, "Spectral line shapes of autoionizing Rydberg series," Phys. Rev. A **35**, 2484–2492.
Valiente, M., and D. Petrosyan, 2009, "Scattering resonances and two-particle bound states of the extended Hubbard model," J. Phys. B **42**, 121001.
van der Hulst, H. C., 1981, *Light Scattering by Small Particles* (Dover, New York).
van der Molen, K. L., K. J. K. Koerkamp, S. Enoch, F. B. Segerink, N. F. van Hulst, and L. Kuipers, 2005, "Role of shape and localized resonances in extraordinary transmission through periodic arrays of subwavelength holes: Experiment and theory," Phys. Rev. B **72**, 045421.
Verellen, N., Y. Sonnefraud, H. Sobhani, F. Hao, V. V. Moshchalkov, P. V. Dorpe, P. Nordlander, and S. A. Maier, 2009, "Fano resonances in individual coherent plasmonic nanocavities," Nano Lett. **9**, 1663–1667.
Vicencio, R. A., J. Brand, and S. Flach, 2007, "Fano blockade by a Bose-Einstein condensate in an optical lattice," Phys. Rev. Lett. **98**, 184102.
Vittorini-Orgeas, A., and A. Bianconi, 2009, "From Majorana theory of atomic autoionization to Feshbach resonances in high temperature superconductors," J. Supercond. Novel Magn. **22**, 215–221.
Vlasov, Y. A., M. O'Boyle, H. F. Hamann, and S. J. McNab, 2005, "Active control of slow light on a chip with photonic crystal waveguides," Nature (London) **438**, 65–69.
von Neumann, J., and E. Wigner, 1929, "Uber merkwurdige diskrete eigenwerte/on unusual discrete eigevalues," Z. Phys. **30**, 465–467.
Waligorski, G., L. Zhou, and W. E. Cooke, 1997, "Technique for measuring the linewidth of autoionizing Rydberg states," Phys. Rev. A **55**, 1544–1547.
Wang, F., X. Wang, H. Zhou, Q. Zhou, Y. Hao, X. Jiang, M. Wang, and J. Yang, 2009, "Fano-resonance-based Mach-Zehnder optical switch employing dual-bus coupled ring resonator as two-beam interferometer," Opt. Express **17**, 7708–7716.
Ward, A. J., and J. B. Pendry, 1998, "Calculating photonic Green's functions using a nonorthogonal finite-difference time-domain method," Phys. Rev. B **58**, 7252–7259.
Weidner, E., S. Combrié, A. de Rossi, N.-V.-Q. Tran, and S. Cassette, 2007, "Nonlinear and bistable behavior of an ultrahigh-Q GaAs photonic crystal nanocavity," Appl. Phys. Lett. **90**, 101118.
Wickenhauser, M., J. Burgdorfer, F. Krausz, and M. Drescher, 2005, "Time resolved Fano resonances," Phys. Rev. Lett. **94**, 023002.
Wiegmann, P. B., and A. M. Tsvelick, 1983, "Exact solution of the Anderson model: I," J. Phys. C **16**, 2281–2319.
Winstead, C., and P. W. Langhoff, 1991, "Feshbach-Fano formalism in Hilbert space: Application to shape resonances in molecular photoionization," J. Chem. Phys. **95**, 3107–3118.
Wood, R., 1902, "On the remarkable case of uneven distribution of light in a diffraction grating spectrum," Proc. R. Soc. London, Ser. A **18**, 269–275.
Wood, R. W., 1935, "Anomalous diffraction gratings," Phys. Rev. **48**, 928–936.
Wulf, U., and V. V. Skalozub, 2005, "Pulse propagation in resonant tunneling," Phys. Rev. B **72**, 165331.
Xu, Q., S. Sandhu, M. L. Povinelli, J. Shakya, S. Fan, and M. Lipson, 2006, "Experimental realization of an on-chip all-optical analogue to electromagnetically induced transparency," Phys. Rev. Lett. **96**, 123901.
Xu, S. J., J. L., S.-J. Xiong, and H. Z. Zheng, 2006, "New type of Fano resonant tunneling via Anderson impurities in superlattice," Europhys. Lett. **74**, 875–881.
Xu, Y., Y. Li, R. K. Lee, and A. Yariv, 2000, "Scattering-theory analysis of waveguide-resonator coupling," Phys. Rev. E **62**, 7389–7404.
Yafet, Y., 1981, "Effect of shake-up transitions on the spectrum of Auger electrons in Fano resonances," Phys. Rev. B **23**, 3558–3559.
Yang, H., H. Pang, Z. Qiang, Z. Ma, and W. Zhou, 2008, "Surface-normal Fano filters based on transferred silicon nanomembranes on glass substrates," Electron. Lett. **44**, 858–860.
Yang, X., C. Husko, C. W. Wong, M. Yu, and D.-L. Kwong, 2007, "Observation of femtojoule optical bistability involving Fano resonances in high-Q/V_m silicon photonic crystal nanocavities," Appl. Phys. Lett. **91**, 051113.
Yanik, M. F., and S. Fan, 2004, "Stopping light all optically," Phys. Rev. Lett. **92**, 083901.
Yanik, M. F., S. Fan, and M. Soljačić, 2003, "High-contrast all-optical bistable switching in photonic crystal microcavities," Appl. Phys. Lett. **83**, 2739–2741.
Yanik, M. F., S. Fan, M. Soljačić, and J. D. Joannopoulos, 2003, "All-optical transistor action with bistable switching in a photonic crystal cross-waveguide geometry," Opt. Lett. **28**, 2506–2508.
Yanik, M. F., W. Suh, Z. Wang, and S. Fan, 2004, "Stopping light in a waveguide with an all-optical analog of electromagnetically induced transparency," Phys. Rev. Lett. **93**, 233903.
Yi, W., L. Lu, H. Hu, Z. W. Pan, and S. S. Xie, 2003, "Tunneling into multiwalled carbon nanotubes: Coulomb blockade and the Fano resonance," Phys. Rev. Lett. **91**, 076801.
Yoon, Y., M.-G. Kang, T. M. L. Mourokh, N. Aoki, J. L. Reno, J. P. Bird, and Y. Ochiai, 2009, "Detector backaction on the self-consistent bound state in quantum point contacts," Phys. Rev. B **79**, 121304.
Zhang, W., A. O. Govorov, and G. W. Bryant, 2006, "Semiconductor-metal nanoparticle molecules: Hybrid excitons and the nonlinear Fano effect," Phys. Rev. Lett. **97**, 146804.
Zhang, Z., and V. Chandrasekhar, 2006, "Signatures of phase coherence in the low-temperature transport properties of multiwall carbon nanotubes," Phys. Rev. B **73**, 075421.
Zhang, Z., D. A. Dikin, R. S. Ruoff, and V. Chandrasekhar, 2004, "Conduction in carbon nanotubes through metastable resonant states," Europhys. Lett. **68**, 713–719.